Physical characterization of Warm Spitzer-observed near-Earth objects

Cristina A. Thomas [a,b,c,*,1], Joshua P. Emery [d,1], David E. Trilling [a,1], Marco Delbó [e,1], Joseph L. Hora [f,1], Michael Mueller [g,1]

[a] Northern Arizona University, Department of Physics and Astronomy, PO Box 6010, Flagstaff, AZ 86011, USA
[b] NASA Goddard Space Flight Center, 8800 Greenbelt Rd., Greenbelt, MD 20771, USA
[c] NASA Postdoctoral Program, Oak Ridge Associated Universities, PO Box 117, MS 36, Oak Ridge, TN 37831, USA
[d] University of Tennessee, Department of Earth and Planetary Sciences, 1412 Circle Dr., Knoxville, TN 37996, USA
[e] Université de Nice Antipolis, CNRS, Observatoire de la Côte d'Azur, BP4229, 06304 Nice Cedex 4, France
[f] Harvard-Smithsonian Center for Astrophysics, 60 Garden Street, MS-65, Cambridge, MA 02138, USA
[g] SRON Netherlands Institute for Space Research, PO Box 800, 9700 AV, Groningen, The Netherlands

ARTICLE INFO

ABSTRACT

Near-infrared spectroscopy of Near-Earth Objects (NEOs) connects diagnostic spectral features to specific surface mineralogies. The combination of spectroscopy with albedos and diameters derived from thermal infrared observations can increase the scientific return beyond that of the individual datasets. For instance, some taxonomic classes can be separated into distinct compositional groupings with albedo and different mineralogies with similar albedos can be distinguished with spectroscopy. To that end, we have completed a spectroscopic observing campaign to complement the ExploreNEOs Warm Spitzer program that obtained albedos and diameters of nearly 600 NEOs (Trilling, D.E. et al. [2010]. Astron. J. 140, 770–784. http://dx.doi.org/10.1088/0004-6256/140/3/770). The spectroscopy campaign included visible and near-infrared observations of ExploreNEOs targets from various observatories. Here we present the results of observations using the low-resolution prism mode ($\sim$0.7–2.5 μm) of the SpeX instrument on the NASA Infrared Telescope Facility (IRTF). We also include near-infrared observations of ExploreNEOs targets from the MIT-UH-IRTF Joint Campaign for Spectral Reconnaissance. Our dataset includes near-infrared spectra of 187 ExploreNEOs targets (125 observations of 92 objects from our survey and 213 observations of 154 objects from the MIT survey). We identify a taxonomic class for each spectrum and use band parameter analysis to investigate the mineralogies for the S-, Q-, and V-complex objects. Our analysis suggests that for spectra that contain near-infrared data but lack the visible wavelength region, the Bus–DeMeo system misidentifies some S-types as Q-types. We find no correlation between spectral band parameters and ExploreNEOs albedos and diameters. We investigate the correlations of phase angle with Band Area Ratio and near-infrared spectral slope. We find slightly negative Band Area Ratio (BAR) correlations with phase angle for Eros and Ivar, but a positive BAR correlation with phase angle for Ganymed. The results of our phase angle study are consistent with those of (Sanchez, J.A., Reddy, V., Nathues, A., Cloutis, E.A., Mann, P., Hiesinger, H. [2012]. Icarus 220, 36–50. http://dx.doi.org/10.1016/j.icarus.2012.04.008, arXiv:1205.0248). We find evidence for spectral phase reddening for Eros, Ganymed, and Ivar. We identify the likely ordinary chondrite type analog for an appropriate subset of our sample. Our resulting proportions of H, L, and LL ordinary chondrites differ from those calculated for meteorite falls and in previous studies of ordinary chondrite-like NEOs.

© 2013 Elsevier Inc. All rights reserved.

1. Introduction

Since many asteroids have diagnostic spectral features in near-infrared wavelengths, we can investigate their mineralogies remo-tely. These connections to mineralogy allow for detailed investigations of individual objects and can be applied to questions regarding the compositional distributions of asteroids throughout the Solar System. In near-Earth space, one puzzle is the relative distribution of ordinary chondrite-like material. Previous work (e.g. Vernazza et al., 2008; Dunn et al., 2013; de León et al., 2010) suggests that a majority of Near-Earth Objects (NEOs) have compositions similar to LL ordinary chondrites. This result was unexpected since LL ordinary chondrites are only $\sim$7.9% of all meteorite falls (Burbine et al., 2002). The gap between these two populations will likely be bridged as we start to observe smaller

objects, the direct precursors to our meteorite collection, and as our spectroscopic observing sample sizes grow.

There are several quantitative approaches to near-infrared spectral analysis. Taxonomic classification based on measurements of the spectral slope and absorption features is often used as a first step. Basic compositional can be inferred if the average compositions of each of the taxonomic classes are known. Taxonomy can suggest the presence of certain minerals, such as mafic silicates, but in many cases the mineralogical interpretation can be ambiguous. For those objects with broad 1-μm and 2-μm absorption features we can study the composition more thoroughly using band parameter analysis. Band parameter analysis has been used in many studies (e.g. Gaffey et al., 1993; Thomas and Binzel, 2010; de León et al., 2010; Dunn et al., 2013; Burbine et al., 2009; Moskovitz et al., 2010; Reddy et al., 2011a) to determine the compositions and relative abundances of the olivines and pyroxenes present on the surface of various asteroids. For olivine–pyroxene mixtures, the band center wavelength of the broad 1-μm absorption feature is a function of the relative abundance and composition of olivine and pyroxene, and the band center of the broad 2-μm absorption is a function of the pyroxene composition. Additionally, the Band Area Ratio (the ratio of the area of the 2-μm band to the area of the 1-μm band) is a function of the relative olivine and pyroxene abundances. Using the derived compositions, the diversity and distribution of material in near-Earth space can be investigated remotely.

The regions within the parameter space defined by calculated band centers and Band Area Ratios provide insight into meteorite analogs and the diversity of compositions among the asteroid sample. These regions are correlated to potential meteorite types using laboratory derived mineralogies of various meteorite analogs. The relationship between band parameters and mineralogical composition is particularly well studied for ordinary chondrites and basaltic achondrites (e.g. Dunn et al., 2010; Burbine et al., 2009, 2007; Reddy et al., 2011a,b, 2012b).

The combination of spectroscopy and albedos and diameters derived from thermal infrared observations can increase the scientific return beyond that of the individual datasets. To that end, we have completed a ground-based observing campaign to measure visible and near-infrared spectra of near-Earth objects in support of the Warm Spitzer project entitled "The Warm Spitzer NEO Survey: Exploring the history of the inner Solar System and near Earth space" or ExploreNEOs (Trilling et al., 2010 and Trilling et al., submitted for publication). This two year program (2009–2011) was allocated 500 h to determine the albedos and diameters of nearly 600 NEOs using the Warm capabilities of the IRAC (Infrared Array Camera, Fazio et al., 2004; Werner et al., 2004). In this paper, we present our near-infrared observations from the SpeX instrument at the NASA Infrared Telescope Facility (IRTF). We supplement our observations with spectra of ExploreNEOs targets from the MIT-UH-IRTF Joint Campaign for NEO Spectral Reconnaissance.

2. Data

2.1. Observations and reduction

The observations presented in this paper were obtained using the low-resolution prism mode of the SpeX instrument (Rayner et al., 2003) on the NASA Infrared Telescope Facility (IRTF) between 1 September 2009 and 28 January 2012. Each object was observed with the dichroic out of the light path, which resulted in spectra covering ~0.7–2.5 μm. We used the 0.8 × 15 arcsec slit with the *abba* 7.5 arcsec dither pattern. Observations were taken at the parallactic angle. Each individual exposure was nominally limited to 120s due to variability of the atmosphere. Brighter object exposure

times were calculated to avoid any non-linearity in the detector. Solar standards were selected using a list provided by S.J. Bus (personal communication) and SIMBAD searches for G-dwarfs with solar-like B–V and V–K colors near the position of the object. We used the internal SpeX calibration macro for flat-field frames and wavelength calibration argon lamp frames.

The spectra were reduced in one of two methods that employed standard near-infrared reduction techniques. One method used IDL tools (e.g. Emery et al., 2011) to perform the reduction, while the other used the IRAF `apextract` package with telluric atmosphere correction by the ATRAN model atmosphere (e.g. Lord, 1992; Rivkin et al., 2004). Both techniques included the creation of bad pixel maps, division by the flat field, subtraction of the dithered pairs to remove atmospheric emission, wavelength calibration, and the extraction of two-dimensional spectra to one-dimensional spectra. We chose solar-like stars as telluric calibrators in order to also correct for the spectroscopic signature of reflected sunlight from the targets. These techniques were tested against each other on a small number of objects and the reductions were nearly identical. Some reduced spectra show evidence of telluric absorption in the ~1.4 and ~1.8–1.9 μm regions, which should not be confused with features that present compositional information. The one exception to these described reduction techniques is the analysis of (3552) Don Quixote. Mommert et al. (submitted for publication) discovered cometary activity on Don Quixote at the time of our ExploreNEOs observation. Therefore, a small reduction artifact found in the spectrum needed to be addressed. The final spectrum presented in this paper and in Mommert et al. (submitted for publication) was reduced using Spextool (Cushing et al., 2004) and the ATRAN atmospheric correction.

We present 125 observations of 92 ExploreNEOs targets (see Table 1 and Fig. 9). Some of these spectra were used to taxonomically classify objects for the study of average albedo by taxonomic complex presented in Thomas et al. (2011). Additional visible and near-infrared spectra from the campaign will be presented in future papers.

2.2. MIT-UH-IRTF Joint Campaign for NEO Spectral Reconnaissance

A number of ExploreNEOs targets were also observed with SpeX as part of the MIT-UH-IRTF Joint Campaign for NEO Spectral Reconnaissance.[2] The objects were identified using the MIT catalog of asteroid spectra and include observations from the MIT Joint Campaign, Binzel et al. (2001), Binzel et al. (2004a), and Rivkin et al. (2004). These objects were also observed with the low-resolution prism mode on SpeX with the 0.8 × 15 arcsec slit and the 7.5 arcsec dither pattern. These objects were reduced using the IRAF `apextract` package and the ATRAN model atmosphere. Data taken prior to mid-2007 (prior to and including `sp61`) used the dichroic to remove light short ward 0.82 μm. The blue end of the data for subsequent observations ranges between ~ 0.7–0.8 μm. Visible wavelength data from the Small Main-Belt Asteroid Spectroscopic Survey (SMASS) are included when available (Xu et al., 1995; Bus and Binzel, 2002).

We include 213 observations of 154 ExploreNEOs targets. Table 2 shows all the spectra used in this study, including the file name from the MIT-UH-IRTF Joint Campaign. The file names are marked with a footnote if the file does not include data at or below 0.75 μm, which affects our band parameter analysis (Section 2.4).

The combination of our survey and the MIT-UH-IRTF Joint Campaign for NEO Spectral Reconnaissance (hereafter "MIT Joint Campaign") yields a total of 340 observations of 187 ExploreNEOs targets.

---

[2] http://smass.mit.edu/minus.html.

Table 1

Table of observations of ExploreNEOs targets from our spectroscopic survey. The table includes object number, name, the UT date and time of observation, the integration time (T_{int}) in minutes, airmass, the solar standard used in the reduction, and the taxonomic classification.

Number	Name	UT	T_{int}	Airmass	Standard	Taxonomic type
433	Eros	01-September-2009 12:06	2	1.20	SAO 127422	Sq/Q
433	Eros	01-November-2009 05:42	18	1.05	L113–276	Q/Sq
433	Eros	06-Mar-2010 04:52	8	1.32	SAO 75438	Q/Sq
433	Eros	28-January-2012 12:17	1.07	1.08	HD 91688	Q/Sq
1036	Ganymed	19-Mar-2010 09:50	16	1.42	HD 111017	Sr/S
1036	Ganymed	10-June-2011 11:48	2	1.14	HD 334883	Sr
1036	Ganymed	04-July-2011 10:31	2.7	1.28	HD 204570	Sr
1036	Ganymed	17-September-2011 14:08	3	1.46	Hya 64	S
1036	Ganymed	26-September-2011 10:21	2.7	1.24	HD 232456	Sr
1036	Ganymed	19-October-2011 07:48	2.7	1.28	SAO 75105	Sr/S
1627	Ivar	19-February-2010 10:26	32	1.01	HD 89547	S
1864	Daedalus	07-Mar-2010 14:41	32	1.42	HD 132076	Sq/Q
1865	Cerberus	05-August-2010 09:08	96	1.08	L110–361 and L112–1333	S
1866	Sisyphus	01-May-2011 11:56	16	1.05	HD 144684	S
1866	Sisyphus A	10-June-2011 06:16	16	1.18	HD 125982	S
1866	Sisyphus B	10-June-2011 06:52	16	1.13	HD 125982	S
1866	Sisyphus C	10-June-2011 07:19	16	1.11	HD 125982	S
1866	Sisyphus D	10-June-2011 08:22	16	1.14	HD 125982	S
1866	Sisyphus E	10-June-2011 09:07	8	1.21	HD 125982	S
1866	Sisyphus F	10-June-2011 09:27	16	1.30	HD 125982	S
1866	Sisyphus A	24-June-2011 06:08	16	1.16	HD 123765	S
1866	Sisyphus B	24-June-2011 06:40	16	1.17	HD 123765	S
1866	Sisyphus C	24-June-2011 07:04	16	1.19	HD 123765	S
1917	Cuyo A	24-June-2011 10:16	16	1.01	HD 342904	Sv
1917	Cuyo B	24-June-2011 10:46	24	1.01	HD 342904	Sr
1917	Cuyo C	24-June-2011 11:31	24	1.02	HD 342904	Sv/Sr
1917	Cuyo D	24-June-2011 12:11	24	1.05	HD 342904	Sr
1917	Cuyo E	24-June-2011 12:48	24	1.11	HD 342904	Sv/Sr
1917	Cuyo F	24-June-2011 13:29	24	1.22	HD 342904	Sr
1917	Cuyo	14-August-2011 06:59	48	1.01	L107–684	Sr
1943	Anteros	02-September-2010 11:30	32	1.15	SAO 107874	Sq
2102	Tantalus	04-July-2011 06:36	16	1.17	HD 234075	Sr
3103	Eger	24-June-2011 14:38	40	1.06	HD 206658	C/X INDET
3122	Florence	05-August-2010 15:26	10	1.03	L115–271	Sq/Q
3200	Phaethon	01-September-2009 13:53	64	1.20	SAO 3963	B
3552	Don Quixote	18-October-2009 05:37	20	1.54	L113–276	D
3554	Amun	01-February-2010 14:44	32	1.12	SAO 97431	D
4015	Wilson–Harrington	02-September-2009 05:02	48	1.40	HD 148116	C*
4055	Magellan	01-September-2010 05:13	32	1.06	HD 156486	V
4283	Cuno	19-October-2011 12:17	32	1.07	HD 16397	Sq/Q
5143	Heracles	27-September-2011 12:58	32	1.04	HD 275948	Q
5587	1990 SB	28-January-2012 14:25	48	1.25	SAO 157011	S/Sr
5626	1991 FE	02-September-2009 06:47	32	1.25	HD 190524	Sq
5646	1990 TR	01-November-2009 14:22	48	1.03	HD 60913	Q
5786	Talos	05-August-2010 11:18	72	1.02	L110–361 and L112–1333	Sq
6239	Minos	01-September-2010 11:49	16	1.12	HD 220685	Q/Sq
7358	Oze	13-August-2011 05:44	48	1.32	SAO 159708	S
7358	Oze	14-August-2011 05:47	48	1.32	L107–684	S
7358	Oze	17-September-2011 05:02	48	1.39	L110–361	S
7822	1991 CS	06-Mar-2010 05:37	48	1.09	HD 288180	S*
8566	1996 EN	02-September-2009 14:58	32	1.13	HD 30947	V
8567	1996 HW1	26-September-2011 15:11	16	1.02	HD 247554	Q
11066	Sigurd	19-February-2010 12:32	48	1.10	HD 129290	Sr
12711	Tukmit	01-September-2009 05:07	48	1.25	BD + 12 2836	Q
12923	Zephyr	04-April-2010 12:19	64	1.19	HD 125982	S
16834	1997 WU22	01-September-2009 12:24	48	1.14	SAO 127422	Sq
17274	2000 LC16	01-September-2009 09:07	16	1.05	HD 205027	D
18882	1999 YN4	27-December-2010 07:52	32	1.33	SAO 13263	Sr
19764	2000 NF5	27-September-2010 09:32	32	1.04	SAO 109095	Sq
20086	1994 LW	24-June-2011 08:29	44	1.18	HD 133600	C/X INDET
21088	1992 BL2	19-February-2010 08:06	64	1.20	HD 70996	Q
23187	2000 PN9	01-September-2010 09:04	80	1.04	HD 206658	Sq
24761	Ahau	06-January-2010 15:07	16	1.20	HD 96995	C/X INDET
27346	2000 DN8	01-February-2010 08:50	48	1.25	HD 43713	Q
36284	2000 DM8	02-February-2011 12:26	32	1.03	HD 249566 and HD 89179	Sq
39572	1993 DQ1	17-September-2011 09:40	80	1.30	L113–276	Q
52750	1998 KK17	19-Mar-2010 14:54	32	1.27	HD 175470	V
53789	2000 ED104	27-September-2010 05:22	80	1.14	SA 115–271 and SAO 86827	Sq
54789	2001 MZ7	01-February-2010 10:51	16	1.05	SAO 97431	C/X INDET
54789	2001 MZ7	19-February-2010 07:21	16	1.11	SAO 60533	C/X INDET
65679	1989 UQ	15-October-2010 08:19	32	1.13	HD 10488	C/Cb
68216	2001 CV26	19-February-2010 14:03	56	1.01	HD 129290	Sq
68216	2001 CV26	07-Mar-2010 11:47	32	1.06	HD 123760	Sq

Table 1 (*continued*)

Number	Name	UT	T_{int}	Airmass	Standard	Taxonomic type
68216	2001 CV26	19-Mar-2010 10:55	32	1.03	HD 115692	S/Sq
68350	2001 MK3	02-February-2011 05:25	72	1.15	HD 23925	S/Sr
85839	1998 YO4	19-February-2010 11:32	32	1.02	HD 96657	Q
86067	1999 RM28	01-February-2010 13:22	32	1.11	HD 87776	Q
88254	2001 FM129	04-April-2010 09:22	32	1.36	HD 82410	Q
96590	1998 XB	15-December-2010 10:16	24	1.09	Hya 64	Sq
100926	1998 MQ	15-October-2010 11:25	24	1.40	SAO 40380	Q
136617	1994 CC	18-October-2009 11:49	80	1.12	L93–101 and L98–978	Sa
137032	1998 UO1	15-October-2010 05:06	32	1.02	SAO 89822	Sq
137062	1998 WM	15-October-2010 09:23	64	1.20	HD 12264	Sq
137084	1998 XS16	02-January-2011 08:09	48	1.05	HD 42160	S
137084	1998 XS16	03-January-2011 07:10	32	1.16	HD 42160	S
137125	1999 CT3	02-February-2011 13:24	84	1.25	HD 92670	Q
137170	1999 HF1	01-May-2011 12:32	16	1.23	HD 177780	C/X INDET
137671	1999 XP35	28-December-2011 10:57	48	1.16	SA 98–978	S
138883	2000 YL29	02-September-2009 14:03	32	1.06	SAO 55805	Q
138911	2001 AE2	28-January-2012 09:26	92	1.05	SAO 97431	S
141498	2002 EZ16	05-December-2010 09:40	32	1.24	HD 30518	Sq
141498	2002 EZ16	12-December-2010 06:55	68	1.08	L93–101	Sq
143381	2003 BC21	27-September-2010 08:00	48	1.05	SAO 127304	Sr/S
152558	1990 SA	01-September-2010 11:19	16	1.02	SAO 90986	Sq/Q
152563	1992 BF	02-February-2011 07:29	72	1.09	HD 249566	K/C/X/ INDET
152931	2000 EA107	07-Mar-2010 13:13	48	1.22	HD 144423	Q
153814	2001 WN5	15-October-2010 06:24	48	1.11	HD 200565	K/L/Sq INDET
153842	2001 XT30	05-December-2010 10:46	80	1.07	HD 288029	C/X INDET
154029	2002 CY46	01-September-2010 12:23	92	1.01	HD 14786	S
159402	1999 AP10	01-September-2009 09:49	16	1.32	HD 216298	Sq
162998	2001 SK162	19-February-2010 05:27	52	1.10	HD 285295	D
163132	2002 CU11	07-Mar-2010 10:23	48	1.29	HD 77066	C/X INDET
163243	2002 FB3	04-April-2010 05:10	64	1.18	HD 296688	Q
163697	2003 EF54	02-September-2009 10:01	48	1.13	SAO 107874	Q
164121	2003 YT1	18-October-2009 13:55	28	1.09	L93–101 and L98–978	V
198856	2005 LR3	12-December-2010 04:50	80	1.15	L115–271	Sq
198856	2005 LR3	16-December-2010 05:58	48	1.11	L115–271	Q
207945	1991 JW	15-December-2010 05:26	72	1.17	L115–271	Q
207945	1991 JW	16-December-2010 04:34	64	1.06	L115–271	Q
214088	2004 JN13	06-January-2010 04:51	48	1.34	L115–271	Sq
218863	2006 WO127	18-October-2009 10:23	64	1.14	L93–101 and L98–978	Sq
219071	1997 US9	05-December-2010 07:41	64	1.34	HD 16472	Q
220124	2002 TE66 A	04-April-2010 10:44	8	1.03	HD 124019	Sq/Q
220124	2002 TE66 B	04-April-2010 14:17	16	1.30	HD 124019	Sq
247517	2002 QY6	05-August-2010 06:25	112	1.18	L110–361 and L112–1333	Sr
265187	2003 YS117	02-February-2011 09:58	88	1.15	HD 68972	Q
275792	2001 QH142	27-January-2012 10:49	136	1.01	L102–1081	C/X INDET
297418	2000 SP43	17-September-2011 14:47	36	1.04	Hya 64	V
347813	2002 NP1	02-September-2009 08:09	48	1.03	HD 199268	Q
	2000 CO101	04-April-2010 07:20	64	1.19	SAO 117128	C/X/T INDET
	2000 TJ1	27-September-2010 10:38	82	1.03	SA 115–271 and HD 5294	Sq
	2001 HC	04-April-2010 14:55	32	1.07	HD 125982	Sq
	2002 OS4	02-January-2011 06:07	64	1.21	SAO 39637	Sr
	2002 RQ25	02-September-2009 12:35	48	1.36	HD 5078	C/X INDET
	2005 MC	06-January-2010 14:18	16	1.25	HD 73668	Sr

2.3. Taxonomic classification

Taxonomic classifications of all 340 observations from both our ExploreNEOs survey and the MIT Joint Campaign determined from the Bus–DeMeo online taxonomic classifier[3] (DeMeo et al., 2009) are presented in Tables 1 and 2. We use the definitions of the complexes adopted by Thomas et al. (2011) and defined in Binzel et al. (2004c).

The online classification system only returns a definitive classification when a spectrum contains visible and near-infrared data. This is the case for a subset of the MIT Joint Campaign data. For all near-infrared only observations (those without visible spectra), the classification system returns a variety of possible subclasses. The additional absorption features and slope information contained in the visible wavelength region are vital to non-ambiguous classification, especially for the relatively featureless C- and X-complexes. DeMeo et al. (2009) show that the lack of visible wave-

length data allow certain classes to occupy the same principal component space. This prevents the data from being formally classified by principal component analysis, and all possible types are returned by the system. Some of these objects can be classified if the presence or absence of weak absorption features or small spectral variations typical to the potential subclasses are taken into account. These features are too small to be distinguished in principal component space and too small to affect the residuals between the input spectrum and the class average spectrum, but are indicative of certain classifications.

For all near-infrared only spectra, we compare the object's spectrum with the average spectra of the possible subclasses. Potential classifications are ruled out when the shapes, slopes, and/or residuals of the object in question are not consistent with the average subclass spectra. For most objects, this examination reveals the most likely or two most likely subclass classifications for the object. Two subclass classifications are given only if the two subclasses are within the same taxonomic complex. If several potential subclass classifications within a single complex are possible

---

Table 2
Table of ExploreNEOs spectra from the MIT-UH-IRTF Joint Campaign for NEO Spectral Reconnaissance. The table includes object number, name, the file name from the MIT survey catalog (smass.mit.edu), the UT date of observation, and the taxonomic classification.

Number	Name	File name	UT date	Taxonomic type
433	Eros	a000433.sp15	17-June-02	Sw
433	Eros	a000433.sp16	17-August-02	Sw
433	Eros	a000433.sp17	16-September-02	Sw
433	Eros	a000433.sp101	22-August-11	Sw
433	Eros	a000433.sp102	25-September-11	Sw
433	Eros	a000433.sp103	24-October-11	Sw
433	Eros	a000433.sp105	28-December-11	Sqw
1036	Ganymed	a001036.sp05	28-Mar-01	Sr
1036	Ganymed	a001036.sp51	03-June-06	Sr
1036	Ganymed	a001036.sp80	27-April-09	Sr
1036	Ganymed	a001036.sp103	24-October-11	S
1036	Ganymed	a001036.sp104	31-October-11	S
1627	Ivar	a001627.sp09	13-January-02	S
1627	Ivar	a001627.sp73	02-September-08	Sqw
1627	Ivar	a001627.sp74	02-October-08	Sw
1627	Ivar	a001627.sp76	03-December-08	S
1627	Ivar	a001627.sp77	27-January-09	Sr
1627	Ivar	a001627.sp88	22-February-10	Sw
1685	Toro	a001685.sp13	08-May-02	S
1685	Toro	a001685.sp17[a]	16-September-02	S
1864	Daedalus	a001864.sp05	29-Mar-01	Sq
1865	Cerberus	a001865.sp75	31-October-08	S
1866	Sisyphus	a001866.sp56	21-November-06	Sw
1916	Boreas	a001916.sp07	14-August-01	Sw
1917	Cuyo	a001917.sp72	07-July-08	Sv
1943	Anteros	a001943.sp09	12-January-02	Sw
1943	Anteros	a001943.sp103	24-October-11	S
1980	Tezcatlipoca	a001980.sp55	25-October-06	Sw
2212	Hephaistos	a002212.sp57[a]	22-December-06	Sq
3102	Krok	a003102.sp02	09-October-00	Sqw
3103	Eger	a003103.sp06	21-June-01	Xe
3199	Nefertiti	a003199.sp03	30-January-01	NO TAX MATCH
3199	Nefertiti	a003199.sp36	03-Mar-05	K
3200	Phaethon	a003200.sp19	27-October-02	NO TAX MATCH
3200	Phaethon	a003200.sp34	10-December-04	B
3552	Don Quixote	a003552.sp85	25-October-09	D
3554	Amun	a003554.sp78[a]	02-Mar-09	C/X INDET
3554	Amun	a003554.sp88[a]	23-February-10	D
3554	Amun	a003554.sp89[a]	16-Mar-10	D
3554	Amun	a003554.sp98[a]	05-April-11	D
3671	Dionysus	a003671.sp91	10-May-10	C/X INDET
3691	Bede	a003691.sp68	10-Mar-08	Cgh
4015	Wilson–Harrington	a004015.sp81[a]	22-June-09	B
4055	Magellan	a004055.sp38	11-April-05	V
4183	Cuno	a004183.sp103	24-October-11	Q
4544	Xanthus	a004544.sp58[a]	21-January-07	Sq/Q
4660	Nereus	a004660.6	15-Mar-02	X*
5011	Ptah	a005011.sp56[a]	21-November-06	Q
5131	1990 BG	a005131.sp67	15-January-08	Sq
5131	1990 BG	a005131.sp87	17-January-10	Sqw
5143	Heracles	a005143.sp55	25-October-06	Q
5332	1990 DA	a005332.sp47[a]	13-November-05	Sr/S
5496	1973 NA	a005496.sp96[a]	06-January-11	C/X INDET
5587	1990 SB	a005587.sp05	28-Mar-01	Sr
5604	1992 FE	a005604.sp05	29-Mar-01	V
5604	1992 FE	a005604.sp80	27-April-09	V
5620	Jasonwheeler	a005620.sp81[a]	22-June-09	K
5626	1991 FE	a005626.sp84	20-September-09	S
5645	1990 SP	a005645.sp12[a]	14-April-02	C/X/T INDET
5653	Camarillo	a005653.sp35[a]	08-January-05	S/Sr
5693	1993 EA	a005693.sp58[a]	21-January-07	Sq
5786	Talos	a005786.sp08[a]	23-August-01	Sq/Q
6047	1991 TB1	a006047.sp45	08-October-05	S
6239	Minos	a006239.sp93	07-September-10	Sq
6455	1992 HE	a006455.sp11	15-Mar-02	Srw
6455	1992 HE	a006455.sp19	28-October-02	Srw
6455	1992 HE	a006455.sp107	21-April-12	Sqw
7350	1993 VA	a007350.sp30[a]	15-September-04	C/X INDET
7350	1993 VA	a007350.sp39[a]	17-April-05	C/X INDET
7358	Oze	a007358.sp100	06-June-11	Sq
8567	1996 HW1	a008567.sp44[a]	04-September-05	Q
8567	1996 HW1	a008567.sp48[a]	22-November-05	Q
8567	1996 HW1	a008567.sp73	02-September-08	Q

Table 2 (*continued*)

Number	Name	File name	UT date	Taxonomic type
8567	1996 HW1	a008567.sp74[a]	02-October-08	Sq
8567	1996 HW1	a008567.sp104[a]	31-October-11	Q
10115	1992 SK	a010115.sp55[a]	24-October-06	Sq/S
10145	1994 CK1	au1994ck1.sp105[a]	30-December-11	S
11066	Sigurd	a011066.sp88	22-February-10	S
11398	1998 YP11	a011398.sp68	10-Mar-08	Sr
11885	1990 SS	a011885.sp98[a]	05-April-11	CLASSIFIER INDET
12923	Zephyr	a012923.sp92[a]	11-July-10	S
14402	1991 DB	a014402.sp78	02-Mar-09	Ch
15745	1991 PM5	a015745.sp82	07-August-09	S
16834	1997 WU22	a016834.sp77	27-January-09	S
16834	1997 WU22	a016834.sp84	20-September-09	S
17274	2000 LC16	a017274.sp02	10-October-00	D
17274	2000 LC16	a017274.sp83	24-August-09	CLASSIFIER INDET[b]
19764	2000 NF5	a019764.sp93[a]	06-September-10	Sq
20086	1994 LW	a020086.sp100[a]	07-June-11	C/Cb
20790	2000 SE45	a020790.sp03	29-January-01	S
21088	1992 BL2	au1992BL2.sp03[a]	30-January-01	Q
22753	1998 WT	a022753.sp19[a]	27-October-02	S/Sq
22753	1998 WT	a022753.sp36[a]	03-Mar-05	Sq
23183	2000 OY21	a023183.sp49[a]	30-January-06	Sq/Q
23187	2000 PN9	a023187.sp05[a]	28-Mar-01	S/Sq
23187	2000 PN9	a023187.sp98[a]	05-April-11	Sq/Q
24761	Ahau	a024761.sp87[a]	17-January-10	C/X INDET
25143	Itokawa	a025143.5	19-February-01 and 28-Mar-01	Sqw
25916	2001 CP44	a025916.sp55[a]	24-October-06	Sq/Q
25916	2001 CP44	a025916.sp93[a]	07-September-10	Sq/Q
31669	1999 JT6	a031669.sp12[a]	15-April-02	Q
35107	1991 VH	a035107.sp20	27-December-02	Sq
35107	1991 VH	a035107.sp71	11-June-08	Sq
36284	2000 DM8	a036284.sp11	16-Mar-02	Sq
36284	2000 DM8	a036284.sp97	07-February-11	NO TAX MATCH
39572	1993 DQ1	a039572.sp73[a]	02-September-08	Q
52387	1993 OM7	au1993OM7.sp20[a]	27-December-02	Sr
52750	1998 KK17	a052750.sp30[a]	15-September-04	V
52768	1998 OR2	a052768.sp79[a]	30-Mar-09	L
53430	1999 TY16	a053430.sp76[a]	03-December-08	Sr
53435	1999 VM40	a053435.sp55	25-October-06	Srw
53789	2000 ED104	au2000ED104.sp17[a]	15-September-02	S
54690	2001EB	au2001EB.sp05	28-Mar-01	S
54789	2001 MZ7	a054789.sp21[a]	16-Mar-03	C/X INDET
54789	2001 MZ7	a054789.sp87[a]	17-January-10	C/X INDET
54789	2001 MZ7	a054789.sp89[a]	16-Mar-10	C/X INDET
65679	1989 UQ	a065679.sp94	13-October-10	C
66251	1999 GJ2	a066251.sp44[a]	05-September-05	Q
66251	1999 GJ2	a066251.sp45[a]	08-October-05	Q
66251	1999 GJ2	a066251.sp46[a]	31-October-05	Q
68216	2001 CV26	a068216.sp89[a]	16-Mar-10	Sq
68359	2001 OZ13	a068359.sp67[a]	16-January-08	Sq
69230	Hermes	a069230.9[a]	16-October-03	Sq
85709	1998 SG36	a085709.sp50[a]	30-April-06	S/Sr
85818	1998 XM4	a085818.sp91	10-May-10	Srw
85839	1998 YO4	a085839.sp89[a]	16-Mar-10	Sq/Q
85989	1999 JD6	a085989.sp92	12-July-10	K
86324	1999 WA2	a086324.sp67[a]	16-January-08	Sr/S
86667	2000 FO10	a086667.sp107[a]	21-April-12	Sq
87684	2000 SY2	au2000SY2.sp30[a]	15-September-04	Q
88254	2001 FM129	a088254.sp89[a]	17-Mar-10	Sq
89355	2001 VS78	au2001VS78.sp11[a]	16-Mar-02	Sr
89355	2001 VS78	au2001VS78.sp12	15-April-02	Sr
90367	2003 LC5	au2003LC5.sp23[a]	05-July-03	C/X/T INDET
96590	1998 XB	a096590.sp96[a]	06-January-11	Q/Sq
99799	2002 LJ3	a099799.sp105[a]	30-December-11	Sq
99907	1989 VA	au1989VA.sp19	27-October-02	Sr
99907	1989 VA	a099907.sp65[a]	11-November-07	S/Sr
99935	2002 AV4	a099935.sp67[a]	16-January-08	B
100926	1998 MQ	a100926.sp94	14-October-10	Sqw
108519	2001 LF	au2001LF.sp23[a]	05-July-03	C
136564	1977 VA	au1977VA.sp44[a]	04-September-05	C/X INDET
137032	1998 UO1	au1998UO1.sp19[a]	27-October-02	S/Sr
137032	1998 UO1	a137032.sp74[a]	02-October-08	Sq/Q
137062	1998 WM	au1998WM.sp19	27-October-02	Sr
137170	1999 HF1	au1999HF1.sp13[a]	07-May-02	C/X INDET
137170	1999 HF1	au1999HF1.sp38[a]	11-April-05	C/X INDET
137170	1999 HF1	a137170.sp98[a]	05-April-11	C/X INDET

Table 2 (*continued*)

Number	Name	File name	UT date	Taxonomic type
137671	1999 XP35	au1999xp35.sp105[a]	30-December-11	S/Sr
137924	2000 BD19	au2000BD19.sp03[a]	29-January-01	V
138258	2000 GD2	au2000GD2.sp11	15-Mar-02	Sq
138883	2000 YL29	a138883.sp84[a]	20-September-09	Q
141052	2001 XR1	a141052.sp77	27-January-09	Sq
141432	2002 CQ11	a141432.sp99[a]	30-April-11	S
143651	2003 QO104	a143651.sp79[a]	30-Mar-09	Sq/Q
143651	2003 QO104	a143651.sp80	27-April-09	Q
144900	2004 VG64	au2004VG64.sp46[a]	31-October-05	Sq
144922	2005 CK38	au2005CK38.sp37[a]	08-Mar-05	Sq
152558	1990 SA	a152558.sp93[a]	07-September-10	Sq
152931	2000 EA107	a152931.sp89	16-Mar-10	Q
153219	2000 YM29	au2000YM29.sp58[a]	21-January-07	C/X INDET
153814	2001 WN5	a153814.sp94[a]	12-October-10	NO TAX MATCH[b]
154029	2002 CY46	a154029.sp93[a]	06-September-10	S
154244	2002 KL6	a154244.sp81[a]	21-June-09	Q
154715	2004 LB6	a154715.sp96[a]	06-January-11	Q
159402	1999 AP10	a159402.sp84[a]	20-September-09	Q
161989	Cacus	au1978CA.sp21[a]	16-Mar-03	Q
161998	1988 PA	a161998.sp92[a]	11-July-10	Q
162483	2000 PJ5	a162483.sp82[a]	08-August-09	Q
162900	2001 HG31	a162900.sp76[a]	03-December-08	Q
163001	2001 SE170	au2001SE170.sp33[a]	24-October-04	Sr
163243	2002 FB3	a163243.dm07[a]	20-Mar-12	Sq/Q
163697	2003 EF54	a163697.sp83[a]	24-August-09	Q
164202	2004 EW	au2004EW.sp36[a]	03-Mar-05	C/X INDET
164400	2005 GN59	a164400.sp73[a]	02-September-08	Q
175706	1996 FG3	a175706.sp79	30-Mar-09	C/Ch
175706	1996 FG3	a175706.sp80	27-April-09	B
175706	1996 FG3	a175706-obsA.sp105	30-December-11	C/Ch[b]
175706	1996 FG3	a175706-obsB.sp105	30-December-11	C/Ch[b]
175706	1996 FG3	a175706.dm04	1-December-11	NO TAX MATCH[b]
184266	2004 VW14	au2004VW14.sp69[a]	13-April-08	Q
200840	2001 XN254	au2001XN254.sp12	14-April-02	S
207945	1991 JW	a207945.sp80	27-April-09	Sq/Q
217796	2000 TO64	a217796.sp85[a]	25-October-09	Sr
217807	2000 XK44	a217807.sp85[a]	25-October-09	Q
218863	2006 WO127	a218863.sp89[a]	17-Mar-10	Sq
219071	1997 US9	a219071.sp104	31-October-11	Q
235756	2004 VC	au2004VC.sp79[a]	30-Mar-09	Sr/S
237442	1999 TA10	a237442.sp91[a]	10-May-10	S/Sr
241662	2000 KO44	a241662.sp92[a]	12-July-10	Sq/Q
248818	2006 SZ217	au2006SZ217.sp76[a]	03-December-08	Sr/S
256412	2007 BT2	au2007BT2.sp79[a]	30-Mar-09	C/Cb
257744	2000 AD205	au2000AD205.sp71[a]	11-June-08	K
260141	2004 QT24	au2004QT24.sp39[a]	18-April-05	Q
260141	2004 QT24	a260141.sp99[a]	30-April-11	Q
267729	2003 FC5	a267729.sp98[a]	05-April-11	S[c]
274138	2008 FU6	au2008FU6.sp98[a]	05-April-11	Sq
274138	2008 FU6	a274138.sp99[a]	30-April-11	Q
297418	2000 SP43	au2000SP43.sp02[a]	09-October-00	V
297418	2000 SP43	au2000sp43.sp102[a]	25-September-11	V
297418	2000 SP43	a297418.sp103[a]	23-October-11	V
301844	1990 UA	au1990ua.sp103[a]	24-October-11	Sq
302831	2003 FH	au2003fh.sp104[a]	31-October-11	Q
310442	2000 CH59	au2000CH59.sp67[a]	16-January-08	Sq
	2000 CO101	au2000co101.sp84	20-September-09	X
	2002 GO5	au2002GO5.sp12[a]	14-April-02	Sq
	2002 LV	au2002lv.sp81[a]	22-June-09	S/Sr
	2002 LV	au2002lv.sp82[a]	07-August-09	Sr
	2005 JE46	au2005JE46n1.sp47[a]	12-November-05	NO TAX MATCH[b]
	2005 JE46	au2005JE46n2.sp47[a]	13-November-05	NO TAX MATCH[b]
	2005 JE46	au2005JE46.sp48[a]	22-November-05	C/X/T INDET
	2005 UL5	au2005UL5.sp47[a]	13-November-05	Sq
	2007 RF5	au2007RF5.sp64[a]	02-October-07	Sq

[a] File does not include data at or below 0.75 μm. Observations were likely taken with the dichroic in the light path.
[b] Objects can not be formally classified due to the presence of a thermal tail.
[c] Object spectrum is very low resolution, only the complex can be identified. Possible classifications include members of the S-complex that are not S-subtypes.

following examination, the object is classified as belonging to that complex and the classification is marked as the complex letter followed by a star (e.g., S*).

If the potential subclass classifications span more than one taxonomic complex, then the object is labeled as being of indeterminate complex and is marked as such. This is particularly prevalent for objects of C- or X-complex. These complexes are often difficult to separate using only near-infrared data. The subtle visible wavelength spectral features are often crucial to making definitive assignments.

We include two labels that indicate an object has not been classified. If the classification system finds no matches in principal component space it returns "Classifier Indeterminate." If the classifier returns several options in principal component space that are not good matches to the spectrum, we do not classify the object and label it as "No Tax Match". These two labels appear in Tables 1 and 2. The problems classifying the "No Tax Match" spectra are caused primarily by thermal tails in the observations. Objects with thermal tails are labeled with a footnote and will be addressed in a future paper.

We do not allow any past classifications to influence the classifications presented in this paper. We compare our classifications with the taxonomic classes reported by the European Asteroid Research Node (EARN) Near-Earth Asteroid Database[4] and find that most classifications from our survey are the same class or are within the same taxonomic complex as previously determined taxonomic classifications. Five objects have distinctly different classifications in our survey than appear in EARN. Three of these objects, (24761) Ahau, (154029) 2002 CY46, and (297418) 2000 SP43, have EARN classifications from broadband photometry observations (Hicks et al., 2010; Somers et al., 2010; Ye, 2011). In these cases, the classification differences are likely due to the low resolution of broadband photometry. We classify (297418) 2000 SP43 as V-type with our ExploreNEOs survey spectrum and with the MIT Joint Campaign spectrum, but the classification on EARN is Sr-type. This discrepancy is likely due to the fact that the previous classification comes from a visible wavelength spectrum with no near-infrared data. The final classification discrepancy is (138911) 2001 AE2. This object was previously classified as T-type (Binzel et al., 2004b). The primitive, carbonaceous-like, material implied by the T-type classification and the low delta-V orbit of the object made this object a candidate for spacecraft exploration. The classification for our observation is S-complex. The S-complex classification suggests the thermal history and evolution of the object is different from the primitive material suggested by the previous T-type classification. The T-type classification was determined with visible wavelength data and our near-infrared S-complex classification is unambiguous. This suggests that (138911) 2001 AE2 is not an appropriate target for missions to primitive objects.

The spectrum for (433) Eros provides an example of a classification mismatch seen in our survey. Eros is often considered a quintessential S-type object; however the near-infrared spectra from the ExploreNEOs survey are formally classified in the Q-complex. Most of the MIT Joint Campaign observations are classified as S-complex. The key difference between the ExploreNEOs and MIT data is the availability of visible wavelength data. Our observations have no visible wavelength component included, while the MIT data uses visible wavelength data from Binzel et al. (2004c). We tested the robustness of these classifications by removing the visible data from the MIT spectra and appending it to each of the ExploreNEOs observations. We reclassified each of these alternate spectra. All MIT spectra with no visible wavelength component classified as Q-complex (either Q/Sq or Q), while most ExploreNEOs spectra with the visible wavelengths added classified as Sw (one classified as Sqw). This suggests that for near-infrared only observations, the Bus–DeMeo system returns more apparent Q-types than truly exist in the population. To address this problem quantitatively, visible spectra should be obtained for objects that have been classified as Q-complex using only near-infrared data. The classifications of the combined visible and near-infrared spectra can be compared against the classifications that use only near-infrared data.

2.4. Band parameters

For objects belonging to the S-, Q-, and V-complexes, which show large 1- and 2-μm absorption features, certain spectral band parameters can be used to infer composition (e.g., Burns et al., 1972; Adams, 1974; Gaffey et al., 1993; Dunn et al., 2010, 2013; Sanchez et al., 2012). These diagnostic absorption features are indicative of crystalline olivine and/or pyroxene. These minerals are common in various meteorites and asteroids. Olivine characteristically shows a broad absorption feature centered near 1.04–1.1 μm that is comprised of three overlapping bands, while pyroxenes show two broad absorption features centered at 0.9–1 μm and 1.9–2 μm. These features are caused by Fe^{2+} in the crystalline structure (e.g., Burns, 1993). For olivine–pyroxene mixtures, the wavelength of the 1 μm feature (Band I, BI) is a function of the relative abundances and compositions of olivine and pyroxene, while the wavelength of the 2 μm feature (Band II, BII) is a function of the pyroxene composition (e.g., Cloutis et al., 1986). The ratio of the area of Band II to Band I, or Band Area Ratio, is also a measure of the relative abundances of olivine and pyroxene. The depths of the bands can be used to investigate phase angle and space weathering effects under the assumption that mafic mineral abundance and particle size are the same (Sanchez et al., 2012; Reddy et al., 2012c). The band parameters that work best for this analysis are 1-μm Band Depth (BID), 1-μm Band Center (BIC), 2-μm Band Center (BIIC), and Band Area Ratio (BAR). For a very small number of taxonomically classified objects, the spectra are too noisy to calculate specific band parameters (e.g., (7358) Oze from 17 September 2011 does not have a BAR calculation). Calculated band parameters are shown in Tables 3 and 4.

All spectral band parameters are calculated based on the procedures described in Gaffey et al. (2002). For consistency between our two reduction techniques, all spectra are normalized to unity at 1-μm. We find no change between the parameters calculated before and after the normalization. The spectra are displayed using this normalization in the appendix (Fig. 9). All parameters are calculated using a spectrum that is smoothed with a boxcar average of a chosen width. This ensures that no individual point can influence the calculation. Most objects are smoothed with a width of 10 spectral points; however, some high signal-to-noise observations use a smaller value. To calculate band centers, a linear continuum between the two local maxima is calculated for each band. The linear continua are divided out of each band and the center is calculated by fitting a fourth-order polynomial to the bottom of the band and finding the local minimum. For some objects, the linear continuum that defines Band I will cut through the spectrum at slightly shorter wavelength than the local maximum at ~1.5 μm. This is defined as a "rollover" spectrum and in these cases a new local maximum is found from the continuum removed spectrum and the Band I Center calculation is repeated. For Band II, the red edge is nominally defined as the end of the spectrum. However, many spectra are noisy in this region and we remove some spectral points without changing the angle of the continuum in order to most accurately calculate the band centers and band areas.

Band center errors are calculated via a Monte Carlo method. We generate offsets to each individual point in a spectrum by multiplying the observational error by a normally distributed random number with a standard deviation of 1. Each spectrum is altered 20,000 times and a new band center is calculated for each trial. The band center error is defined as the standard deviation of these trials. We define a minimum band center error of 0.01 for all observations to account for uncertainties that have not been quantified. Calculated uncertainties are only reported if they exceed this minimum. Band II centers often have a much higher error than Band I centers. This is not only due to increased noise in Band II, but also to the shallowness and relative flatness of Band II, and therefore

Table 3

Calculated band parameters for our ExploreNEOs observations. In order to distinguish between multiple observations of the same object, the objects appear in the same order as they appear in Table 1. The table includes object number, name, phase angle (α), heliocentric distance (r), calculated temperature (in K), Band I Depth (BID), Band I Center (BIC), BIC error (σ_{BIC}), calculated BIC temperature correction (δ_{BIC}), corrected BIC (ΔBIC), Band II Center (BIIC), BIIC error (σ_{BIIC}), calculated BIIC temperature correction (δ_{BIIC}), corrected BIIC (ΔBIIC), Band Area Ratio (BAR), BAR error (σ_{BAR}), calculated BAR temperature correction (δ_{BAR}), corrected BAR (ΔBAR), Warm Spitzer diameter (D), positive diameter error (σ_{D^+}), negative diameter error (σ_{D^-}), Warm Spitzer albedo (p_V), positive albedo error ($\sigma_{p_V^+}$), and negative albedo error ($\sigma_{p_V^-}$).

Number	Name	α	r (AU)	T (K)	BID	BIC	σ_{BIC}	δ_{BIC}	ΔBIC	BIIC	σ_{BIIC}	δ_{BIIC}	ΔBIIC	BAR	σ_{BAR}	δ_{BAR}	ΔBAR	D	σ_{D^+}	σ_{D^-}	p_V	$\sigma_{p_V^+}$	$\sigma_{p_V^-}$
433	Eros	9.1	1.69	206	14.3	0.984	0.010	0.000	0.983	1.931	0.010	0.019	1.949	0.473	0.100	-0.075	0.398	22.30			0.23		
433	Eros	37.7	1.54	216	16.5	0.995	0.010	0.000	0.995	2.015	0.010	0.017	2.032	0.392	0.100	-0.068	0.324	22.30			0.23		
433	Eros	45.7	1.17	247	17.2	0.962	0.010	0.000	0.962	1.963	0.010	0.011	1.974	0.390	0.100	-0.045	0.345	22.30			0.23		
433	Eros	29.7	1.14	251	16.9	0.976	0.010	0.000	0.976	1.987	0.010	0.010	1.996	0.550	0.100	-0.042	0.507	22.30			0.23		
1036	Ganymed	6.3	3.76	137	16.2	0.921	0.010	-0.001	0.919	1.853	0.010	0.033	1.885	1.114	0.100	-0.125	0.989						
1036	Ganymed	39.2	1.54	214	18.2	0.929	0.010	0.000	0.929	1.908	0.010	0.017	1.925	1.156	0.100	-0.069	1.086						
1036	Ganymed	44.7	1.40	224	18.1	0.923	0.010	0.000	0.923	1.933	0.010	0.015	1.949	1.288	0.100	-0.062	1.226						
1036	Ganymed	46.1	1.25	237	14.1	0.925	0.010	0.000	0.925	1.950	0.010	0.013	1.963	1.575	0.100	-0.053	1.522						
1036	Ganymed	39.9	1.27	235	17.6	0.920	0.010	0.000	0.920	1.982	0.010	0.013	1.995	1.771	0.100	-0.054	1.717						
1036	Ganymed	12.8	1.35	228	15.3	0.922	0.010	0.000	0.922	1.953	0.010	0.014	1.967	1.489	0.100	-0.059	1.430						
1627	Ivar	2.0	2.38	181	12.6	1.025	0.010	-0.001	1.024	1.937	0.010	0.024	1.961	0.710	0.100	-0.093	0.616	10.03	3.27	2.77	0.09	0.12	0.05
1864	Daedalus	33.4	1.61	207	18.9	1.049	0.010	0.000	1.049	1.885	0.070	0.019	1.903	0.531	0.100	-0.075	0.457						
1865	Cerberus	40.3	1.31	209	20.0	0.930	0.010	0.000	0.930	1.945	0.010	0.018	1.963	0.605	0.100	-0.073	0.533	0.82	0.15	0.13	0.50	0.29	0.21
1866	Sisyphus	13.1	2.09	194	13.3	0.929	0.010	0.000	0.929	2.011	0.015	0.021	2.032	0.633	0.100	-0.084	0.549	12.94	4.57	3.66	0.07	0.09	0.04
1866	Sisyphus A	22.2	1.83	207	11.7	0.930	0.010	0.000	0.930	1.880	0.008	0.019	1.899	1.418	0.100	-0.074	1.344	12.94	4.57	3.66	0.07	0.09	0.04
1866	Sisyphus B	22.2	1.83	207	11.4	0.930	0.010	0.000	0.930	1.957	0.010	0.019	1.976	2.258	0.100	-0.074	2.184	12.94	4.57	3.66	0.07	0.09	0.04
1866	Sisyphus C	22.2	1.83	207	12.8	0.920	0.010	0.000	0.920	1.905	0.011	0.019	1.923	1.262	0.100	-0.074	1.188	12.94	4.57	3.66	0.07	0.09	0.04
1866	Sisyphus D	22.2	1.83	207	11.9	0.919	0.010	0.000	0.918	1.883	0.018	0.019	1.901	1.205	0.100	-0.074	1.131	12.94	4.57	3.66	0.07	0.09	0.04
1866	Sisyphus E	22.2	1.83	207	11.7	0.915	0.010	0.000	0.915	1.991	0.057	0.019	2.009	1.677	0.100	-0.074	1.603	12.94	4.57	3.66	0.07	0.09	0.04
1866	Sisyphus F	22.2	1.83	207	11.8	0.919	0.010	0.000	0.918	1.858	0.013	0.019	1.876	0.844	0.100	-0.074	0.770	12.94	4.57	3.66	0.07	0.09	0.04
1866	Sisyphus A	30.7	1.73	213	12.9	0.926	0.010	0.000	0.925	1.883	0.010	0.017	1.900	1.360	0.100	-0.070	1.290	12.94	4.57	3.66	0.07	0.09	0.04
1866	Sisyphus B	30.7	1.73	213	18.2	0.933	0.010	0.000	0.932	1.967	0.010	0.017	1.984	1.061	0.100	-0.070	0.991	12.94	4.57	3.66	0.07	0.09	0.04
1866	Sisyphus C	30.7	1.73	213	13.1	0.926	0.010	0.000	0.925	1.946	0.010	0.017	1.963	1.736	0.100	-0.070	1.667	12.94	4.57	3.66	0.07	0.09	0.04
1917	Cuyo A	24.8	1.01	263	28.3	0.922	0.010	0.001	0.922	1.889	0.010	0.007	1.897	2.458	0.100	-0.033	2.425	4.36	1.16	0.93	0.27	0.21	0.14
1917	Cuyo B	24.8	1.01	263	20.1	0.922	0.010	0.001	0.922	1.932	0.010	0.007	1.939	2.003	0.100	-0.033	1.969	4.36	1.16	0.93	0.27	0.21	0.14
1917	Cuyo C	24.8	1.01	263	21.7	0.922	0.010	0.001	0.922	1.925	0.010	0.007	1.932	1.355	0.100	-0.033	1.322	4.36	1.16	0.93	0.27	0.21	0.14
1917	Cuyo D	24.8	1.01	263	18.1	0.925	0.010	0.001	0.926	1.914	0.010	0.007	1.921	1.618	0.100	-0.033	1.585	4.36	1.16	0.93	0.27	0.21	0.14
1917	Cuyo E	24.8	1.01	263	23.6	0.922	0.010	0.001	0.922	1.907	0.033	0.007	1.914	1.429	0.100	-0.033	1.396	4.36	1.16	0.93	0.27	0.21	0.14
1917	Cuyo F	24.8	1.01	263	23.9	0.922	0.010	0.001	0.922	1.928	0.007	0.007	1.935	1.746	0.100	-0.033	1.713	4.36	1.16	0.93	0.27	0.21	0.14
1917	Cuyo	38.5	1.49	216	19.7	0.925	0.010	0.000	0.925	1.890	0.010	0.017	1.907	0.800	0.100	-0.068	0.733	4.36	1.16	0.93	0.27	0.21	0.14
1943	Anteros	16.7	1.51	223	9.8	0.987	0.010	0.000	0.987	1.993	0.010	0.015	2.008	0.694	0.100	-0.063	0.631	2.40	0.67	0.56	0.17	0.15	0.08
2102	Tantalus	61.0	1.15	247	23.1	0.916	0.010	0.000	0.917	1.891	0.014	0.011	1.902	1.383	0.100	-0.045	1.338						
3122	Florence	71.4	1.07	261	35.3	1.030	0.010	0.000	1.030	2.055	0.022	0.008	2.063	0.535	0.100	-0.035	0.499	4.25	1.22	0.90	0.21	0.20	0.10
4055	Magellan	54.2	1.23	230	53.2	0.935	0.010	0.003	0.938	1.951	0.010	0.010	1.962	2.289	0.100	0.000	2.289	2.46	0.53	0.41	0.36	0.27	0.17
4283	Cuno	11.7	2.11	191	18.7	0.980	0.010	-0.001	0.979	1.966	0.190	0.022	1.988	0.639	0.100	-0.086	0.554	5.44	1.20	1.11	0.10	0.10	0.05
5143	Heracles	28.1	1.87	184	23.5	1.017	0.010	-0.001	1.016	1.937	0.013	0.023	1.960	0.388	0.100	-0.091	0.297	3.39	0.60	0.55	0.40	0.22	0.16
5587	1990 SB	22.8	2.18	178	16.8	0.925	0.010	-0.001	0.925	1.904	0.025	0.024	1.928	1.426	0.100	-0.095	1.330	3.73	2.26	1.22	0.29	0.43	0.19
5626	1991 FE	22.6	1.62	216	12.7	0.943	0.010	0.000	0.943	1.924	0.031	0.017	1.941	0.656	0.100	-0.068	0.588	3.90	1.14	0.93	0.15	0.18	0.08
5646	1990 TR	33.8	1.69	169	28.4	1.025	0.010	-0.001	1.025	2.033	0.042	0.026	2.060	0.349	0.100	-0.102	0.247	2.09	0.45	0.36	0.66	0.42	0.29
5786	Talos	42.6	1.22	247	30.4	0.935	0.010	0.000	0.935	1.970	0.032	0.011	1.981	0.441	0.100	-0.046	0.395	1.29	0.32	0.27	0.17	0.15	0.08
6239	Minos	11.7	1.17	213	16.9	0.982	0.010	0.000	0.981	1.898	0.010	0.017	1.915	0.337	0.100	-0.070	0.267	0.47	0.13	0.08	0.57	0.37	0.29
7358	Oze	45.2	1.39	237	12.3	0.924	0.010	0.000	0.924	1.941	0.010	0.013	1.953	1.166	0.100	-0.052	1.114	6.17	2.03	1.62	0.08	0.10	0.04
7358	Oze	45.7	1.38	238	11.8	0.930	0.010	0.000	0.930	1.970	0.019	0.012	1.982	2.324	0.100	-0.052	2.272	6.17	2.03	1.62	0.08	0.10	0.04
7358	Oze	57.0	1.19	256	8.7	0.920	0.010	0.000	0.920	2.020	0.015	0.009	2.029					6.17	2.03	1.62	0.08	0.10	0.04
7822	1991 CS	60.9	1.12	249	19.1	0.908	0.010	0.000	0.909	1.977	0.029	0.010	1.987	0.982	0.100	-0.044	0.938	0.84	0.16	0.13	0.28	0.18	0.12
8566	1996 EN	79.5	1.03	258	51.0	0.950	0.010	0.002	0.952	1.993	0.010	0.006	1.999	1.754	0.100	0.000	1.754	1.25	0.26	0.22	0.30	0.22	0.14
8567	1996 HW1	56.2	1.20	239	17.7	1.002	0.010	0.000	1.002	2.020	0.036	0.012	2.032	0.587	0.100	-0.051	0.536						
11066	Sigurd	17.4	1.65	197	17.3	0.924	0.010	0.000	0.923	1.954	0.010	0.021	1.975	1.187	0.100	-0.081	1.105	1.98	0.45	0.38	0.38	0.31	0.18
12711	Tukmit	80.1	0.97	275	22.1	0.978	0.010	0.001	0.979	1.965	0.224	0.005	1.970	0.332	0.100	-0.025	0.307	1.95	0.40	0.34	0.19	0.14	0.09
12923	Zephyr	12.9	1.79	202	12.2	0.942	0.010	0.000	0.942	1.969	0.091	0.020	1.989	1.162	0.100	-0.078	1.084	1.82	0.42	0.34	0.20	0.16	0.09
16834	1997 WU22	33.6	1.48	204	14.8	0.961	0.010	0.000	0.961	1.969	0.010	0.019	1.988	0.552	0.100	-0.077	0.476	1.50	0.32	0.26	0.43	0.28	0.20
18882	1999 YN4	22.7	1.58	216	17.9	0.911	0.010	0.000	0.911	1.987	0.224	0.017	2.004	1.813	0.100	-0.068	1.746	1.74	0.47	0.36	0.18	0.15	0.09

Table 3 (*continued*)

Number	Name	α	r (AU)	T (K)	BID	BIC	σ_{BIC}	δ_{BIC}	ΔBIC	BIIC	σ_{BIIC}	δ_{BIIC}	ΔBIIC	BAR	σ_{BAR}	δ_{BAR}	ΔBAR	D	σ_{D^+}	σ_{D^-}	p_V	σ_{pV^+}	σ_{pV^-}
19764	2000 NF5	2.4	1.59	210	15.2	0.971	0.010	0.000	0.971	1.996	0.010	0.018	2.014	0.469	0.100	−0.072	0.397	1.67	0.43	0.37	0.26	0.23	0.14
21088	1992 BL2	15.7	2.11	182	18.6	1.048	0.010	−0.001	1.048	2.072	0.135	0.024	2.096	0.330	0.100	−0.092	0.238	3.44	1.10	0.86	0.26	0.32	0.14
23187	2000 PN9	12.9	1.90	196	17.2	1.032	0.010	0.000	1.031	1.933	0.228	0.021	1.954	0.728	0.100	−0.082	0.646	1.84	0.37	0.35	0.20	0.15	0.10
27346	2000 DN8	31.2	1.40	229	13.0	1.028	0.010	0.000	1.028	1.988	0.022	0.014	2.002	0.415	0.100	−0.059	0.356	1.93	0.43	0.39	0.19	0.17	0.09
36284	2000 DM8	11.0	1.78	204	20.9	1.018	0.010	0.000	1.018	1.942	0.017	0.019	1.961	0.367	0.100	−0.077	0.291	3.08	0.72	0.55	0.19	0.16	0.09
39572	1993 DQ1	38.7	1.34	227	16.4	0.985	0.010	0.000	0.985	1.990	0.011	0.015	2.005	0.669	0.100	−0.060	0.609						
52750	1998 KK17	85.1	0.96	250	47.1	0.939	0.010	0.002	0.941	1.928	0.050	0.007	1.935	1.339	0.100	0.000	1.339	1.03	0.17	0.16	0.46	0.25	0.20
53789	2000 ED104	61.3	1.12	244	12.7	0.949	0.010	0.000	0.949	2.033	0.019	0.011	2.044	0.813	0.100	−0.047	0.766	0.84	0.19	0.17	0.32	0.24	0.15
68216	2001 CV26	46.3	1.24	238	15.8	0.934	0.010	0.000	0.934	2.082	0.039	0.012	2.095	0.588	0.100	−0.052	0.536	1.39	0.37	0.29	0.26	0.21	0.13
68216	2001 CV26	30.9	1.32	231	15.6	0.960	0.010	0.000	0.960	1.885	0.010	0.014	1.899	0.484	0.100	−0.057	0.427	1.39	0.37	0.29	0.26	0.21	0.13
68216	2001 CV26	17.0	1.38	226	14.4	0.949	0.010	0.000	0.949	1.938	0.010	0.015	1.952	0.808	0.100	−0.060	0.747	1.39	0.37	0.29	0.26	0.21	0.13
68350	2001 MK3	51.1	1.26	237	14.0	0.918	0.010	0.000	0.918	2.027	0.058	0.013	2.040	2.094	0.100	−0.052	2.042	1.71	0.37	0.33	0.25	0.17	0.10
85839	1998 YO4	16.1	1.46	226	21.4	1.001	0.010	0.000	1.001	2.049	0.012	0.015	2.064	0.332	0.100	−0.061	0.271	1.81	0.41	0.40	0.17	0.16	0.08
86067	1999 RM28	11.8	1.40	231	18.9	0.966	0.010	0.000	0.966	1.957	0.011	0.014	1.971	0.495	0.100	−0.057	0.438	1.58	0.44	0.36	0.17	0.16	0.09
88254	2001 FM129	43.0	1.20	236	22.3	0.976	0.010	0.000	0.976	2.034	0.170	0.013	2.046	0.657	0.100	−0.053	0.604	0.81	0.17	0.14	0.33	0.23	0.14
96590	1998 XB	19.2	1.21	252	19.0	1.000	0.010	0.000	1.000	2.025	0.010	0.010	2.035	0.606	0.100	−0.042	0.564	2.29	0.47	0.42	0.11	0.09	0.05
100926	1998 MQ	56.2	1.10	243	21.6	0.945	0.010	0.000	0.945	2.019	0.023	0.011	2.031	0.612	0.100	−0.048	0.564	1.08	0.23	0.19	0.37	0.22	0.16
136617	1994 CC	13.2	1.41	219	29.9	1.065	0.010	0.000	1.065	2.190	0.154	0.016	2.206	0.407	0.100	−0.066	0.341	0.67	0.11	0.12	0.32	0.22	0.14
137032	1998 UO1	45.3	1.16	256	22.8	0.967	0.010	0.000	0.968	1.992	0.010	0.009	2.001	0.524	0.100	−0.039	0.485	1.66	0.37	0.35	0.13	0.11	0.06
137062	1998 WM	14.8	1.58	207	24.3	0.931	0.010	0.000	0.930	1.941	0.221	0.019	1.959	0.781	0.100	−0.075	0.706	1.13	0.28	0.23	0.32	0.23	0.14
137084	1998 XS16	5.0	1.80	195	17.3	0.909	0.010	0.000	0.908	1.872	0.186	0.021	1.893	1.096	0.125	−0.083	1.013	1.36	0.28	0.29	0.30	0.23	0.14
137084	1998 XS16	5.8	1.80	195	19.3	0.909	0.010	0.000	0.908	1.844	0.217	0.021	1.865	1.101	0.109	−0.083	1.018	1.36	0.28	0.29	0.30	0.23	0.14
137125	1999 CT3	18.2	1.40	223	21.5	1.038	0.010	0.000	1.038	1.994	0.179	0.015	2.009	0.743	0.100	−0.063	0.680	0.54	0.12	0.10	0.28	0.22	0.13
137671	1999 XP35	23.6	1.17	252	15.9	0.936	0.010	0.000	0.937	1.977	0.191	0.010	1.987	1.826	0.100	−0.041	1.785	0.60	0.17	0.13	0.17	0.16	0.08
138883	2000 YL29	58.4	1.11	256	23.5	0.957	0.010	0.000	0.958	1.907	0.010	0.009	1.915	0.424	0.100	−0.038	0.385	1.40	0.30	0.30	0.19	0.17	0.09
138911	2001 AE2	9.3	1.34	222	9.1	0.911	0.010	0.000	0.911	2.061	0.122	0.016	2.076	2.824	0.183	−0.064	2.760	0.35	0.08	0.07	0.35	0.24	0.15
141498	2002 EZ16	28.1	1.15	247	21.7	0.966	0.010	0.000	0.967	2.039	0.019	0.011	2.049	0.557	0.100	−0.045	0.512	0.59	0.11	0.09	0.25	0.18	0.11
141498	2002 EZ16	19.5	1.20	242	20.8	0.990	0.010	0.000	0.990	1.950	0.010	0.012	1.962	0.207	0.100	−0.049	0.158	0.59	0.11	0.09	0.25	0.18	0.11
143381	2003 BC21	20.2	1.46	212	16.9	0.924	0.010	0.000	0.924	1.924	0.010	0.018	1.941	1.008	0.100	−0.070	0.937	1.50	0.33	0.25	0.35	0.23	0.15
152558	1990 SA	27.4	1.28	232	7.9	0.970	0.010	0.000	0.970	2.005	0.011	0.014	2.019	1.169	0.100	−0.056	1.113						
152931	2000 EA107	48.4	1.28	232	22.8	1.010	0.010	0.000	1.010	1.910	0.280	0.014	1.923	0.339	0.100	−0.056	0.283						
154029	2002 CY46	52.9	1.10	261	12.1	0.934	0.010	0.001	0.934	1.944	0.010	0.008	1.951	1.511	0.100	−0.035	1.476	1.76	0.40	0.38	0.16	0.16	0.08
159402	1999 AP10	9.0	1.29	226	9.7	0.950	0.010	0.000	0.950	1.907	0.010	0.015	1.921	0.723	0.100	−0.060	0.663	1.22	0.25	0.22	0.35	0.24	0.16
163243	2002 FB3	56.2	1.20	238	26.3	0.939	0.010	0.000	0.939	1.913	0.218	0.012	1.926	0.354	0.100	−0.052	0.303	1.36	0.27	0.24	0.30	0.20	0.14
163697	2003 EF54	26.7	1.12	248	25.1	0.965	0.010	0.000	0.965	1.917	0.014	0.010	1.927	0.520	0.100	−0.044	0.476	0.25	0.04	0.04	0.29	0.20	0.12
164121	2003 YT1	68.7	1.05	252	57.1	0.935	0.010	0.002	0.937	1.950	0.010	0.007	1.957	1.594	0.100	0.000	1.594	1.37	0.28	0.24	0.34	0.23	0.15
198856	2005 LR3	52.7	1.16	253	21.2	0.995	0.010	0.000	0.995	1.940	0.236	0.009	1.949	0.258	0.100	−0.041	0.217	1.19	0.27	0.22	0.17	0.15	0.08
198856	2005 LR3	54.4	1.15	255	23.4	1.005	0.010	0.001	1.005	1.970	0.071	0.009	1.979	0.227	0.100	−0.040	0.188	1.19	0.27	0.22	0.17	0.15	0.08
207945	1991 JW	75.3	1.01	261	14.9	1.000	0.010	0.001	1.001	2.010	0.232	0.008	2.018	0.178	0.100	−0.035	0.143						
207945	1991 JW	74.5	1.01	261	18.5	0.990	0.010	0.001	0.991	1.945	0.024	0.008	1.953	0.358	0.100	−0.035	0.323						
214088	2004 JN13	62.6	1.03	261	18.8	0.980	0.010	0.001	0.981	1.955	0.161	0.008	1.963	0.601	0.100	−0.035	0.566	3.01	0.76	0.65	0.26	0.20	0.13
218863	2006 WO127	9.8	1.65	209	18.5	0.990	0.010	0.000	0.990	1.985	0.024	0.018	2.003	0.351	0.100	−0.073	0.278	1.69	0.43	0.38	0.22	0.18	0.10
219071	1997 US9	39.1	1.26	228	23.7	1.024	0.010	0.000	1.024	1.985	0.159	0.014	1.999	0.306	0.100	−0.059	0.248	0.79	0.15	0.13	0.35	0.22	0.15
220124	2002 TE66 A	30.5	1.14	235	20.1	0.976	0.010	0.000	0.976	2.020	0.176	0.013	2.033	0.339	0.100	−0.054	0.286	0.48	0.09	0.08	0.40	0.24	0.17
220124	2002 TE66 B	30.5	1.14	235	20.0	0.957	0.010	0.000	0.957	1.993	0.093	0.013	2.006	0.519	0.100	−0.054	0.465	0.48	0.09	0.08	0.40	0.24	0.17
247517	2002 QY6	51.7	1.10	253	24.0	0.925	0.010	0.000	0.925	1.890	0.010	0.009	1.899	1.453	0.100	−0.041	1.411						
265187	2003 YS117	13.8	1.41	212	24.6	0.972	0.010	0.000	0.972	1.956	0.072	0.018	1.973	0.531	0.100	−0.071	0.460	0.53	0.09	0.09	0.40	0.24	0.17
297418	2000 SP43	70.9	1.04	244	29.0	0.935	0.010	0.003	0.938	1.835	0.013	0.008	1.843	1.126	0.100	0.000	1.126						
347813	2002 NP1	24.1	1.34	228	17.0	0.961	0.010	0.000	0.961	1.969	0.015	0.014	1.984	0.293	0.100	−0.059	0.235	0.81	0.17	0.13	0.26	0.19	0.12
	2000 TJ1	19.5	1.21	236	22.4	0.946	0.010	0.000	0.946	1.927	0.010	0.013	1.940	0.619	0.100	−0.054	0.566	0.36	0.06	0.06	0.33	0.20	0.13
	2001 HC	60.6	1.08	252	22.1	0.968	0.010	0.000	0.968	1.986	0.166	0.010	1.996	0.287	0.100	−0.041	0.246						
	2002 OS4	28.9	1.26	232	19.8	0.912	0.010	0.001	0.912	2.001	0.092	0.014	2.015	1.903	0.100	−0.056	1.846	0.59	0.12	0.10	0.31	0.22	0.12
	2005 MC	20.9	1.32	236	18.4	0.915	0.010	0.000	0.916	2.005	0.036	0.013	2.017	1.876	0.100	−0.054	1.822	1.63	0.50	0.41	0.19	0.21	0.09

Table 4

Calculated band parameters for ExploreNEOs objects in the MIT–UH–IRTF Joint Campaign. As with Table 3, in order to distinguish between multiple observations of the same object the objects appear in the same order as they appear in Table 2. The table includes the same parameters as Table 3.

Number	Name	α	r (AU)	T (K)	BID	BIC	σ_{BIC}	δ_{BIC}	ΔBIC	BIIC	σ_{BIIC}	δ_{BIIC}	$\Delta BIIC$	BAR	σ_{BAR}	δ_{BAR}	ΔBAR	D	σ_{D^+}	σ_{D^-}	p_V	$\sigma_{p_V^+}$	$\sigma_{p_V^-}$
433	Eros	34.9	1.77	201	17.2	0.995	0.010	0.000	0.995	1.975	0.010	0.020	1.995	0.417	0.100	−0.078	0.339	22.30			0.23		
433	Eros	21.6	1.69	206	18.0	0.955	0.010	0.000	0.955	1.955	0.010	0.019	1.974	0.453	0.100	−0.075	0.378	22.30			0.23		
433	Eros	12.8	1.62	210	17.2	0.950	0.010	0.000	0.950	1.970	0.010	0.018	1.988	0.434	0.100	−0.072	0.362	22.30			0.23		
433	Eros	42.8	1.49	219	18.9	0.990	0.010	0.000	0.990	1.990	0.010	0.016	2.006	0.244	0.100	−0.065	0.179	22.30			0.23		
433	Eros	45.5	1.38	228	19.0	0.960	0.010	0.000	0.960	1.990	0.010	0.014	2.004	0.500	0.100	−0.059	0.440	22.30			0.23		
433	Eros	47.2	1.29	236	19.5	0.980	0.010	0.000	0.980	2.005	0.010	0.013	2.018	0.329	0.100	−0.053	0.276	22.30			0.23		
433	Eros	43.7	1.14	250	19.7	1.020	0.010	0.000	1.020	2.015	0.010	0.010	2.025	0.197	0.100	−0.043	0.154	22.30			0.23		
1036	Ganymed	5.0	3.97	133	16.6	0.910	0.010	−0.001	0.909	1.850	0.010	0.033	1.883	0.907	0.100	−0.128	0.779						
1036	Ganymed	15.7	3.00	153	17.9	0.915	0.010	−0.001	0.914	1.890	0.010	0.029	1.919	1.049	0.100	−0.114	0.936						
1036	Ganymed	13.2	4.07	131	18.0	0.915	0.010	−0.001	0.914	1.860	0.010	0.034	1.894	0.731	0.100	−0.129	0.602						
1036	Ganymed	6.1	1.37	226	17.0	0.925	0.010	0.000	0.925	1.925	0.010	0.015	1.940	0.750	0.100	−0.060	0.690						
1036	Ganymed	2.9	1.40	224	16.6	0.930	0.010	0.000	0.930	1.930	0.010	0.015	1.945	0.932	0.100	−0.062	0.869						
1627	Ivar	3.7	2.60	173	17.3	0.955	0.010	−0.001	0.954	1.970	0.011	0.025	1.995	0.596	0.100	−0.099	0.497	10.03	3.27	2.77	0.09	0.12	0.05
1627	Ivar	44.5	1.42	234	20.4	0.960	0.010	0.000	0.960	1.960	0.011	0.013	1.973	0.267	0.100	−0.054	0.213	10.03	3.27	2.77	0.09	0.12	0.05
1627	Ivar	31.0	1.58	222	20.6	0.950	0.010	0.000	0.950	1.970	0.007	0.016	1.986	0.262	0.100	−0.063	0.199	10.03	3.27	2.77	0.09	0.12	0.05
1627	Ivar	16.3	1.90	202	18.8	0.945	0.010	0.000	0.945	1.900	0.014	0.020	1.920	0.423	0.100	−0.078	0.345	10.03	3.27	2.77	0.09	0.12	0.05
1627	Ivar	26.9	2.15	190	21.5	0.950	0.010	−0.001	0.949	1.975	0.015	0.022	1.997	0.589	0.100	−0.086	0.503	10.03	3.27	2.77	0.09	0.12	0.05
1627	Ivar	2.2	2.37	181	17.2	0.950	0.010	−0.001	0.949	1.780	0.009	0.024	1.804	0.283	0.100	−0.093	0.190	10.03	3.27	2.77	0.09	0.12	0.05
1685	Toro	8.9	1.96	181	15.9	0.940	0.010	−0.001	0.939	2.045	0.090	0.024	2.069	0.324	0.100	−0.093	0.232	3.09	0.72	0.59	0.38	0.33	0.18
1685	Toro	31.2	1.65	198	10.2	1.015	0.010	0.000	1.015	2.050	0.092	0.020	2.070					3.09	0.72	0.59	0.38	0.33	0.18
1864	Daedalus	4.4	1.89	191	22.0	0.960	0.010	−0.001	0.959	1.915	0.033	0.022	1.937	0.238	0.100	−0.086	0.152	0.82	0.15	0.13	0.50	0.29	0.21
1865	Cerberus	20.2	1.41	202	17.7	0.925	0.010	0.000	0.925	1.890	0.049	0.020	1.910	0.484	0.100	−0.078	0.406	12.94	4.57	3.66	0.07	0.09	0.04
1866	Sisyphus	41.6	1.44	234	15.9	0.930	0.010	0.000	0.930	1.980	0.009	0.013	1.993	0.256	0.100	−0.055	0.202	3.24	0.78	0.71	0.20	0.17	0.11
1916	Boreas	38.2	1.27	240	16.3	0.955	0.010	0.000	0.955	1.985	0.010	0.012	1.997	0.461	0.100	−0.050	0.411	4.36	1.16	0.93	0.27	0.21	0.14
1917	Cuyo	47.6	1.37	226	21.0	0.940	0.010	0.000	0.940	1.860	0.008	0.015	1.875	1.213	0.100	−0.060	1.152						
1943	Anteros	14.4	1.46	226	11.3	0.940	0.010	0.000	0.940	2.025	0.032	0.015	2.040	0.424	0.100	−0.060	0.363	2.40	0.67	0.56	0.17	0.15	0.08
1943	Anteros	15.9	1.80	204	10.1	1.010	0.010	0.000	1.010	2.015	0.006	0.019	2.034	0.601	0.100	−0.077	0.525	2.40	0.67	0.56	0.17	0.15	0.08
1980	Tezcatlipoca	53.8	1.17	225	20.6	0.955	0.010	0.000	0.955	1.995	0.011	0.015	2.010	0.188	0.100	−0.061	0.127	3.14	0.80	0.60	0.47	0.43	0.24
2212	Hephaistos	14.2	1.81	209	13.5	1.010	0.010	0.000	1.010	1.995	0.010	0.018	2.013					9.02	3.13	2.49	0.06	0.08	0.03
3102	Krok	19.7	1.38	223	20.7	1.000	0.010	0.000	1.000	2.050	0.033	0.015	2.065	0.528	0.100	−0.063	0.465						
4055	Magellan	17.7	1.84	188	51.2	0.925	0.010	0.005	0.930	1.915	0.010	0.017	1.932	2.182	0.100	0.000	2.182	2.46	0.53	0.41	0.36	0.27	0.17
4183	Cuno	9.4	2.07	193	19.8	1.015	0.010	−0.001	1.014	1.925	0.021	0.021	1.946	0.264	0.100	−0.084	0.179	5.44	1.20	1.11	0.10	0.10	0.05
4544	Xanthus	50.5	1.18	234	12.4	0.930	0.010	0.000	0.930	1.940	0.162	0.013	1.953					0.85	0.16	0.14	0.37	0.23	0.16
5011	Ptah	63.2	1.10	265	18.0	0.965	0.010	0.001	0.966	1.995	0.020	0.007	2.002					1.54	0.42	0.39	0.11	0.11	0.05
5131	1990 BG	13.9	1.90	95	26.2	1.020	0.010	−0.002	1.018	2.020	0.032	0.041	2.061	0.278	0.100	−0.156	0.122	1.31	0.29	0.19	0.96	0.38	0.39
5131	1990 BG	22.6	1.41	110	26.6	1.040	0.010	−0.002	1.038	2.000	0.152	0.038	2.038	0.119	0.100	−0.144	−0.026	1.31	0.29	0.19	0.96	0.38	0.39
5143	Heracles	16.2	1.70	193	23.4	1.010	0.010	−0.001	1.009	1.960	0.016	0.021	1.981	0.232	0.100	−0.085	0.148	3.39	0.60	0.55	0.40	0.22	0.16
5332	1990 DA	56.1	1.18	242	12.9	0.935	0.010	0.000	0.935	1.950	0.010	0.012	1.962					3.73	2.26	1.22	0.29	0.43	0.19
5587	1990 SB	21.9	1.49	215	16.4	0.925	0.010	0.000	0.925	1.905	0.010	0.017	1.922	0.979	0.100	−0.068	0.911						
5604	1992 FE	28.1	1.26	188	48.3	0.925	0.010	0.005	0.930	1.925	0.010	0.017	1.942	1.960	0.100	0.000	1.960	0.85	0.10	0.11	0.71	0.32	0.23
5604	1992 FE	36.7	1.29	185	51.6	0.925	0.010	0.005	0.930	1.915	0.012	0.017	1.932	2.038	0.100	0.000	2.038	0.85	0.10	0.11	0.71	0.32	0.23
5626	1991 FE	33.8	1.51	223	15.1	0.930	0.010	0.000	0.930	1.955	0.012	0.015	1.970	0.559	0.100	−0.063	0.496	3.90	1.14	0.93	0.15	0.18	0.08
5653	Camarillo	30.3	1.30	222	11.0	0.925	0.010	0.000	0.925	1.980	0.011	0.016	1.996					1.74	0.45	0.34	0.39	0.37	0.19
5693	1993 EA	19.5	1.40	232	13.7	1.025	0.010	0.000	1.025	2.040	0.183	0.014	2.054					1.39	0.28	0.24	0.15	0.11	0.07
5786	Talos	16.3	1.41	230	16.1	0.960	0.010	0.000	0.960	1.990	0.023	0.014	2.004					1.29	0.32	0.27	0.17	0.15	0.08
6047	1991 TB1	20.3	1.39	162	14.7	0.930	0.010	−0.001	0.929	2.005	0.028	0.028	2.033	1.889	0.130	−0.107	1.782	0.55	0.10	0.08	0.80	0.44	0.35
6239	Minos	0.8	1.21	210	16.8	0.985	0.010	0.000	0.985	2.020	0.113	0.018	2.038	0.268	0.100	−0.072	0.196	0.47	0.13	0.08	0.57	0.37	0.29
6455	1992 HE	24.5	1.70	200	31.4	0.935	0.010	0.000	0.935	1.980	0.054	0.020	2.000	0.727	0.100	−0.079	0.648	3.96	1.72	1.10	0.31	0.42	0.18
6455	1992 HE	14.2	1.59	207	24.4	0.940	0.010	0.000	0.940	1.955	0.011	0.019	1.974	0.482	0.100	−0.075	0.407	3.96	1.72	1.10	0.31	0.42	0.18
6455	1992 HE	23.4	1.56	209	25.4	0.980	0.010	0.000	0.980	1.930	0.010	0.018	1.948	0.373	0.100	−0.073	0.300	3.96	1.72	1.10	0.31	0.42	0.18
7358	Oze	1.1	1.84	206	13.7	0.940	0.010	0.000	0.940	1.950	0.018	0.019	1.969	0.312	0.100	−0.075	0.237	6.17	2.03	1.62	0.08	0.10	0.04
8567	1996 HW1	55.8	1.19	243	14.7	1.015	0.010	0.000	1.015	2.005	0.010	0.011	2.016										
8567	1996 HW1	53.0	1.22	240	13.5	1.015	0.010	0.000	1.015	2.080	0.064	0.012	2.092										
8567	1996 HW1	27.1	1.13	249	17.9	0.995	0.010	0.000	0.995	1.955	0.086	0.010	1.965	0.246	0.100	−0.044	0.202						

Table 4 (continued)

Number	Name	α	r (AU)	T (K)	BID	BIC	σ_{BIC}	δ_{BIC}	ΔBIC	BIIC	σ_{BIIC}	δ_{BIIC}	ΔBIIC	BAR	σ_{BAR}	δ_{BAR}	ΔBAR	D	σ_{D^+}	σ_{D^-}	p_V	σ_{pV^+}	σ_{pV^-}
8567	1996 HW1	23.9	1.15	248	17.4	1.005	0.010	0.000	1.005	2.000	0.010	0.010	2.010					1.98	0.45	0.38	0.38	0.31	0.18
8567	1996 HW1	39.6	1.36	227	14.9	1.005	0.010	0.000	1.005	1.980	0.026	0.015	1.995					1.73	0.47	0.39	0.18	0.17	0.09
10145	1994 CK1	10.2	1.35	226	15.3	0.960	0.010	0.000	0.960	2.015	0.032	0.015	2.030					1.82	0.42	0.34	0.20	0.16	0.09
11066	Sigurd	16.2	1.66	196	14.0	0.925	0.010	0.000	0.925	1.900	0.005	0.021	1.921	0.915	0.100	−0.082	0.833	0.78	0.17	0.16	0.24	0.18	0.11
11398	1998 YP11	32.9	1.16	252	19.0	0.925	0.010	0.000	0.925	1.940	0.003	0.010	1.950	0.645	0.100	−0.042	0.603	1.50	0.32	0.26	0.43	0.28	0.20
12923	Zephyr	62.6	1.15	253	15.2	0.960	0.010	0.000	0.960	1.905	0.010	0.009	1.914					1.50	0.32	0.26	0.43	0.28	0.20
15745	1991 PM5	27.1	1.32	232	11.0	0.945	0.010	0.000	0.945	1.970	0.027	0.014	1.984	0.639	0.100	−0.056	0.583	1.67	0.43	0.37	0.26	0.23	0.14
16834	1997 WU22	27.8	1.35	214	11.3	1.020	0.010	0.000	1.020	1.955	0.039	0.017	1.972	2.428	0.100	−0.069	2.359	2.02	0.63	0.51	0.10	0.11	0.05
16834	1997 WU22	24.0	1.59	197	14.2	0.960	0.010	0.000	0.960	1.975	0.016	0.021	1.996	0.487	0.100	−0.082	0.406	3.44	1.10	0.86	0.26	0.32	0.14
19764	2000 NF5	18.4	1.48	218	17.6	1.010	0.010	0.000	1.010	1.975	0.010	0.016	1.991					0.74	0.14	0.12	0.27	0.17	0.11
20790	2000 SE45	13.3	1.26	248	12.9	0.945	0.010	0.000	0.945	1.975	0.010	0.010	1.985					0.74	0.14	0.12	0.27	0.17	0.11
21088	1992 BL2	7.6	2.10	183	14.2	1.040	0.010	−0.001	1.039	2.025	0.083	0.023	2.048	1.894	0.100	−0.044	1.849	0.74	0.11	0.10	0.92	0.39	0.39
22753	1998 WT	54.2	1.08	254	14.4	0.970	0.010	0.000	0.970	2.010	0.010	0.009	2.019					1.84	0.37	0.35	0.20	0.15	0.10
22753	1998 WT	44.5	1.05	257	15.4	1.000	0.010	0.000	1.000	1.965	0.010	0.009	1.974					1.84	0.37	0.35	0.20	0.15	0.10
23183	2000 OY21	32.6	1.26	134	20.7	1.025	0.010	−0.001	1.024	2.110	0.018	0.033	2.143										
23187	2000 PN9	50.8	1.22	245	14.5	1.025	0.010	0.000	1.025	2.060	0.033	0.011	2.071										
23187	2000 PN9	55.6	1.19	248	18.1	1.040	0.010	0.000	1.040	1.995	0.047	0.010	2.005										
25143	Itokawa	22.1046–69.3187	1.08	246	19.5	0.970	0.010	0.000	0.970	2.020	0.010	0.011	2.031	0.284	0.100	−0.046	0.238	0.32	0.05	0.04	0.36	0.22	0.15
25916	2001 CP44	12.4	2.22	181	10.5	1.020	0.010	−0.001	1.019	1.880	0.074	0.024	1.904					6.49	1.98	1.49	0.21	0.22	0.11
25916	2001 CP44	30.7	1.70	207	13.1	1.020	0.010	0.000	1.020	1.950	0.193	0.019	1.969					6.49	1.98	1.49	0.21	0.22	0.11
31669	1999 JT6	33.3	1.28	234	14.3	1.035	0.010	0.000	1.035	2.105	0.030	0.013	2.118										
35107	1991 VH	45.0	1.20	242	19.4	0.980	0.010	0.000	0.980	2.035	0.025	0.012	2.047	0.360	0.100	−0.049	0.311	1.09	0.22	0.19	0.26	0.20	0.11
35107	1991 VH	61.7	1.11	252	19.8	1.005	0.010	0.000	1.005	1.945	0.013	0.010	1.955	0.287	0.100	−0.042	0.245	1.09	0.22	0.19	0.26	0.20	0.11
36284	2000 DM8	40.3	1.37	231	17.0	0.985	0.018	0.000	0.985	2.075	0.166	0.014	2.089	0.452	0.111	−0.057	0.396	3.08	0.72	0.55	0.19	0.16	0.09
39572	1993 DQ1	64.8	1.08	255	19.1	0.990	0.010	0.000	0.990	1.960	0.011	0.009	1.969					1.21	0.32	0.30	0.09	0.10	0.05
52387	1993 OM7	58.8	1.07	270	11.1	0.925	0.010	0.001	0.926	1.975	0.104	0.006	1.981					1.03	0.17	0.16	0.46	0.25	0.20
52750	1998 KK17	21.0	1.36	210	30.8	0.935	0.010	0.004	0.939	1.970	0.010	0.013	1.983										
53430	1999 TY16	24.0	1.29	231	22.6	0.930	0.010	0.000	0.930	1.935	0.010	0.014	1.949										
53435	1999 VM40	55.0	1.21	241	17.3	0.930	0.010	0.000	0.930	1.920	0.008	0.012	1.932	1.135	0.100	−0.050	1.085	0.84	0.19	0.17	0.32	0.24	0.15
53789	2000 ED104	58.8	1.14	243	8.9	0.925	0.045	0.000	0.925	1.890	0.257	0.011	1.901	0.567	0.325	−0.058	0.509	0.96	0.25	0.20	0.24	0.21	0.11
54690	2001 EB	33.0	1.36	229	6.9	0.940	0.035	0.000	0.940	1.975	0.279	0.014	1.989					0.88	0.29	0.17	0.37	0.32	0.21
66251	1999 GJ2	37.2	1.24	229	11.6	0.955	0.010	0.000	0.955	2.015	0.012	0.015	2.029					0.88	0.29	0.17	0.37	0.32	0.21
66251	1999 GJ2	7.4	1.28	226	11.0	0.945	0.010	0.000	0.945	2.005	0.011	0.016	2.020										
66251	1999 GJ2	16.6	1.32	222	9.8	0.945	0.010	0.000	0.945	1.925	0.017	0.016	1.941										
68216	2001 CV26	20.5	1.36	227	11.3	0.980	0.010	0.000	0.980	2.000	0.010	0.015	2.015					1.39	0.37	0.29	0.26	0.21	0.13
68359	2001 OZ13	21.5	1.26	217	18.0	0.995	0.010	0.000	0.995	1.845	0.308	0.017	1.862					0.61	0.14	0.11	0.47	0.32	0.22
69230	Hermes	6.5	1.19	254	14.2	0.975	0.010	0.000	0.975	1.965	0.010	0.009	1.974					1.25	0.27	0.21	0.12	0.10	0.05
85709	1998 SG36	66.1	1.10	248	11.9	0.930	0.010	0.000	0.930	1.960	0.010	0.010	1.970					1.53	0.37	0.30	0.32	0.27	0.15
85818	1998 XM4	48.5	1.18	241	18.1	0.935	0.010	0.000	0.935	1.985	0.010	0.012	1.997	1.401	0.100	−0.050	1.351	2.00	0.50	0.40	0.30	0.23	0.15
85839	1998 YO4	22.2	1.38	232	21.4	1.025	0.010	0.000	1.025	2.035	0.034	0.014	2.049					1.81	0.41	0.40	0.17	0.16	0.08
86324	1999 WA2	37.4	1.47	217	16.3	0.935	0.010	0.000	0.935	1.940	0.112	0.017	1.957										
86667	2000 FO10	3.3	1.34	238	15.2	1.035	0.010	0.000	1.035	1.945	0.012	0.012	1.957					1.22	0.29	0.25	0.13	0.11	0.06
87684	2000 SY2	44.9	1.18	244	19.6	0.965	0.010	0.000	0.965	1.950	0.010	0.011	1.961										
88254	2001 FM129	79.5	1.01	257	21.6	0.985	0.010	0.000	0.985	2.005	0.035	0.009	2.014										
89355	2001 VS78	51.9	1.24	236	12.0	0.945	0.010	0.000	0.945	1.950	0.042	0.013	1.963										
89355	2001 VS78	49.0	1.27	233	18.5	0.925	0.010	0.000	0.925	2.065	0.015	0.013	2.078	0.907	0.100	−0.055	0.852	0.81	0.17	0.14	0.33	0.23	0.14
96590	1998 XB	28.6	1.23	251	17.4	1.010	0.010	0.000	1.010	1.995	0.010	0.010	2.005					2.29	0.47	0.42	0.11	0.09	0.05
99799	2002 LJ3	16.0	1.36	214	20.4	1.005	0.010	0.000	1.005	1.875	0.234	0.017	1.892					0.50	0.09	0.09	0.42	0.26	0.17
99907	1989 VA	62.8	1.06	259	24.5	0.905	0.010	0.000	0.905	1.965	0.008	0.008	1.973	0.589	0.100	−0.036	0.552	0.74	0.14	0.14	0.24	0.19	0.11
99907	1989 VA	36.7	1.15	249	21.5	0.975	0.010	0.000	0.975	1.965	0.010	0.010	1.975					0.74	0.14	0.14	0.24	0.19	0.11
100926	1998 MQ	57.4	1.10	244	23.2	0.945	0.010	0.000	0.945	2.030	0.012	0.011	2.041	0.311	0.100	−0.048	0.263	1.08	0.23	0.19	0.37	0.22	0.16
137032	1998 UO1	22.2	1.57	220	14.3	0.925	0.010	0.000	0.925	1.890	0.019	0.016	1.906					1.66	0.37	0.35	0.13	0.11	0.06
137032	1998 UO1	52.0	1.07	267	21.0	0.985	0.010	0.001	0.986	2.010	0.010	0.007	2.017					1.66	0.37	0.35	0.13	0.11	0.06
137062	1998 WM	18.1	1.60	205	22.7	0.915	0.010	0.000	0.915	1.990	0.010	0.019	2.009	0.778	0.100	−0.076	0.702	1.13	0.28	0.23	0.32	0.23	0.14
137671	1999 XP35	26.1	1.17	252	16.1	0.925	0.010	0.000	0.925	2.020	0.012	0.010	2.030					0.60	0.17	0.13	0.17	0.16	0.08
137924	2000 BD19	19.8	1.50	226	55.8	0.950	0.010	0.004	0.954	1.965	0.010	0.011	1.976					1.46	0.31	0.29	0.11	0.09	0.05

Number	Designation	C1	C2	C3	C4	C5	C6	C7	C8	C9	C10	C11	C12	C13	C14	C15	C16	C17	T	σ1	σ2	σ3	σ4	σ5
138258	2000 GD2	26.5	1.06	257	21.0	1.010	0.010	0.000	1.010	1.950	0.038	0.009	1.959	0.499	0.100	−0.038	0.461	1.40	0.30	0.30	0.19	0.17	0.09
138883	2000 YL29	34.8	1.19	248	26.2	0.995	0.010	0.000	0.995	1.965	0.047	0.009	1.974	0.395	0.100	−0.039	0.356	0.94	0.16	0.16	0.20	0.16	0.09
141052	2001 XR1	39.9	1.12	255	16.8	0.960	0.010	0.000	0.960									0.91	0.16	0.16	0.22	0.16	0.09
141052	2001 XR1																	0.82	0.14	0.12	0.27	0.18	0.12
141052	2001 XR1																	0.96	0.22	0.19	0.20	0.15	0.09
141052	2001 XR1																						
141432	2002 CQ11	12.4	1.15	245	17.2	0.925	0.010	0.000	0.925	2.005	0.058	0.011	2.016										
143651	2003 QO104	40.8	1.24	247	21.4	0.985	0.010	0.000	0.985	2.060	0.010	0.011	2.071					2.30	0.56	0.49	0.14	0.12	0.07
143651	2003 QO104	64.3	1.09	264	27.1	0.995	0.010	0.001	0.996	1.905	0.014	0.007	1.912	0.329	0.100	−0.033	0.296	2.30	0.56	0.49	0.14	0.12	0.07
144900	2004 VG64	44.2	1.10	249	10.7	0.980	0.010	0.000	0.980	2.020	0.021	0.010	2.030					0.55	0.11	0.09	0.30	0.20	0.13
144922	2005 CK38	11.4	1.40	230	13.1	1.000	0.010	0.000	1.000	1.990	0.013	0.014	2.004					1.15	0.28	0.26	0.17	0.16	0.08
152558	1990 SA	15.7	1.31	232	5.7	0.950	0.010	0.000	0.950	2.025	0.019	0.014	2.039										
152931	2000 EA107	50.2	1.24	238	27.0	1.005	0.010	0.000	1.005	1.950	0.025	0.012	1.962	0.326	0.100	−0.052	0.274	1.76	0.40	0.38	0.16	0.16	0.08
154029	2002 CY46	45.5	1.12	258	11.0	0.935	0.010	0.000	0.935	1.980	0.010	0.008	1.988										
154244	2002 KL6	48.7	1.11	251	22.5	1.000	0.010	0.000	1.000	1.920	0.127	0.010	1.930					1.22	0.25	0.22	0.35	0.24	0.16
154715	2004 LB6	50.9	1.13	249	22.0	1.015	0.010	0.000	1.015	1.965	0.045	0.010	1.975					0.95	0.19	0.16	0.29	0.21	0.13
159402	1999 AP10	19.3	1.16	238	9.8	0.970	0.010	0.000	0.970	1.955	0.013	0.012	1.967					1.10	0.29	0.23	0.16	0.14	0.08
161989	Cacus	53.6	1.10	250	14.8	1.010	0.010	0.000	1.010	1.988	0.012	0.012	2.000					0.93	0.21	0.17	0.22	0.17	0.10
161998	1988 PA	25.7	1.29	241	16.8	0.980	0.010	0.000	0.980	1.935	0.151	0.012	1.947					1.02	0.30	0.23	0.09	0.10	0.05
162483	2000 PJ5	52.8	1.18	248	26.3	0.965	0.010	0.000	0.965	1.915	0.265	0.010	1.925					1.36	0.27	0.24	0.30	0.20	0.14
162900	2001 HG31	16.4	1.31	232	17.4	1.065	0.010	0.000	1.065	1.945	0.011	0.014	1.959					0.25	0.04	0.04	0.29	0.20	0.12
163001	2001 SE170	28.0	1.26	248	10.3	0.925	0.010	0.000	0.925	1.980	0.028	0.010	1.990					1.30	0.29	0.26	0.13	0.11	0.05
163243	2002 FB3	57.6	1.17	242	15.2	1.015	0.010	0.000	1.015	1.943	0.015	0.012	1.954					0.44	0.10	0.09	0.17	0.14	0.08
163697	2003 EF54	46.4	1.06	255	20.8	0.990	0.010	0.000	0.990	1.965	0.227	0.009	1.974										
164400	2005 GN59	27.0	1.20	252	18.1	0.995	0.010	0.000	0.995	1.940	0.016	0.010	1.950										
184266	2004 VW14	50.8	1.06	265	24.0	1.025	0.010	0.001	1.026	2.020	0.015	0.007	2.027										
200840	2001 XN254	63.8	1.03	258	17.1	0.950	0.010	0.000	0.950	2.000	0.010	0.008	2.008	0.732	0.100	−0.037	0.695	1.14	0.25	0.21	0.28	0.21	0.12
207945	1991 JW	23.1	1.12	250	19.9	0.970	0.010	0.000	0.970	1.955	0.087	0.010	1.965	0.318	0.100	−0.043	0.275	0.73	0.15	0.13	0.29	0.19	0.13
217796	2000 TO64	64.9	1.07	255	26.4	0.935	0.010	0.000	0.935	1.890	0.028	0.009	1.899					1.69	0.43	0.38	0.22	0.18	0.10
217807	2000 XK44	38.8	1.06	255	16.5	1.000	0.010	0.000	1.000	1.980	0.019	0.009	1.989					0.79	0.15	0.13	0.35	0.22	0.15
218863	2006 WO127	66.1	1.07	259	19.1	0.970	0.010	0.000	0.970	1.995	0.044	0.008	2.003					0.52	0.10	0.09	0.21	0.16	0.09
219071	1997 US9	23.5	1.35	221	23.9	1.030	0.010	0.000	1.030	1.965	0.131	0.016	1.981	0.265	0.100	−0.064	0.201	0.75	0.16	0.13	0.25	0.18	0.11
235756	2004 VC	59.2	1.06	261	18.7	0.915	0.010	0.001	0.916	1.875	0.026	0.008	1.883										
237442	1999 TA10	20.8	1.30	233	17.4	0.930	0.010	0.000	0.930	1.960	0.017	0.013	1.973										
241662	2000 KO44	24.0	1.26	236	16.3	1.005	0.010	0.000	1.005	1.945	0.012	0.013	1.958										
248818	2006 SZ217	21.7	1.23	246	16.1	0.925	0.010	0.000	0.925	1.910	0.010	0.011	1.921					1.08	0.26	0.20	0.16	0.14	0.07
260141	2004 QT24	27.4	1.10	238	14.1	0.995	0.010	0.000	0.995	2.000	0.010	0.012	2.012					0.46	0.08	0.07	0.42	0.24	0.17
260141	2004 QT24	51.4	1.10	238	17.7	0.980	0.010	0.000	0.980	1.985	0.019	0.012	1.997					0.46	0.08	0.07	0.42	0.24	0.17
274138	2008 FU6	4.0	1.34	229	18.2	1.045	0.010	0.000	1.045	1.960	0.227	0.014	1.974										
274138	2008 FU6	53.2	1.11	251	20.8	1.025	0.010	0.000	1.025	1.965	0.148	0.010	1.975										
297418	2000 SP43	56.6	1.09	239	26.3	0.940	0.010	0.003	0.943	2.000	0.010	0.009	2.009										
297418	2000 SP43	51.3	1.08	239	30.5	0.945	0.010	0.003	0.948	1.945	0.010	0.009	1.954										
297418	2000 SP43	35.6	1.17	230	29.2	0.945	0.010	0.003	0.948	1.985	0.010	0.010	1.995										
301844	1990 UA	44.1	1.08	236	16.1	0.990	0.010	0.000	0.990	1.965	0.106	0.013	1.978					0.24	0.04	0.04	0.46	0.25	0.19
302831	2003 FH	64.2	1.04	258	24.9	1.000	0.010	0.000	1.000	2.065	0.094	0.008	2.073					0.40	0.08	0.07	0.28	0.19	0.13
310442	2000 CH59	21.2	1.14	229	19.7	0.985	0.010	0.000	0.985	2.100	0.143	0.014	2.114					0.23	0.03	0.03	0.46	0.23	0.19
	2002 GO5	11.2	1.15	249	14.5	1.000	0.010	0.000	1.000	1.990	0.010	0.010	2.000					0.76	0.16	0.14	0.25	0.20	0.11
	2002 LV	34.8	1.47	227	22.1	0.960	0.010	0.000	0.960	1.995	0.284	0.015	2.010					1.73	0.36	0.30	0.15	0.13	0.07
	2002 LV	65.3	1.09	263	13.2	0.930	0.010	0.001	0.931	1.890	0.013	0.007	1.897					1.73	0.36	0.30	0.15	0.13	0.07
	2005 UL5	27.6	1.10	253	18.5	0.975	0.010	0.000	0.975	2.000	0.010	0.009	2.009										
	2007 RF5	16.7	1.28	238	14.6	1.035	0.010	0.000	1.035	1.955	0.010	0.012	1.967					0.62	0.12	0.12	0.21	0.18	0.09

the polynomial fit, which allows for subtle polynomial shifts to result in relatively large shifts in the band center calculations.

Since some observations do not contain data that extend to ∼0.75 μm on the blue end, they do not contain a complete Band I. These Band I Centers are calculated using a linear continuum that begins at the start of the data, not at the local maximum blue-ward of Band I. Dividing Band I by this data-start continuum will produce a differently sloped continuum-divided Band I than if it had been divided by an appropriate local maxima continuum. Therefore, there is an additional source of error on objects that do not include data short ward of 0.75 μm. We quantify this error by removing the spectral data <0.82 μm for a few high signal-to-noise observations to simulate an observation taken with the SpeX dichroic in the light path. We find that the BICs tend to shift to higher wavelength by values smaller than the defined minimum band center error of 0.01.

Band Area Ratio (BAR) is defined as the ratio of the area of Band II to the area of Band I. Each band area is calculated by using the trapezoidal rule to determine the area between the linear continuum and the continuum-divided spectral band. The error for each band area is calculated using the same Monte Carlo method used for band center errors. The error is defined as the standard deviation of the 20,000 altered area trials. The BAR error uses the individual area errors and propagates them with standard error analysis techniques. We define a minimum BAR error of 0.1 for all observations to account for uncertainties that have not been quantified such as the definition of the continuum slope and band depth changes due to phase angle. Calculated uncertainties are only reported if they exceed this minimum. This minimum error was also used by Reddy et al. (2010). The Band Area Ratio is not calculated for observations with no data <0.75 μm. Using a data-start continuum instead of a local maxima continuum removes a significant amount of area from the Band I area calculation. Therefore, the BARs calculated in this manner would not be directly comparable to the BARs calculated for asteroids using the complete Band I and the BARs calculated for laboratory meteorite spectra.

Band depth is a measure of the ratio of the spectrum to the continuum at the calculated band center. The depth of a band is diagnostic of mafic mineral abundance and grain size, but is less diagnostic of composition than the other presented band parameters. The nominal band depth for an object can be modified by factors such as phase angle and lunar-style space weathering. We present only Band I depth in this paper because the telluric absorption remnants in Band II often make depth difficult to constrain. We use the smoothed, continuum-divided spectrum to determine Band I depth using the following equation:

$$\text{Band I Depth } (\%) = \left[1 - \frac{R_b}{R_c}\right] * 100 \tag{1}$$

where R_b is the reflectance spectrum value at the Band I center location and R_c is the linear continuum value at the Band I center location (Clark and Roush, 1984).

2.5. Temperature corrections of band parameters

Surface temperature variations on asteroids shift the band centers and change the width of the absorption feature (e.g., Moroz et al., 2000; Hinrichs and Lucey, 2002; Sanchez et al., 2012; Dunn et al., 2013). These temperature changes are of little importance for Main-Belt asteroids, but can be significant for the higher eccentricity near-Earth objects. Most importantly, in order to directly compare room temperature (∼300 K) laboratory spectra with observational spectra, temperature corrections are necessary.

In order to apply temperature corrections to our sample, we need to identify the best laboratory matches to the two types of compositions in our band parameter sample. The S- and Q-complex objects are olivine–pyroxene assemblages. For these objects, we apply corrections derived from ordinary chondrites by Sanchez et al. (2012) and Dunn et al. (2013) using data from Moroz et al. (2000) and Hinrichs and Lucey (2002). The near-infrared spectra of the V-complex objects are dominated by the pyroxene features. For these objects, we apply corrections derived by Reddy et al. (2012c) using laboratory spectra of howardite, eucrite, and diogenite (HED) meteorites measured at various temperatures. All band parameters are corrected to room temperature values. Tables 3 and 4 contain the temperature corrections and corrected band parameters.

For each object, we calculate the average surface temperature (T) in Kelvin using the equation defined in Burbine et al. (2009).

$$T = [(1 - A)L_0/16\eta\varepsilon\sigma\pi r^2]^{1/4} \tag{2}$$

where A is the asteroid albedo, L_0 is the solar luminosity (3.827×10^{26} W), η is the beaming parameter (in this case, assumed to be unity, Cohen et al., 1998), ε is the asteroid's infrared emissivity (assumed to be 0.9, Salisbury et al., 1991), σ is the Stefan Boltzmann constant (5.67×10^{-8} J s^{-1} m^{-2} K^{-4}), and r is the asteroid's distance from the Sun in meters. When available, we use ExploreNEOs geometric albedos. Due to a small number of target list changes over the course of the Warm Spitzer observations, there are some objects on the ExploreNEOs target list for which albedos and diameters have not been measured. For those objects, we use the average albedo of the taxonomic complex ($S = 0.26$, $Q = 0.29$, and $V = 0.42$) derived by Thomas et al. (2011). All calculated corrections are added to the spectrally derived values. Corrections are on order of 0.001 for BIC, 0.01 for BIIC, and 0.1 for BAR. We use Eq. (2) to calculate the asteroid surface temperatures to be consistent with previous asteroid spectroscopy temperature corrections (e.g. Burbine et al., 2009; Moskovitz et al., 2010). The temperature calculated by this equation gives the temperature of a fast-rotating spherical asteroid with high thermal inertia and uniform temperature. This is known as the Fast-Rotating Model (FRM, Lebofsky and Spencer, 1989) and assumes that energy is absorbed over the side of the asteroid facing the Sun, but is radiated from the entire sphere. The temperatures determined using Eq. (2) are lower than those calculated using the Standard Thermal Model (STM, Lebofsky et al., 1986). If we calculate the sub-solar temperature using the STM we get higher temperatures, which correspond to smaller corrections compared to the FRM temperature corrections. Both the FRM and STM corrections are on the order of our defined minimum band parameter errors and therefore the differences between them do not contribute significantly to the overall error budget. We note that the FRM is not consistent with asteroids in this size range with known rotation periods (e.g., Delbó et al., 2003; Müller et al., 2012; Emery et al., 2010).

The majority of our objects in the band parameter sample belong to the olivine–pyroxene-rich S- and Q-complexes. Sanchez et al. (2012) shows that Band II is the most affected by temperature variations and that Band II center shifts to longer wavelength as temperature increases. The equation derived by Sanchez et al. (2012) for the temperature correction of the Band II center is the following:

$$\Delta\text{BIIC } (\mu m) = 0.06 - 0.0002 \times T \text{ (K)} \tag{3}$$

The calculated BIIC correction is added to the spectrally derived BIIC values.

Sanchez et al. (2012) find the correction for Band I center to be very small in general (∼0.003 μm) and do not calculate a temperature correction for it. Dunn et al. (2013) use different corrections from the LL chondrite Soko-Banja and the L chondrite Elenovka and also find the correction to be small. However, since the direction of

movement of the Band I center depends on the amount of olivine in the sample, the temperature corrections derived from these two ordinary chondrites do not shift in the same directions. Since both corrections are small, Dunn et al. (2013) apply a correction based on the average of the two corrections. We apply this method from Dunn et al. (2013) to our sample using the average of the following corrections:

$$\Delta BIC, \text{ LL correction } (\mu m) = 0.000078 \times T \text{ (K)} - 0.02194 \quad (4)$$

$$\Delta BIC, \text{ L correction } (\mu m) = -0.000048 \times T \text{ (K)} + 0.01512 \quad (5)$$

We note that the constant in Eq. (4) is printed incorrectly as 0.2194 in Dunn et al. (2013). If we use 0.2194 instead of 0.02194, we calculate a temperature correction that is two orders of magnitude different from the corrections calculated using the complementary L chondrites BIC correction (Eq. (5)). This would result in a correction of order 0.1 μm instead of <0.001 μm. Dunn et al. (2013) state that the corrections are consistent with Burbine et al. (2009) and are on order <0.001 μm. Therefore we use 0.02194 throughout our analysis.

Sanchez et al. (2012) determine the correction for Band Area Ratio (BAR) to be the following:

$$\Delta BAR = 0.00075 \times T \text{ (K)} - 0.23 \quad (6)$$

Dunn et al. (2013) again use different corrections from the two meteorites and apply the average correction:

$$\Delta BAR, \text{ LL correction } = 0.0009 \times T \text{ (K)} - 0.2666 \quad (7)$$

$$\Delta BAR, \text{ L correction } = 0.0005 \times T \text{ (K)} - 0.1708. \quad (8)$$

We find the Sanchez and Dunn BAR corrections to be nearly identical and use the average of the two in our analysis.

Band I depth was not addressed by Dunn et al. (2013) and Sanchez et al. (2012) found no obvious correlation between Band I depth and temperature. No correction was applied.

For the few pyroxene-rich V-types in our sample, we apply temperature corrections derived by Reddy et al. (2012c) using laboratory spectra of howardite, eucrite, and diogenite (HED) meteorites measured at various temperatures. The band center corrections for howardites and eucrites were calculated using spectra from Hinrichs and Lucey (2002) and the corrections for diogenites were calculated using spectra from Schade and Wäsch (1999). We apply an offset to each nominal V-type band center equal to the average of the two calculated corrections for the appropriate band. The corrections for Band I center are defined as the following:

$$\Delta BIC, \text{ Howardites } \& \text{ Eucrites } (\mu m)$$
$$= 0.01656 - 0.0000552 \times T \text{ (K)} \quad (9)$$

$$\Delta BIC, \text{ Diogenites } (\mu m) = 0.0000000017 \times T^3 \text{ (K)}$$
$$- 0.0000012602 \times T^2 \text{ (K)}$$
$$+ 0.0002664351 \times T \text{ (K)}$$
$$- 0.0124 \quad (10)$$

while the corrections for Band II center are the following:

$$\Delta BIIC, \text{ Howardites } \& \text{ Eucrites } (\mu m)$$
$$= 0.05067 - 0.00017 \times T \text{ (K)} \quad (11)$$

$$\Delta BIIC, \text{ Diogenites } (\mu m) = 0.038544 - 0.000128 \times T \text{ (K)} \quad (12)$$

The resulting corrections are similar to those calculated with equations derived by Burbine et al. (2009) who used spectra of enstatites at multiple temperatures measured by Moroz et al. (2000). Temperature corrections for Band Area Ratio were not addressed in Reddy et al. (2012c), Burbine et al. (2009) or Moskovitz et al. (2010). Therefore, we do not correct the BARs of V-types for temperature variations.

3. Results

3.1. Band Parameters

The results of our band parameter analysis are shown in Fig. 1. Panel (a) shows all band parameters for observed Q-, S-, and V-complex ExploreNEO targets in our survey (black circles) and in the MIT Joint Campaign for NEO Spectral Reconnaissance (red triangles). The Gaffey S-subtypes are shown in panel (b). These subtypes are the result of the S-complex containing a progression of mixtures that range from pure olivine (S(I)) to pure pyroxene (S(VII) and the basaltic acondrites (BA)). The comparison of the Gaffey S-subclasses and our calculated band parameters is shown in panel (c). Our data closely match the region defined by the continuum of S-subtypes defined by Gaffey et al. (1993) and the olivine–orthopyroxene mixing line determined by Cloutis et al. (1986). However, it seems that a small offset to higher BAR could improve the fit. A calibration offset between laboratory derived data and telescopic data was proposed in Gaffey (1984) to explain a discrepancy between their results and calibrations in Adams (1974). It was not determined whether this correction was correct. We do not calculate an offset correction for our data, but do allow for an extra margin when investigating S(IV)-subclass members (panel (d), Section 3.5).

Only one outlying object is excluded from this figure, (16834) 1997 WU22 from sp77 of the MIT Joint Campaign. Visual inspection of the spectrum shows an anomalous 2-micron band that is significantly different from other observations of 1997 WU22. We deem this spectrum to be anomalous and not indicative of the true composition and band parameters of the object.

3.2. ExploreNEOs albedos and diameters

We combine ExploreNEOs albedos with our calculated Band I Centers (BICs). For this analysis we use the albedos calculated via the method described in Mueller et al. (2011) and Trilling et al. (submitted for publication). The analysis produces an albedo and error bars generated by a Monte Carlo procedure. The calculations include a robust error analysis that considers the various sources of uncertainty present in the ExploreNEOs data and asymmetric error bars to capture the true uncertainty. The band parameter sample in this paper is taken from the Q-, S-, and V-complexes which are the higher albedo objects in our NEO sample. Due to the relatively large reflected light component for these objects, the albedo and diameter errors are correspondingly larger than for the low albedo objects (Harris et al., 2011; Mueller et al., 2011).

To potentially identify correlations using the albedo data, we limit the sample to those with $\sigma_{p_V^+}$ and $\sigma_{p_V^-} < 0.20$. This error cutoff was chosen to eliminate the albedos with the highest error. Of the band parameters, we choose Band I Centers because they are the most accurate and precise measurements within our sample and the values can be used to determine the olivine and pyroxene chemistries (Dunn et al., 2010).

As discussed in Trilling et al. (2010), the nominal albedo and diameter values for Eros are quite different from those reported by the NEAR mission and supporting ground-based observations. This discrepancy is due to the near pole-on geometry for the Spitzer observations. Using a beaming parameter (η) and absolute magnitude (H) that were more appropriate for the viewing geometry of the observation, Trilling et al. (2010) recalculated the albedo (p_V) and diameter (D) to be 0.23 and 22.3 km respectively. These recalculated values agree with previous observations of Eros (e.g. Harris and Davies, 1999; Li et al., 2004). We incorporate these recalculated values in our analysis. All other ExploreNEOs albedos
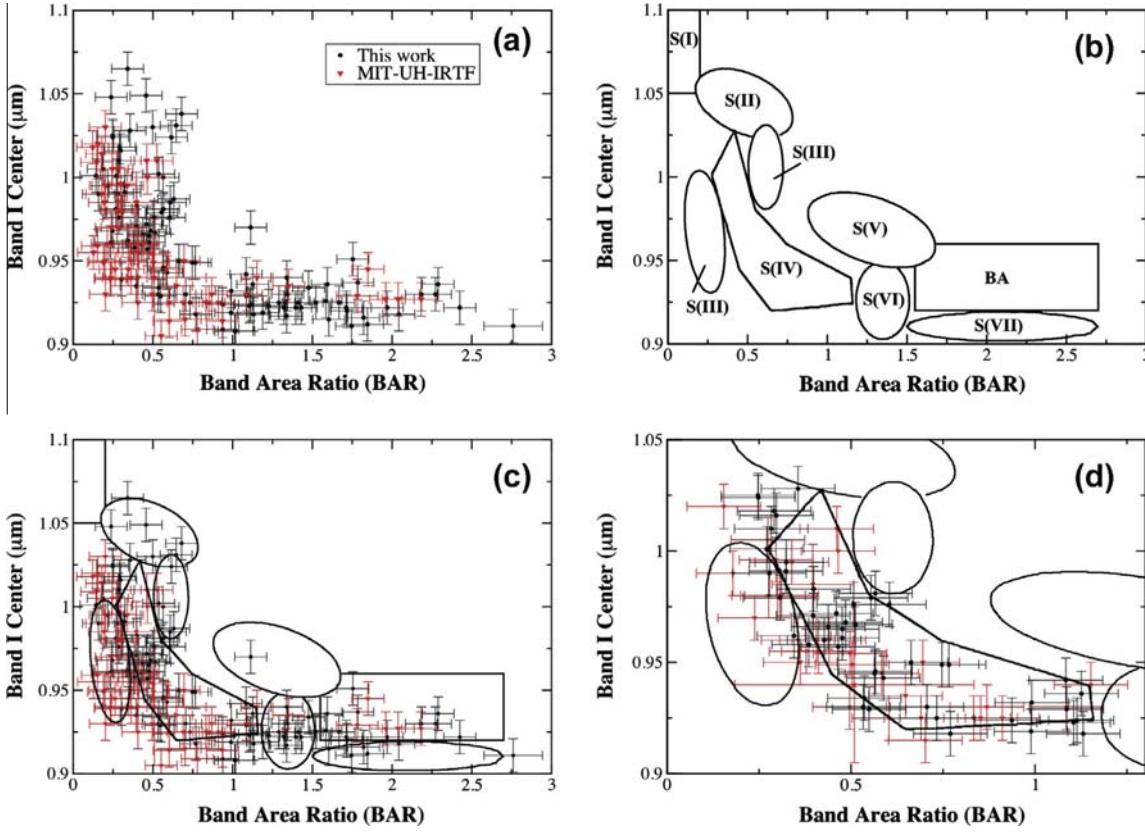
Fig. 1. (a) Band I Centers (BICs) versus Band Area Ratios (BARs) for all S-, Q-, and V-complex objects in our full spectral sample. Objects observed as part of the ExploreNEOs survey are displayed using black circles and those from the MIT Joint Campaign are shown using red triangles. (b) The Gaffey et al. (1993) S-subclasses and basaltic achondrites (BA) in BIC–BAR space. (c) The comparison of our spectral band parameters with the Gaffey et al. (1993) S-subclasses. The shape of the distribution of S-subclasses matches the distribution of objects in our analysis. (d) We use the S(IV) region as one method of identifying potential ordinary chondrites in our sample. This panel shows the S(IV) region with objects classified as S(IV) in our analysis. We include Eros and Itokawa because of their confirmed ordinary chondritic nature. (For interpretation of the references to color in this figure legend, the reader is referred to the web version of this article.)

and diameters are the nominal values (Trilling et al., submitted for publication).

One object, (141052) 2001 XR1, from the MIT Joint Campaign observations has multiple Warm Spitzer observations. This object was part of a subset of ExploreNEOs objects that were observed multiple times in order to study phase angle effects. We use the average of the four albedos and diameters in our analysis. We propagate the errors using standard error propagation techniques. The individual albedo and diameter values are shown in Table 4. The average values are $p_V = 0.22^{+0.08}_{-0.05}$ and $D = 0.91^{+0.09}_{-0.08}$ km.

We add NEOWISE (Mainzer et al., 2011) albedos and diameters to our analysis. For objects that lacked ExploreNEOs albedo and diameter solutions, we include the NEOWISE solutions. When the object appeared in both the ExploreNEOs and NEOWISE catalog, we average the albedos and diameters and propagated the errors using standard techniques in order to reduce the errors for these multiply observed objects.

We find no correlation between our error-limited albedos or diameters (ExploreNEOs and NEOWISE) with respect to Band I Centers (Fig. 2). Since object albedos can depend on object chemistry and olivine is more reflective on average than pyroxene (e.g. Reddy et al., 2011c, 2012a), one might expect to see a trend of increasing albedo with increasing Band I Center. We find no correlation between albedo and BIC down to error limits of 0.05 in albedo. This suggests that processes such as space weathering and photometric effects due to various factors including regolith grain size have a non-negligible contribution to the observed albedo.
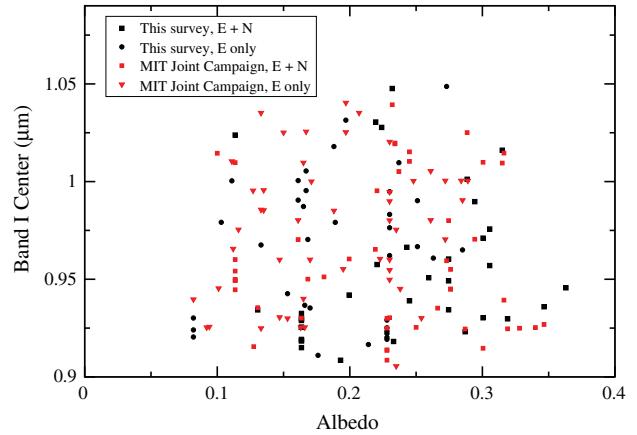
Fig. 2. We find no correlation between ExploreNEOs (E) and NEOWISE (N) albedos and Band I Center for our spectral sample. Objects observed as part of the ExploreNEOs survey are shown in black. The circles represent ExploreNEOs-only albedos and the squares are an average of ExploreNEOs and NEOWISE albedos. Objects from the MIT Joint Campaign are shown in red. The triangles represent ExploreNEOs-only albedos and the squares are an average of ExploreNEOs and NEOWISE albedos. The errors on the ExploreNEOs albedos of these objects are higher than the ExploreNEOs average since we are targeting the high albedo objects in this band parameter analysis. We place an upper limit on the errors σ_{pV^+} and σ_{pV^-} of 0.20. We discard all observations with errors larger than this limit. We find no correlation down to error limits on σ_{pV^+} and σ_{pV^-} of 0.05. (For interpretation of the references to color in this figure legend, the reader is referred to the web version of this article.)

3.3. Phase angle–Band Area Ratio correlations

Band parameters can be influenced by factors not related to compositional variation. One important factor to consider is the phase angle of the observation. Phase angle (α) is the angle between the light incident on the asteroid surface and the light reflected from the surface towards an observer. Increased phase angle can result in an increase of spectral slope known as phase reddening and changes in the strength of the absorption bands.

In Section 3.1 we note that a small offset to higher Band Area Ratio (BAR) could improve the match between our data and the laboratory-derived Gaffey S-subclasses and olivine–orthopyroxene
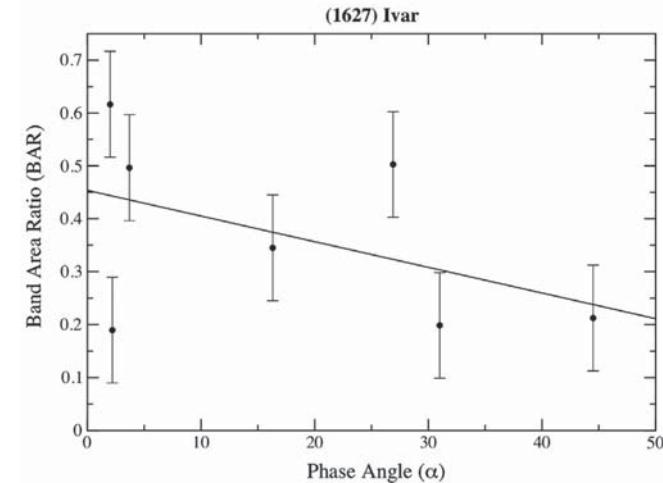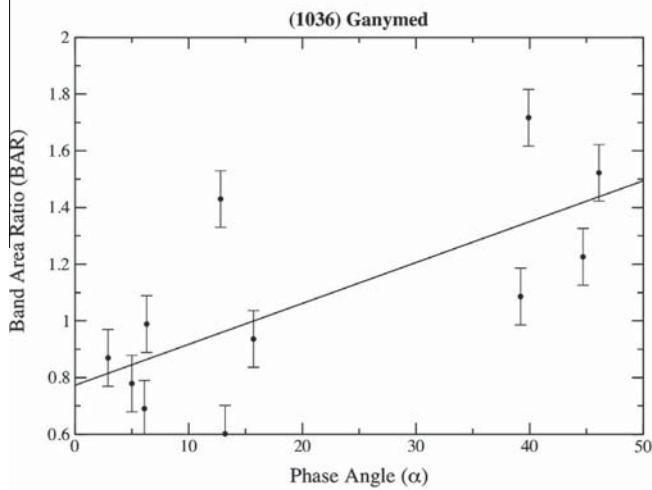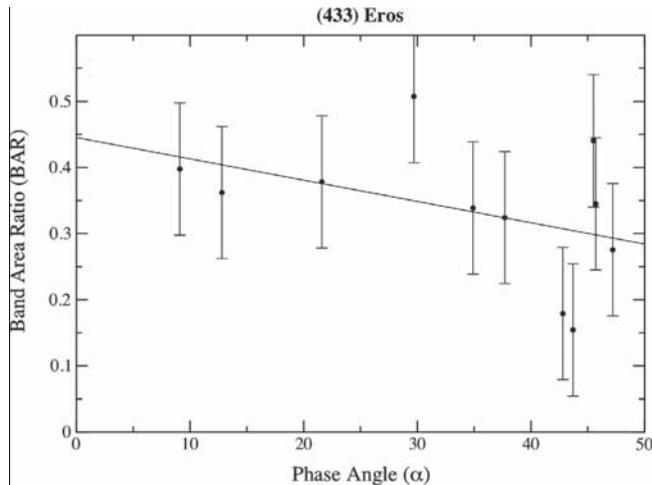
Fig. 3. Band Area Ratio (BAR) versus phase angle (α) for (433) Eros, (1036) Ganymed, and (1627) Ivar. For Eros and Ivar, BAR is anti-correlated with phase angle. Ganymed has an opposite correlation with a trend of increasing BAR with increasing phase angle.
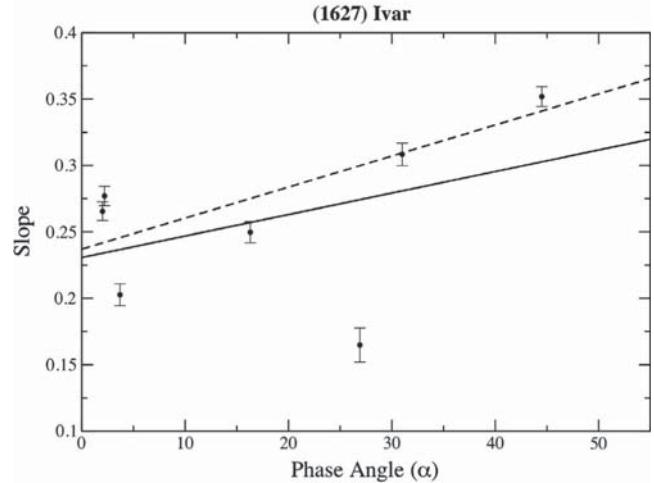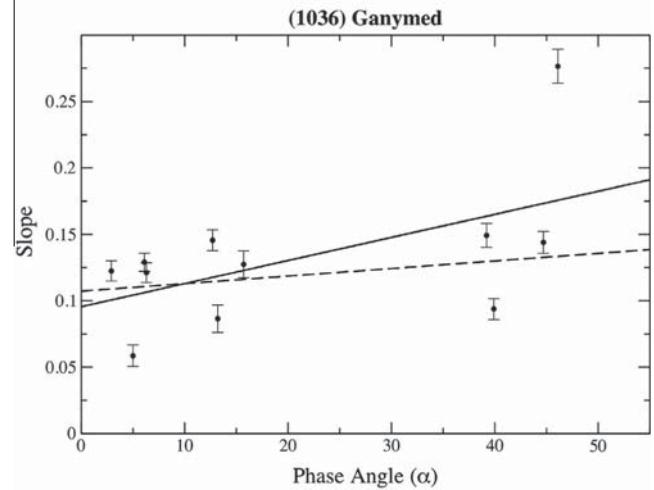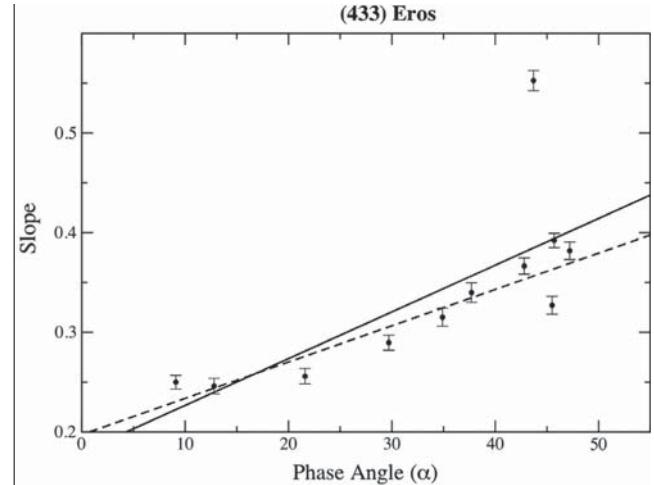
Fig. 4. Near-infrared spectral slope versus phase angle (α) for (433) Eros, (1036) Ganymed, and (1627) Ivar. All three objects show evidence of phase reddening. The solid lines indicate the nominal correlations and the dashed lines indicate the correlations calculated without the outlying points.

mixing line. To investigate potential causes of this offset, we investigate the effect of phase angle on BAR. We examine the relationship between phase angle and BAR on individual objects, not the full population, to understand the effects of varying compositions and optical properties. Our data has not been corrected for phase angle effects although data presented in Sanchez et al. (2012) demonstrates that changes in phase angle will affect the spectral band depth. Ideally, we would correct BAR to a phase angle of 30° to best match laboratory spectra. Sanchez et al. (2012) did not find any correlations between increasing phase angle and BAR values. Our observations demonstrate that individual objects can show different spectral responses to changing phase angle and that there is not a universal phase angle–BAR correlation that can be applied to our spectral sample (Fig. 3).

Three objects in our sample were observed at multiple phase angles: (433) Eros, (1036) Ganymed, and (1627) Ivar. Eros was observed 11 times total by the ExploreNEOs and MIT Joint Campaign surveys. Using the phase angles (α) of the observations and the temperature corrected BARs, we calculate a least-squares linear fit of BAR = $(-0.003 \pm 0.002) \times \alpha + (0.445 \pm 0.083)$ with $R^2 = 0.180$. R^2 is the coefficient of determination, which ranges from 0 to 1 and indicates how well data fits a line (1 indicates the line perfectly fits the data). Ganymed also has 11 observations from the two surveys. We find a least-squares linear fit for Ganymed of BAR = $(0.014 \pm 0.005) \times \alpha + (0.773 \pm 0.131)$ with $R^2 = 0.494$. Ivar has 7 observations from the two surveys, which we use to find a least-squares linear fit of BAR = $(-0.005 \pm 0.004) \times \alpha + (0.454 \pm 0.098)$ with $R^2 = 0.215$.

Eros and Ivar have similar phase angle–Band Area Ratio correlations: for these objects, BAR is anti correlated with phase angle. However, for Ganymed the correlation is opposite with a trend of increasing BAR with increasing phase angle. If most S-type objects behaved in a manner similar to Eros and Ivar, a correction from high phase angle to 30° could cause a shift in our BAR distribution to better match the Gaffey S-subclasses. Sanchez et al. (2012) saw similar correlations of BAR with respect to phase angle. Their two observations of Ganymed also displayed a correlation opposite to the other objects'.

We find no consistent correlation between phase angle and BAR in our data. The large differences between the phase angle–BAR relationships for our three objects suggest that no individual correction should be applied to all objects. Therefore, we do not correct our sample for phase angle variations.

3.4. Phase angle-near-infrared spectral slope correlations

We also examine the relationship between phase angle and spectral slope in near-infrared wavelengths for (433) Eros, (1036) Ganymed, and (1627) Ivar. To investigate these correlations we use phase angles (α) and the near-infrared spectral slope between 0.82 and 2.4 μm. We choose this wavelength range to be consistent for all spectra. Spectra from the ExploreNEOs survey do not include visible wavelength observations. Since we do not want to include data points from visible wavelength observations and several of the MIT Joint Campaign near-infrared spectra were taken with the SpeX dichroic in the light path, we select a lower wavelength of 0.82 μm. We choose the upper limit of wavelength to be 2.4 μm to avoid contributions to the spectral slope from spectral noise at higher wavelengths.

For the 11 observations of Eros we calculate a nominal least-squares linear fit of Near-Infrared Spectral Slope (NISS) = $(0.005 \pm 0.001) \times \alpha + (0.180 \pm 0.053)$ with $R^2 = 0.530$. We find a least-squares linear fit for the 11 observations of Ganymed of NISS = $(0.002 \pm 0.001) \times \alpha + (0.096 \pm 0.024)$ with $R^2 = 0.302$. We find a least-squares linear fit for the 7 observations of Ivar of NISS = $(0.002 \pm 0.002) \times \alpha + (0.231 \pm 0.036)$ with $R^2 = 0.186$.

Each of the three datasets has a single datapoint that lies far from the nominal correlation (Fig. 4). We also calculate each correlation without the single outlying datapoint. For Eros the outlying point is from the MIT Joint Campaign (sp105 on 28 December 2011). Without that observation we calculate a least-squares linear fit of NISS = $(0.004 \pm 0.001) \times \alpha + (0.197 \pm 0.018)$ with $R^2 = 0.867$. For Ganymed the outlying point is from the ExploreNEOs survey on 17 September 2011. Without the outlying observation we calculate a least-squares linear fit of NISS = $(0.001 \pm 0.001) \times \alpha + (0.107 \pm 0.15)$ with $R^2 = 0.099$. The outlying point for Ivar is from the MIT Joint Campaign (sp77 on 27 January 2009). Without this outlying observation we calculate a least-squares linear fit of NISS = $(0.002 \pm 0.001) \times \alpha(0.237 \pm 0.019)$ with $R^2 = 0.661$. The R^2 values improve for Eros and Ivar when the outlying points are removed.

We find evidence for phase reddening for all three objects. Fig. 4 shows the correlations for Eros, Ganymed, and Ivar. The solid lines indicate the nominal correlations and the dashed lines indicate the correlations calculated without the outlying points.

3.5. Ordinary chondrite-like mineralogies

A subset of the olivine–pyroxene mixtures represented in the Band I Center versus Band Area Ratio diagram represent mineralogies consistent with the ordinary chondrites. We identify the potential ordinary chondrites via two methods. First, we use the S(IV) region defined by Gaffey et al. (1993) to include the mineralogical assemblages typical of ordinary chondrites. Fig. 1d shows the Gaffey S(IV) region and the S(IV) objects that were identified in our sample. This region, and similarly shaped regions, have been used by various other studies. For example, Dunn et al. (2010) used the S(IV) region defined by Gaffey et al. (1993) to determine the potential ordinary chondrites and de León et al. (2010) identified ordinary chondrite-like objects by calculating a similar, but slightly larger, region using the spectral band parameters of ordinary chondrite spectra. We identify S(IV) objects by first selecting all objects with data and error bars wholly within the S(IV) subclass. Objects in the nearby S(III) region and with lower Band I Centers than the S(IV) region are included if the datum is close to the boundary and at least half of the associated error bar falls within the S(IV) region. We include some objects with higher Band I Centers than the S(IV) region if the datum and error fall wholly outside of all other Gaffey regions.

We established these generous selection criteria to allow for the possible shift in BAR due to phase angle effects. All spectra of Eros and Itokawa that are not selected by this procedure are added to the sample due to the confirmed ordinary chondritic nature of these asteroids (e.g. Trombka et al., 2000; Nakamura et al., 2011; Foley et al., 2006). Some of the Eros and Itokawa spectra fall in the S(III) region to the left of the S(IV) region. For Eros this is consistent with the S(III) and S(IV) spectra observed with the near-infrared spectrometer on the Near Earth Asteroid Rendezvous (NEAR) mission (Bell et al., 2002).

The second method used to identify potential ordinary chondrite analogues is by calculating the BIC–BAR regions that correspond to the Dunn et al. (2010) ordinary chondrite mineralogies. Dunn et al. (2010) used laboratory derived values of Fayalite (Fa, the iron-rich end member of the olivine solid solution series), Ferrosilite (Fs, the iron-rich end member of the pyroxene solid solution series), and olivine/(olivine + pyroxene) in 48 equilibrated ordinary chondrites to define regions (with and without errors) for the H, L, and LL ordinary chondrites. The derived mineralogies and spectral band parameters for the same 48 ordinary chondrites enabled Dunn et al. (2010) to calculate the relationships between the mineralogical parameters (Fa, Fs, and ol/(ol + px)) and the spectral parameters (BIC and BAR). We use the defined H, L, and LL or-
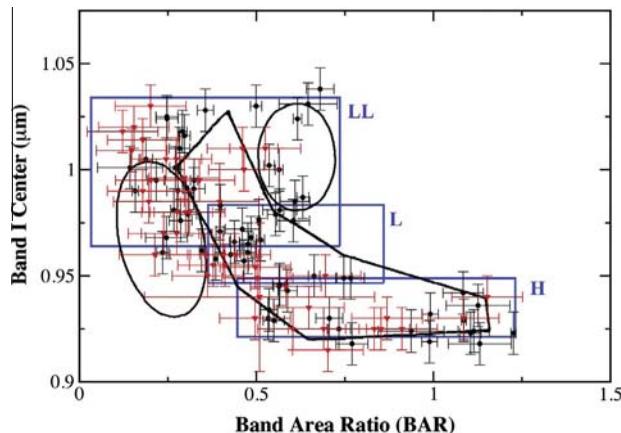
Fig. 5. Our second method of identifying potential ordinary chondrites uses the Dunn ordinary chondrite regions calculated from the ranges of mineralogies determined in Dunn et al. (2010). We calculated the regions in Band I Center-Band Area Ratio space and used the regions to determine potential ordinary chondrite types. Each ordinary chondrite region is labeled with its type. The Gaffey S(III) and S(IV) regions are included for comparison. The L and H regions closely approximate the S(IV) region, but the LL region is much larger than the corresponding subset of the S(IV) region. The Dunn LL region includes most of the Gaffey S(III) regions.

dinary chondrite regions to determine the corresponding region in B1C–BAR space. Objects are selected as potential ordinary chondrites if the datum is inside one of the three regions or if at least half of the corresponding error bar enters one of the regions. Fig. 5 shows the three ordinary chondrite type regions compared to the S(IV) region and includes all the objects determined to be ordinary chondrite-like via this method. All of the objects inside the Gaffey S(IV) region are included as a subset of the Dunn region objects. Using this method, all observations of Eros and Itokawa are automatically included in the sample. The Dunn et al. (2010) H and L regions are reasonably consistent with the Gaffey S(IV) region. However, the LL region is much larger than the S(IV) region and includes the majority of the S(III) region which Gaffey et al. (1993) suggests contains different meteorite analogs (urelites).

We calculate the mineralogies for all of our potential ordinary chondrites identified via both the S(IV) region and the Dunn regions using the following three equations from Dunn et al. (2010):

$$\text{ol}/(\text{ol} + \text{px}) = -0.242 \times \text{BAR} + 0.728 \qquad (13)$$

$$\text{Fa (mol\%)} = -1284.9 \times (\text{BIC})^2 + 2656.5 \times (\text{BIC}) - 1342.3 \qquad (14)$$

$$\text{Fs (mol\%)} = -879.1 \times (\text{BIC})^2 + 1824.9 \times (\text{BIC}) - 921.7 \qquad (15)$$

ol/(ol + px) is a modal ratio of olivine to olivine and pyroxene. Fa is the amount (in mol%) of fayalite and Fs is the amount (in mol%) of ferrosilite. The root mean square errors presented by Dunn et al. (2010) are 0.03 for ol/(ol + px), 1.3 mol% for Fa, and 1.4 mol% for Fs.

We classify each of our potential ordinary chondrite analogs into a subtype using the Dunn et al. (2010) ordinary chondrite mineralogy regions with errors included (Fig. 5). The regions available for analysis are Fa (mol%) with respect to ol/(ol + px) and Fs (mol%) with respect to ol/(ol + px). We classify each object in both of these regimes to determine our final classification. Each object is determined to be a type if it falls within a region that is unique to a specific ordinary chondrite type. Objects that fall in the overlap regions are classified as potentially belonging to either class. In both regimes, there are several outliers near the H and LL ordinary chondrite regions. These are potentially not ordinary chondrite analogues and are classified as "H?" and "LL?". These are the
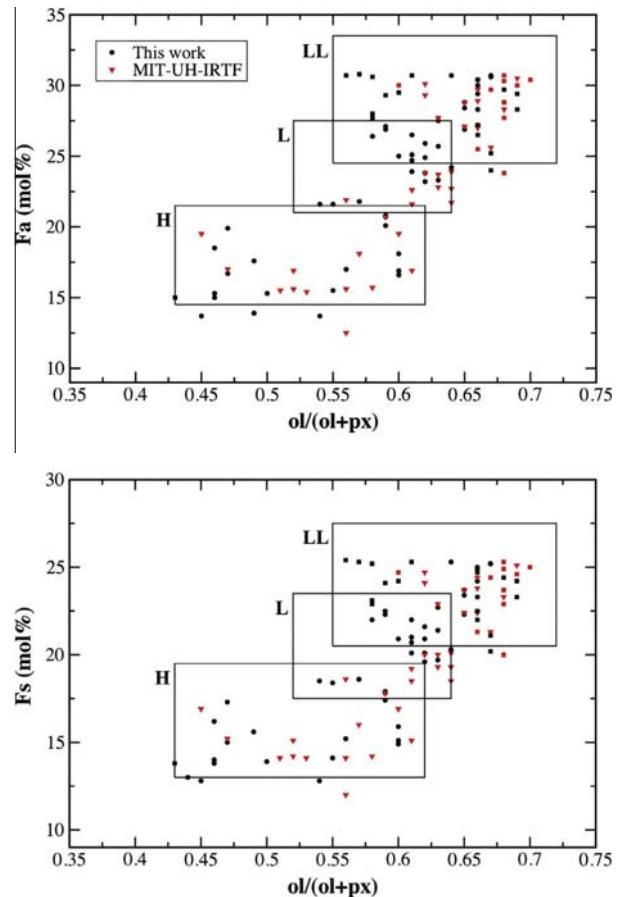
Fig. 6. We use the Dunn et al. (2010) equations to derive the mol% of Fayalite (Fa) and Ferrosilite (Fs) and olivine/(olivine + pyroxene) ratio from band parameters of ordinary chondrite-like spectra. The nominal errors on the chemistry calculations are 0.03 for the ol/(ol + px) calculation, 1.3 for the calculation of the mol% of Fa, and 1.4 for the calculation of mol% of Fs. The top panel shows mol% Fayalite versus ol/(ol + px). The bottom panel shows mol% of Ferrosilite versus ol/(ol + px). We determine a potential ordinary chondrite subtype (H, L, LL) based on the location of the objects in each of these compositional regions. The quadratic equations impose an artificial upper limit on Fayalite and Ferrosilite within the LL ordinary chondrite subclass that can be clearly seen.

objects whose BIC–BAR data placed them outside of the defined regions, but whose error bars did not allow for exclusion from the sample. In order to be conservative, the final classification given is the least certain of the two classifications. For example, if one calculation is H, but another is H/L, then the final classification is H/L. Fig. 6 displays the ordinary chondrite mineralogies of our selected objects. Objects in the Gaffey S(IV) sample are shown with black circles (this ExploreNEOs survey) or red[5] triangles (MIT Joint Campaign). As mentioned previously, all S(IV) objects are a subset of the Dunn regions sample. The Dunn classified objects that are not part of the S(IV) sample are displayed as squares and use the same color scheme to differentiate between this survey and the MIT Joint Campaign. The ordinary chondrite mineralogies calculated often identify Eros and Itokawa as LL ordinary chondrites. This suggests that, at least for the high signal-to-noise objects, this method is a reliable indicator of object composition. Objects with ordinary chondrite-like spectra, their mineralogies, and ordinary chondrite subtype analogs are listed in Tables 5 and 6.

---

[5] For interpretation of color in Fig. 6, the reader is referred to the web version of this article.

Table 5

Calculated mineralogies and ordinary chondrite types for all potential ordinary chondrite types in the ExploreNEOs spectral survey. Potential ordinary chondrites were determined using the S(IV) region and the Dunn et al. (2010) ordinary chondrite regions. Since the objects in S(IV) region are a subset of the Dunn classified objects, they are listed first. The table includes object number, object name, spectral type, corrected Band I Center (ΔBIC), corrected Band Area Ratio (ΔBAR), olivine/(olivine + pyroxene), Mol % of Fayalite (Fa), Mol % of Ferrosilite (Fs), ordinary chondrite type using Fa - ol/(ol + px), ordinary chondrite type using Fsol/(ol + px), and the final ordinary chondrite type classification using the least certain of the two classifications.

Number	Name	Type	ΔBIC	ΔBAR	ol/(ol + px)	Fa	Fs	OC type Fa	OC type Fs	OC type
S(IV)										
433	Eros	Q/Sq	0.962	0.345	0.64	24.2	20.3	L	L	L
433	Eros	Q/Sq	0.976	0.507	0.61	26.5	22.0	L/LL	L/LL	L/LL
433	Eros	Sq/Q	0.983	0.398	0.63	27.5	22.7	L/LL	L/LL	L/LL
433	Eros	Q/Sq	0.995	0.324	0.65	28.8	23.7	LL	LL	LL
1036	Ganymed	Sr/S	0.919	0.989	0.49	13.9	13.0	H?	H	H?
1036	Ganymed	Sr	0.929	1.086	0.47	16.7	15.0	H	H	H
1865	Cerberus	S	0.930	0.533	0.60	16.9	15.1	H	H	H
1866	Sisyphus	S	0.929	0.549	0.60	16.6	14.9	H	H	H
1866	Sisyphus B	S	0.932	0.991	0.49	17.6	15.6	H	H	H
1866	Sisyphus D	S	0.918	1.131	0.45	13.7	12.8	H?	H?	H?
1866	Sisyphus F	S	0.918	0.770	0.54	13.7	12.8	H?	H?	H?
1917	Cuyo	Sr	0.925	0.733	0.55	15.5	14.1	H	H	H
4283	Cuno	Sq/Q	0.979	0.554	0.59	26.9	22.3	L/LL	L/LL	L/LL
5143	Heracles	Q	1.016	0.297	0.66	30.4	24.9	LL	LL	LL
5626	1991 FE	Sq	0.943	0.588	0.59	20.1	17.4	H	H	H
5646	1990 TR	Q	1.025	0.247	0.67	30.7	25.2	LL	LL	LL
7358	Oze	S	0.924	1.114	0.46	15.3	14.0	H	H	H
11066	Sigurd	Sr	0.923	1.105	0.46	15.0	13.8	H	H	H
12711	Tukmit	Q	0.979	0.307	0.65	26.9	22.3	LL	LL	LL
12923	Zephyr	S	0.942	1.084	0.47	19.9	17.3	H	H	H
16834	1997 WU22	Sq	0.961	0.476	0.61	23.9	20.1	L	L	L
19764	2000 NF5	Sq	0.971	0.397	0.63	25.7	21.4	L/LL	L/LL	L/LL
27346	2000 DN8	Q	1.028	0.356	0.64	30.7	25.3	LL	LL	LL
36284	2000 DM8	Sq	1.018	0.291	0.66	30.4	25.0	LL	LL	LL
53789	2000 ED104	Sq	0.949	0.766	0.54	21.6	18.5	L	H/L	H/L
68216	2001 CV26	Sq	0.934	0.536	0.60	18.1	15.9	H	H	H
68216	2001 CV26	S/Sq	0.949	0.747	0.55	21.6	18.4	L	H/L	H/L
68216	2001 CV26	Sq	0.960	0.427	0.62	23.8	20.1	L	L	L
85839	1998 YO4	Q	1.001	0.271	0.66	29.4	24.2	LL	LL	LL
86067	1999 RM28	Q	0.966	0.438	0.62	24.9	20.9	L/LL	L/LL	L/LL
88254	2001 FM129	Q	0.976	0.604	0.58	26.4	22.0	L/LL	L/LL	L/LL
100926	1998 MQ	Q	0.945	0.564	0.59	20.7	17.8	H	H/L	H/L
137032	1998 UO1	Sq	0.968	0.485	0.61	25.1	21.0	L/LL	L/LL	L/LL
137062	1998 WM	Sq	0.930	0.706	0.56	17.0	15.2	H	H	H
138883	2000 YL29	Q	0.958	0.385	0.63	23.3	19.7	L	L	L
141498	2002 EZ16	Sq	0.967	0.512	0.60	25.0	20.9	L/LL	L/LL	L/LL
143381	2003 BC21	Sr/S	0.924	0.937	0.50	15.3	13.9	H	H	H
152931	2000 EA107	Q	1.010	0.283	0.66	30.0	24.7	LL	LL	LL
159402	1999 AP10	Sq	0.950	0.663	0.57	21.8	18.6	L	H/L	H/L
163697	2003 EF54	Q	0.965	0.476	0.61	24.7	20.7	L/LL	L/LL	L/LL
207945	1991 JW	Q	0.991	0.323	0.65	28.4	23.4	LL	LL	LL
214088	2004 JN13	Sq	0.981	0.566	0.59	27.1	22.5	L/LL	L/LL	L/LL
218863	2006 WO127	Sq	0.990	0.278	0.66	28.3	23.3	LL	LL	LL
219071	1997 US9	Q	1.024	0.248	0.67	30.6	25.2	LL	LL	LL
220124	2002 TE66 B	Sq	0.957	0.465	0.62	23.2	19.6	L	L	L
265187	2003 YS117	Q	0.972	0.460	0.62	25.9	21.6	L/LL	L/LL	L/LL
297418	2000 SP43	V	0.936	1.126	0.46	18.5	16.2	H	H	H
	2000 TJ1	Sq	0.946	0.566	0.59	20.8	17.9	H	H/L	H/L
Dunn regions										
1036	Ganymed	Sr	0.923	1.226	0.43	15.0	13.8	H	H	H
1627	Ivar	S	1.024	0.616	0.58	30.6	25.2	LL	LL	LL
1943	Anteros	Sq	0.987	0.631	0.58	28.0	23.1	LL	L/LL	L/LL
3122	Florence	Sq/Q	1.030	0.499	0.61	30.7	25.3	LL	LL	LL
6239	Minos	Q/Sq	0.981	0.267	0.66	27.2	22.5	LL	LL	LL
8567	1996 HW1	Q	1.002	0.536	0.60	29.5	24.2	LL	LL	LL
23187	2000 PN9	Sq	1.031	0.646	0.57	30.8	25.3	LL	LL	LL
39572	1993 DQ1	Q	0.985	0.609	0.58	27.7	22.9	LL	L/LL	L/LL
96590	1998 XB	Sq	1.000	0.564	0.59	29.3	24.1	LL	LL	LL
137125	1999 CT3	Q	1.038	0.680	0.56	30.7	25.4	LL	LL	LL
141498	2002 EZ16	Sq	0.990	0.158	0.69	28.3	23.3	LL	LL	LL
198856	2005 LR3	Sq	0.995	0.217	0.68	28.8	23.7	LL	LL	LL
198856	2005 LR3	Q	1.005	0.188	0.68	29.7	24.4	LL	LL	LL
207945	1991 JW	Q	1.001	0.143	0.69	29.4	24.2	LL	LL	LL
220124	2002 TE66 A	Sq/Q	0.976	0.286	0.66	26.5	22.0	LL	LL	LL
347813	2002 NP1	Q	0.961	0.235	0.67	24.0	20.2	LL?	LL?	LL?
	2001 HC	Sq	0.968	0.246	0.67	25.2	21.1	LL	LL	LL

Table 6
Calculated mineralogies and ordinary chondrite types for all potential ordinary chondrite types for ExploreNEOs objects in the MITJoint Campaign. As with Table 5, the S(IV) objects are listed first. The table includes the same parameters as Table 5.

Number	Name	Type	ΔBIC	ΔBAR	ol/(ol + px)	Fa	Fs	OC type Fa	OC type Fs	OC type
S(IV)										
433	Eros	Sw	0.950	0.362	0.64	21.7	18.5	L	L	L
433	Eros	Sw	0.955	0.378	0.64	22.7	19.3	L	L	L
433	Eros	Sw	0.960	0.440	0.62	23.8	20.0	L	L	L
433	Eros	Sw	0.980	0.276	0.66	27.1	22.4	LL	LL	LL
433	Eros	Sw	0.990	0.179	0.68	28.3	23.3	LL	LL	LL
433	Eros	Sw	0.995	0.339	0.65	28.8	23.7	LL	LL	LL
433	Eros	Sqw	1.020	0.154	0.69	30.5	25.1	LL	LL	LL
1036	Ganymed	S	0.925	0.690	0.56	15.6	14.1	H	H	H
1036	Ganymed	S	0.930	0.869	0.52	16.9	15.1	H	H	H
1627	Ivar	Sr	0.949	0.503	0.61	21.6	18.5	H/L	H/L	H/L
1627	Ivar	S	0.954	0.497	0.61	22.6	19.2	L	H/L	H/L
1916	Boreas	Sw	0.955	0.411	0.63	22.8	19.3	L	L	L
1917	Cuyo	Sv	0.940	1.152	0.45	19.5	16.9	H	H	H
3102	Krok	Sqw	1.000	0.465	0.62	29.3	24.1	LL	LL	LL
5587	1990 SB	Sr	0.925	0.911	0.51	15.5	14.1	H	H	H
5626	1991 FE	S	0.930	0.496	0.61	16.9	15.1	H	H	H
6455	1992 HE	Srw	0.935	0.648	0.57	18.1	16.0	H	H	H
6455	1992 HE	Sqw	0.980	0.300	0.66	27.0	22.4	LL	LL	LL
11066	Sigurd	S	0.925	0.833	0.53	15.4	14.1	H	H	H
11398	1998 YP11	Sr	0.925	0.603	0.58	15.7	14.2	H	H	H
15745	1991 PM5	S	0.945	0.583	0.59	20.7	17.8	H	H/L	H/L
16834	1997 WU22	S	0.960	0.406	0.63	23.7	20.0	L	L	L
25143	Itokawa	Sqw	0.970	0.238	0.67	25.6	21.3	LL	LL	LL
35107	1991 VH	Sq	0.980	0.311	0.65	27.1	22.4	LL	LL	LL
36284	2000 DM8	Sq	0.985	0.396	0.63	27.7	22.9	LL	L/LL	L/LL
53435	1999 VM40	Srw	0.930	1.085	0.47	17.0	15.2	H	H	H
54690	2001EB	S	0.940	0.509	0.60	19.5	16.9	H	H	H
89355	2001 VS78	Sr	0.925	0.852	0.52	15.6	14.2	H	H	H
137062	1998 WM	Sr	0.915	0.702	0.56	12.5	12.0	H?	H?	H?
138258	2000 GD2	Sq	1.010	0.461	0.62	30.1	24.7	LL	LL	LL
141052	2001 XR1	Sq	0.960	0.356	0.64	23.9	20.1	L	L	L
143651	2003 QO104	Q	0.996	0.296	0.66	28.9	23.8	LL	LL	LL
152931	2000 EA107	Q	1.005	0.274	0.66	29.7	24.4	LL	LL	LL
200840	2001 XN254	S	0.950	0.695	0.56	21.9	18.6	L	H/L	H/L
Dunn regions										
1627	Ivar	Sqw	0.960	0.213	0.68	23.8	20.0	LL?	LL?	LL?
1943	Anteros	S	1.010	0.525	0.60	30.0	24.7	LL	LL	LL
4183	Cuno	Q	1.014	0.179	0.68	30.3	24.9	LL	LL	LL
5131	1990 BG	Sq	1.018	0.122	0.70	30.4	25.0	LL	LL	LL
5143	Heracles	Q	1.009	0.148	0.69	30.0	24.6	LL	LL	LL
6239	Minos	Sq	0.985	0.196	0.68	27.7	22.9	LL	LL	LL
8567	1996 HW1	Q	0.995	0.202	0.68	28.8	23.7	LL	LL	LL
35107	1991 VH	Sq	1.005	0.245	0.67	29.7	24.4	LL	LL	LL
207945	1991 JW	Sq/Q	0.970	0.275	0.66	25.5	21.3	LL	LL	LL
219071	1997 US9	Q	1.030	0.201	0.68	30.7	25.3	LL	LL	LL

We have a total of 82 objects in the Gaffey S(IV) sample, which breaks down into 4.9% "H?", 29.3% H, 11.0% H/L, 13.4% L, 14.6% L/LL, and 26.8% LL. The sample determined using the Dunn ordinary chondrite regions contains 109 objects and breaks down into 3.7% "H?", 22.9% H, 8.3% H/L, 10.1% L, 12.8% L/LL, 40.4% LL, and 1.8% "LL?". We discuss the sample statistics and the comparison to the meteorite population in Section 4.

3.6. Spectral variation: Sisyphus and Cuyo

As part of the survey, we obtained rotationally resolved spectra of two near-Earth Asteroids: (1866) Sisyphus and (1917) Cuyo. Sisyphus was observed once on 1 May 2011, in six sequential observations on 10 June 2011, and in three sequential observations on 24 June 2011. Cuyo was observed in six sequential observations on 24 June 2011 and once on 14 August 2011. Fig. 7 shows Band I Center for Sisyphus (top panel) and Cuyo (bottom panel) for our sequences of observations. The x-axis is not directly correlated with time. Each set of observations are connected and presented sequentially. Additional observations for each object are offset along the x-axis.

The Band I Centers of the Sisyphus spectra vary from 0.915 to 0.932 μm among the ten observations, implying that the amounts of fayalite and ferrosilite vary across the surface. While the variations are not greater than the errors associated with the BICs, it should be noted that the errors on BIC are artificially limited to be equal to or greater than 0.01. This error limit accounts for many unquantified sources of error, but this limit is much higher than the nominal Sisyphus BIC errors which are ~0.001–0.002. The nominal errors are low due to the high signal-to-noise of the observations that also enable us to separate the observations into rotationally resolved components instead of requiring the co-addition of the frames over the rotating body. The low nominal errors suggest that Sisyphus likely contains compositional changes over its surface. The variation corresponds to the difference between the S(VII) region (for the 0.915 μm BIC) and the S(IV) region with H chondrite mineralogy (for the 0.932 μm BIC).
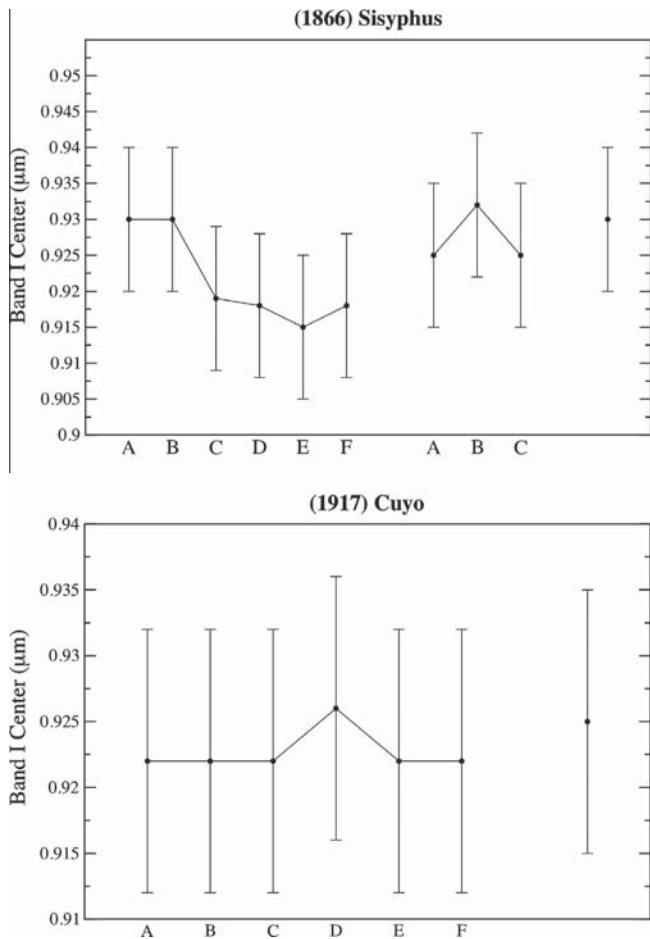
Fig. 7. Band I Center for Sisyphus (top panel) and Cuyo (bottom panel) for our sequences of observations. The x-axis is not directly correlated with time. Each set of observations is connected and presented sequentially. Additional observations for each object are offset in x. We see potential compositional variation on the surface of Sisyphus. Any variation is within the errors, but we set a hard minimum on the errors in order to better include several unquantified sources of error. The differences in BIC exceed the nominal calculated errors for the observations. Cuyo does not show indications of compositional variation on the surface.

Cuyo shows a much smaller variation in Band I Center from 0.922 to 0.926 μm. These BICs are also presented with the error limit of 0.01. Even within the low nominal Cuyo BIC errors (~0.001–0.002, similar to those of Sisyphus), there is no evidence for compositional variation across the surface of Cuyo.

4. Discussion

We found no correlation between albedo and Band I Center. The absence of a correlation could be due to the large uncertainties in the ExploreNEOs albedo calculations (±50%, Harris et al., 2011). Other datasets should be used to confirm the lack of a relationship between these parameters before it is concluded that another process, such as space weathering or regolith evolution, is masking the nominal albedo of the grains.

Our investigation of the relationship between phase angle and Band Area Ratio for (433) Eros, (1036) Ganymed, and (1627) Ivar confirms the phase angle–BAR correlations seen in Sanchez et al. (2012). The Sanchez et al. (2012) sample contained only two or three observations for each object and most correlations were flat or slightly negative in slope. Our results for Eros (11 spectra) and Ivar (7 spectra) show similarly negative slopes. Ganymed is an exception in both our ExploreNEOs sample and in the Sanchez

et al. work with a positive slope that correlates increasing BAR with increasing phase angle. There is no *a priori* reason to expect the optical properties of Ganymed to be different than other objects. All three objects investigated in this work are classified as potential ordinary chondrites in our analysis. One difference of note that separates Ganymed from Eros and Ivar is the higher calculated BARs. This leads to Ganymed's classification as a potential H chondrite while Eros is often correctly identified as an LL chondrite (e.g. Trombka et al., 2000; McCoy et al., 2001) and Ivar has band parameters associated with a range of potential ordinary chondrite types. While the BARs calculated for Ganymed are much larger than those of Eros and Ivar, Sanchez et al. (2012) presents band parameters of one other object at similar BAR, (4954) Eric, which shows a nearly flat, slightly negative correlation. This object also has band parameters correlating to classification as a potential H chondrite. Therefore, it is unlikely that the differing slopes can be solely attributed to the compositions associated with the higher BARs calculated for Ganymed and Eric. Additional studies of the phase angle–BAR relationship should focus on examining objects with a variety of BARs. The Sanchez et al. (2012) sample had 12 different objects and 10 of those had BARs less than or equal to ~0.6. Another possible explanation is that Ganymed is much larger than many other NEOs (D = 35.01 km, Usui et al., 2011). The variations observed in the BARs for Ganymed could be partially attributed to compositional heterogeneities on the surface. The potential for large objects to display surface heterogeneity does not apply to Eros, which displays spectral homogeneity that was observed during the Near-Earth Asteroid Rendezvous (NEAR) mission (Bell et al., 2002).

Our 11 near-infrared spectra of Ganymed suggest compositional heterogeneity on the surface. Five of the Ganymed spectra are classified as potential H chondrites. The other six fall either in the region with lower BIC than the S(IV) region (outside of any S subclass region), in the S(VI) region, or in the S(VII) region. Fieber-Beyer et al. (2011) classified Ganymed as S(VI) and suggested that it was a mesosiderite analog containing HED pyroxenes and NiFe metal. Our analysis does not confirm this result. If the entire range of mineralogies suggested by our band parameters exist on Ganymed, it is possible that the Fieber-Beyer et al. (2011) spectrum observed only the S(VI)-type surface assemblages since their observations were taken in a time period (3.6 h) shorter than the rotational period of Ganymed (10.31 h, Skiff et al., 2012).

The Dunn et al. (2010) equations for olivine and pyroxene chemistry used in Section 3.5 are quadratic. Unfortunately, the local maxima for both the fayalite and ferrosilite equations are within the range of laboratory derived chemistries of the LL ordinary chondrite. This implies that there is a range of fayalite and ferrosilite values that exists in the ordinary chondrite population, but will never be predicted by the Dunn et al. (2010) equations. The maximum calculable value for fayalite is ~30.76 which corresponds to a Band I Center of 1.034 and the maximum calculable value for ferrosilite is ~25.37 which corresponds to a Band I Center of 1.038. This upper limit falls within the true LL ordinary chondrite region, not the larger region that includes the root square mean errors associated with spectrally derived values that is used in our analysis. The artificial limit caused by the turnover of the fayalite and ferrosilite equations is clear in Fig. 6 and does not appear to affect our ordinary chondrite class assignments. However, we note that the limit causes an artificial enhancement of objects with similar fayalite and ferrosilite values near the limit and an artificial dearth of objects with fayalite and ferrosilite values above the limit.

One large unanswered question in the study of the compositions of near-Earth objects is the apparent mismatch between the relative proportions of the ordinary chondrite subclasses (H, L, LL) seen in meteorite falls compared to the relative proportions of the ordinary chondrite subclass analogues observed spectro-

scopically in near-Earth space. Burbine et al. (2002) calculate that the H, L, and LL ordinary chondrites are 34.1%, 38.0%, and 7.9% of all meteorite falls, respectively. This corresponds to H, L, and LL ordinary chondrites being 42.6%, 47.5%, and 9.8% of ordinary chondrite falls. However, the majority of near-Earth asteroids that are ordinary chondrite analogs have spectra consistent with LL chondrite mineralogies (e.g. Vernazza et al., 2008). The analysis of the 47 NEOs with ordinary chondrite compositions by Dunn et al. (2013) found that H, L, and LL ordinary chondrite analogs are 15%, 10%, and 60%, respectively, with objects that could not be distinguished between L and LL accounting for 15%. de León et al. (2010) showed that the concentration of BAR and BIC values in the NEO population is consistent with a more significant presence of olivine in NEOs compared to Main Belt objects (see Fig. 5 of de León et al. (2010)). This concentration mostly occupies the LL ordinary chondrite region.

The 82 objects from our sample that fall in the Gaffey S(IV) sample break down into 4.9% "H?", 29.3% H, 11.0% H/L, 13.4% L, 14.6% L/LL, and 26.8% LL. If we include the "H?" objects in the H chondrite group, the Gaffey S(IV) sample contains 34.1% potential H chondrites. The 109 objects from our sample in the Dunn ordinary chondrite regions sample break down into 3.7% "H?", 22.9% H, 8.3% H/L, 10.1% L, 12.8% L/LL, 40.4% LL, and 1.8% "LL?". If we include the "H?" and "LL?" objects into their respective groups, the Dunn sample contains 26.6% potential H chondrites and 42.2% potential LL chondrites. The relative proportions of the ordinary chondrites in our samples (the S(IV) and Dunn regions) are between the H and L chondrite dominant meteorite statistics (Burbine et al., 2002) and the LL chondrite dominant NEO statistics calculated by Dunn et al. (2013) and seen in Vernazza et al. (2008) and de León et al. (2010). Our samples have elevated percentages of potential LL ordinary chondrites compared to the meteorite fall statistics, but do not have values as high as the Dunn et al. (2013) sample. Similarly, we do not show the same concentration of NEOs in BIC–BAR space (near the LL ordinary chondrites) as was seen in de León et al. (2010). Instead we show a broader distribution of NEOs in BIC–BAR space. This suggests that our objects are more distributed over the possible mineralogies than previous surveys.

Our sample could be a step forward in finding the link between the meteorite population and previous NEO observations. However, there are no clear physical distinctions between our sample and the Dunn et al. (2013) sample that would explain the discrepancies between them. There are 13 objects that are present in both our sample and the Dunn et al. (2013) sample. Most ordinary chondrite classifications are consistent between the samples (there are two exceptions). One initial possibility was the sizes of the objects in each sample: small asteroids are the immediate precursors to meteorite falls and therefore should show mineralogies similar to meteorite falls. We can not directly compare diameters since not all of the objects in the Dunn et al. (2013) sample have thermal diameters. In order to be consistent, we compared the samples using H magnitudes from the Minor Planet Center as a proxy for diameter. The H magnitude ranges for both samples are nearly identical with a peak in the distribution around $H \sim 16$–17. Fig. 8 shows the histograms with the ExploreNEOs sample in blue and the Dunn et al. (2013) sample in green. The ExploreNEOs sample is clearly not sampling a smaller size regime than the Dunn et al. (2013) sample. We also compared the orbital elements of the objects in our survey to the objects in the Dunn et al. (2013) sample. There were no clear differences in semi-major axis (a), eccentricity (e), inclination (i), perihelion distance (q), or aphelion distance (Q).

It is important to note that some observations of Eros and Itokawa fall outside of the S(IV) region, but are included in the Dunn regions. Since these spectra have been observed with high signal-to-noise, this suggests that their positions outside of the S(IV) region are not due to spectral errors and are an accurate representa-
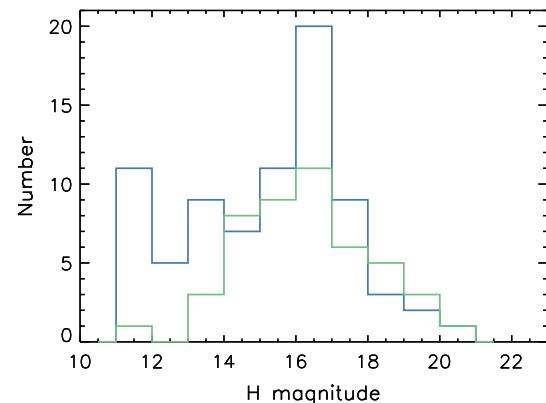
Fig. 8. We compared the distribution of H magnitudes (as a proxy for size) of our ExploreNEOs spectra to the spectral sample analyzed in Dunn et al. (2013) to determine if we were investigating different size regimes. We have different relative proportions of the ordinary chondrite types within our samples, which cannot be explained by differences in object sizes.

tion of the Band I Centers, Band Area Ratios, and the resulting mineralogy. Additionally, our spectral samples have several objects with multiple spectral observations (e.g. Ganymed). In several cases, only a subset of the spectra for each object are classified as ordinary chondrite analogues using the S(IV) region. When the larger Dunn region is considered, many of the spectra from these multiply observed objects that did not fall into the S(IV) region are also classified as ordinary chondrite analogues. Ganymed, 2002 EZ16, and 2002 TE66 are among the objects whose full set of observations were split between ordinary chondrite analogues and non-ordinary chondrite-like objects prior to the inclusion of the Dunn regions. This suggests that classification using the larger Dunn regions (or at minimum, some subset of them that is larger than the S(IV) region) is a valid way to identify potential ordinary chondrites.

It is clear that ordinary chondrite-like spectra can fall outside of the S(IV) region. However, it does not necessarily follow that the area outside the S(IV) region that is covered by the Dunn ordinary chondrite regions contains only ordinary chondrites. Gaffey et al. (1993) suggest that other mineralogies could be present in the regions labeled as S(III). The spectral signatures quantified by the band parameters used in this work are those caused by FeO. Other pyroxene and olivine chemistries that are not as well suited to band parameter analysis can overlap the ordinary chondrite regions in BIC–BAR space. For example, previous spectral studies (e.g. Gaffey et al., 1993; Sunshine et al., 2004) have cautioned that high-calcium pyroxene, a pyroxene variation that is not being measured by the Dunn equations, can affect the calculated band area ratios. If this BIC–BAR overlap in compositions is primarily in the LL ordinary chondrite region then it could help explain the over abundance of NEOs with LL ordinary chondrite-like compositions compared to the meteorite fall population.

5. Conclusions and future work

We have completed a ground-based near-infrared spectral survey of near-Earth objects in support of the ExploreNEOs Warm Spitzer project and complement our observations with near-infrared spectra of ExploreNEOs targets from the MIT Joint Campaign for NEO Spectral Reconnaissance. We report taxonomic classifications, spectral band parameters, and ordinary chondrite mineralogies for objects within our combined dataset of 340 observations of 187 targets. We find no correlation between spectral band parameters and ExploreNEOs albedos and diameters. This suggests that

various optical effects, such as space weathering, can change the nominal albedo expected from composition alone. Our analysis suggests that for spectra that contain near-infrared data but lack the visible wavelength region, the Bus–DeMeo system returns more apparent Q-types than exist in the NEO population. We find negative Band Area Ratio correlations with phase angle for (433) Eros and (1627) Ivar, but a positive Band Area Ratio correlation with phase angle for (1036) Ganymed, confirming the findings of Sanchez et al. (2012). We find evidence for spectral phase reddening for Eros, Ganymed, and Ivar. We identify ordinary chondrite subtypes for all potential ordinary chondrites in our sample using equations from Dunn et al. (2010). Our resulting proportions of H, L, and LL ordinary chondrites differ from those calculated for meteorite falls and in previous studies of ordinary chondrite-like NEOs.

One complementary investigation that has not been completed is a source region analysis for our various taxonomic types and ordinary chondrite types. Future work will use the source region model described in Bottke et al. (2002) to do a full source region analysis of the sample. We will also incorporate our visible wavelength observations that were not described in this paper.

Acknowledgments

Appendix A

We show our near-infrared spectroscopic observations from the SpeX component of our ExploreNEOs spectroscopy survey in Fig. 9. All spectra have been normalized to unity at 1-μm.
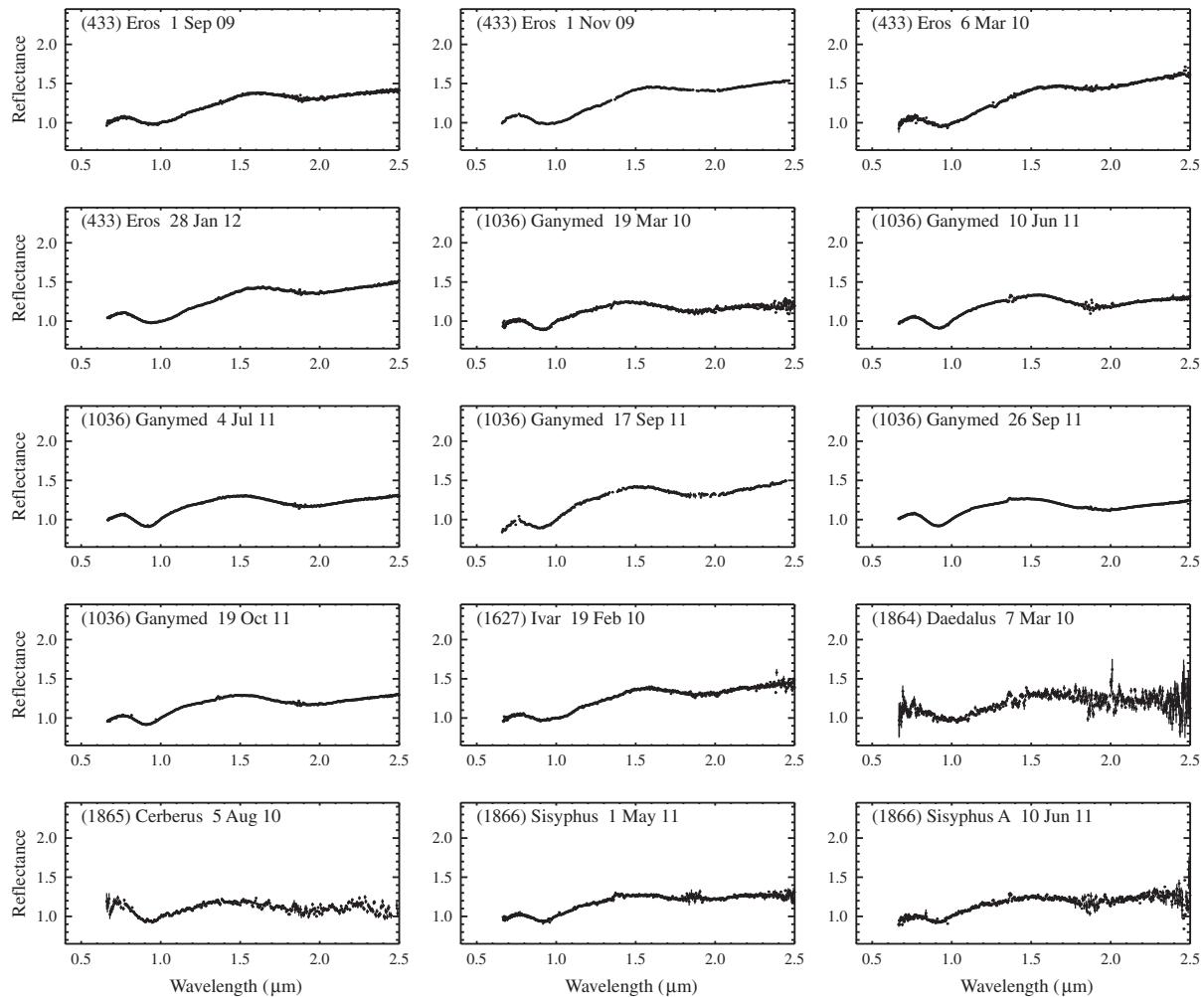
Fig. 9. This paper presents the near-infrared spectra observed at the NASA Infrared Telescope Facility (IRTF) using the SpeX instrument as part of the ExploreNEOs spectral survey. We include the spectra of all 125 observations of 92 ExploreNEOs targets. Each spectrum contains the object name and number, the UT date of observation, and, when appropriate, a letter designating the sequence order for all rotationally resolved observations. All spectra are normalized to unity at 1-μm.
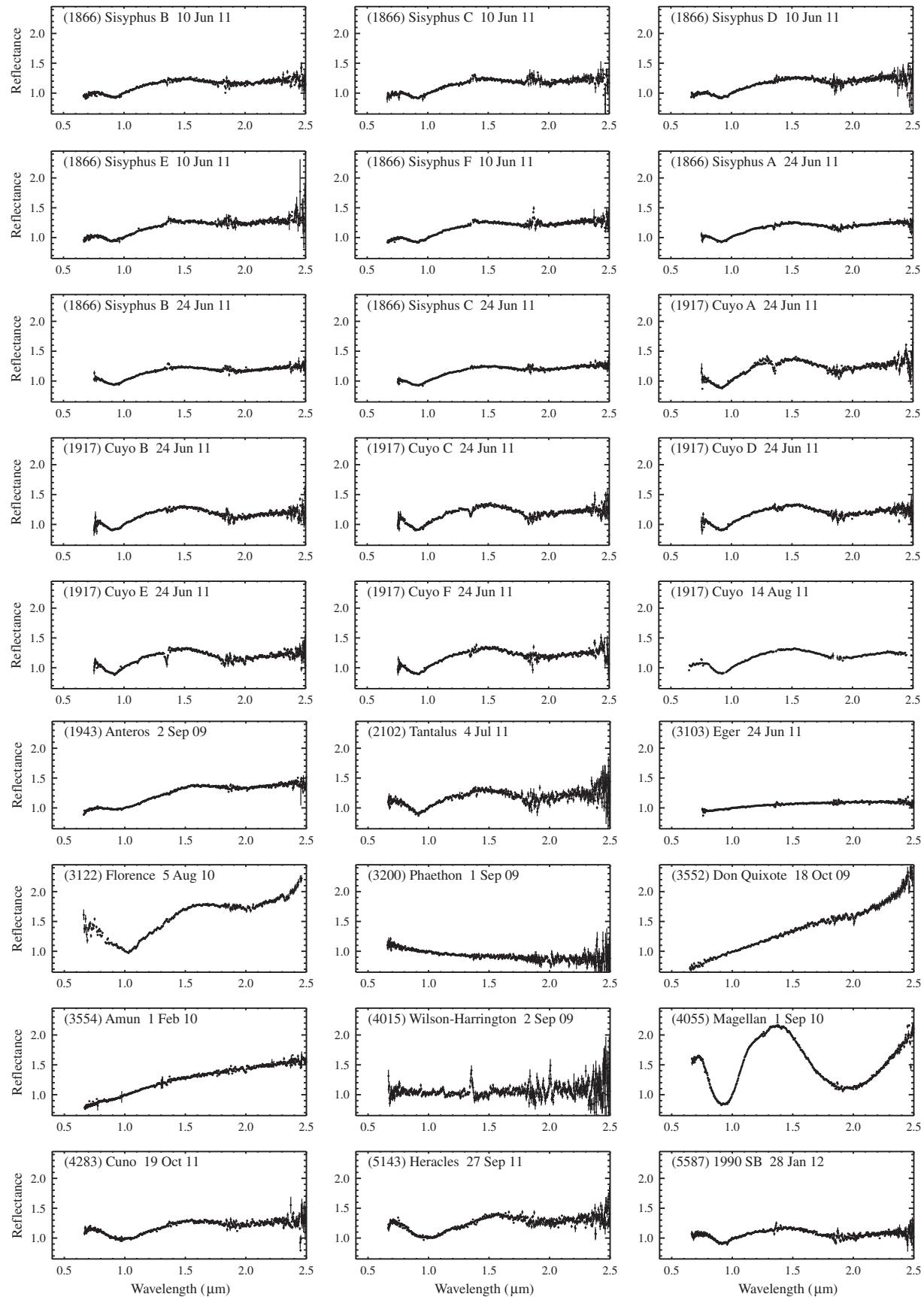
Fig. 9 (*continued*)
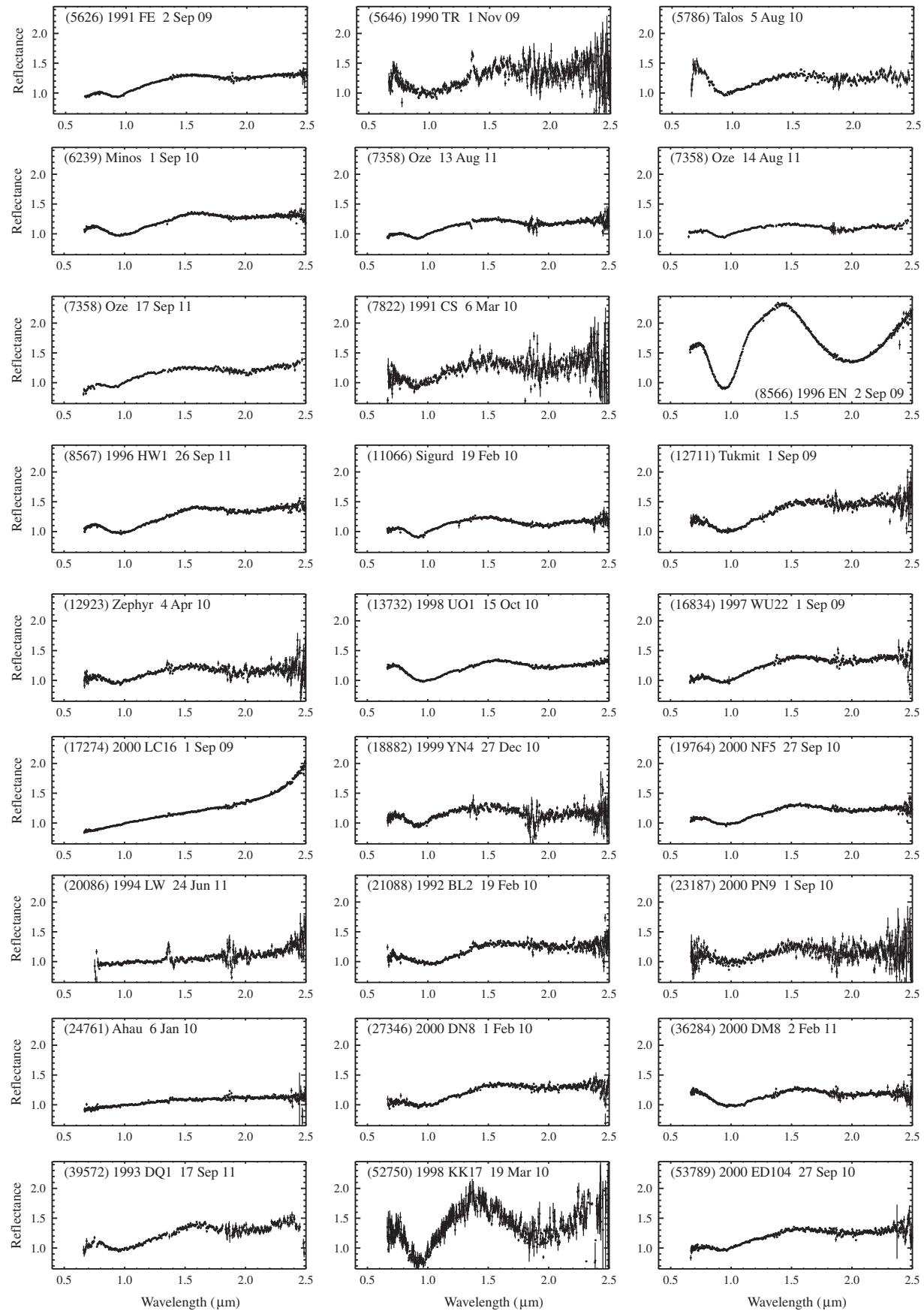
Fig. 9 (*continued*)
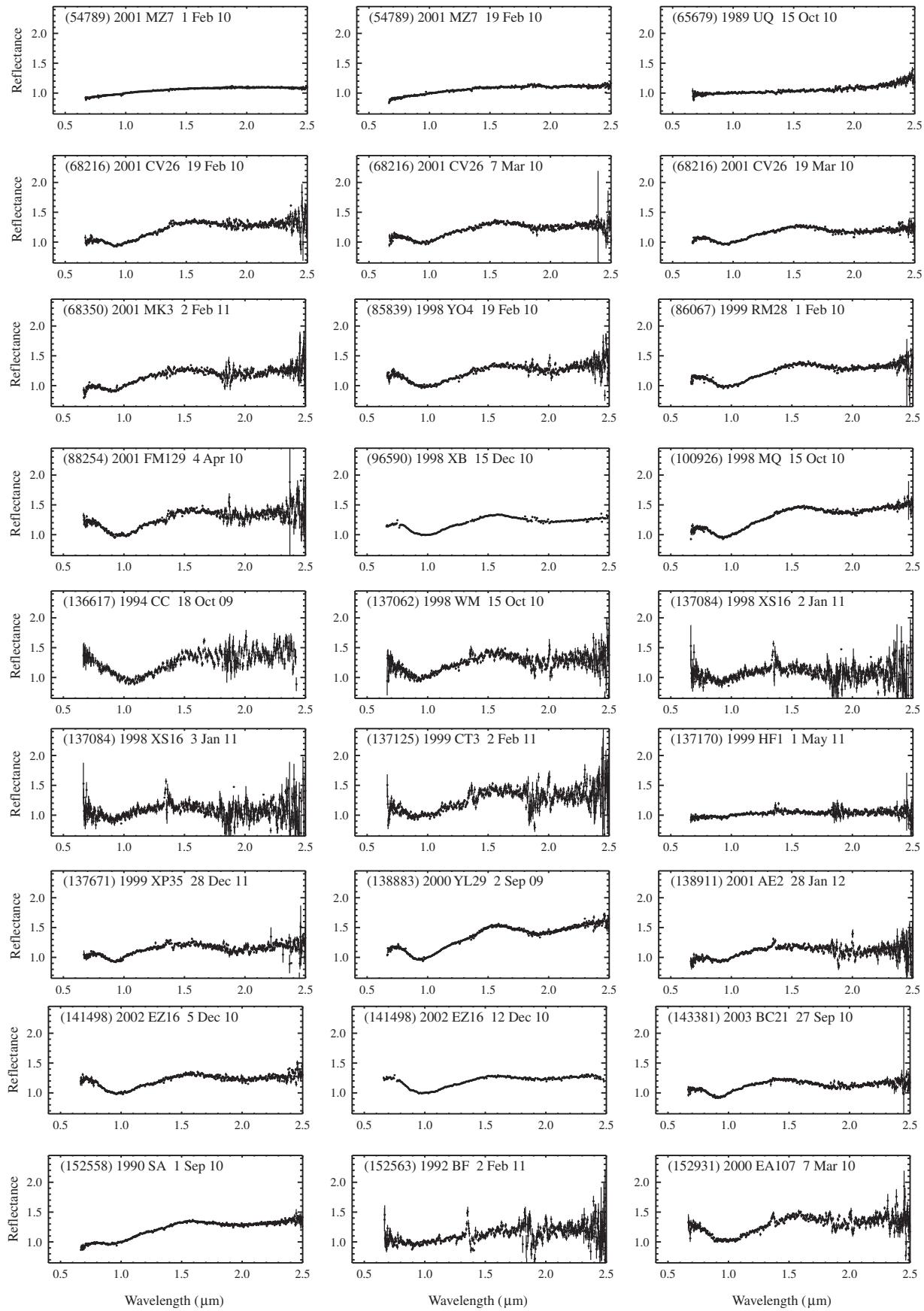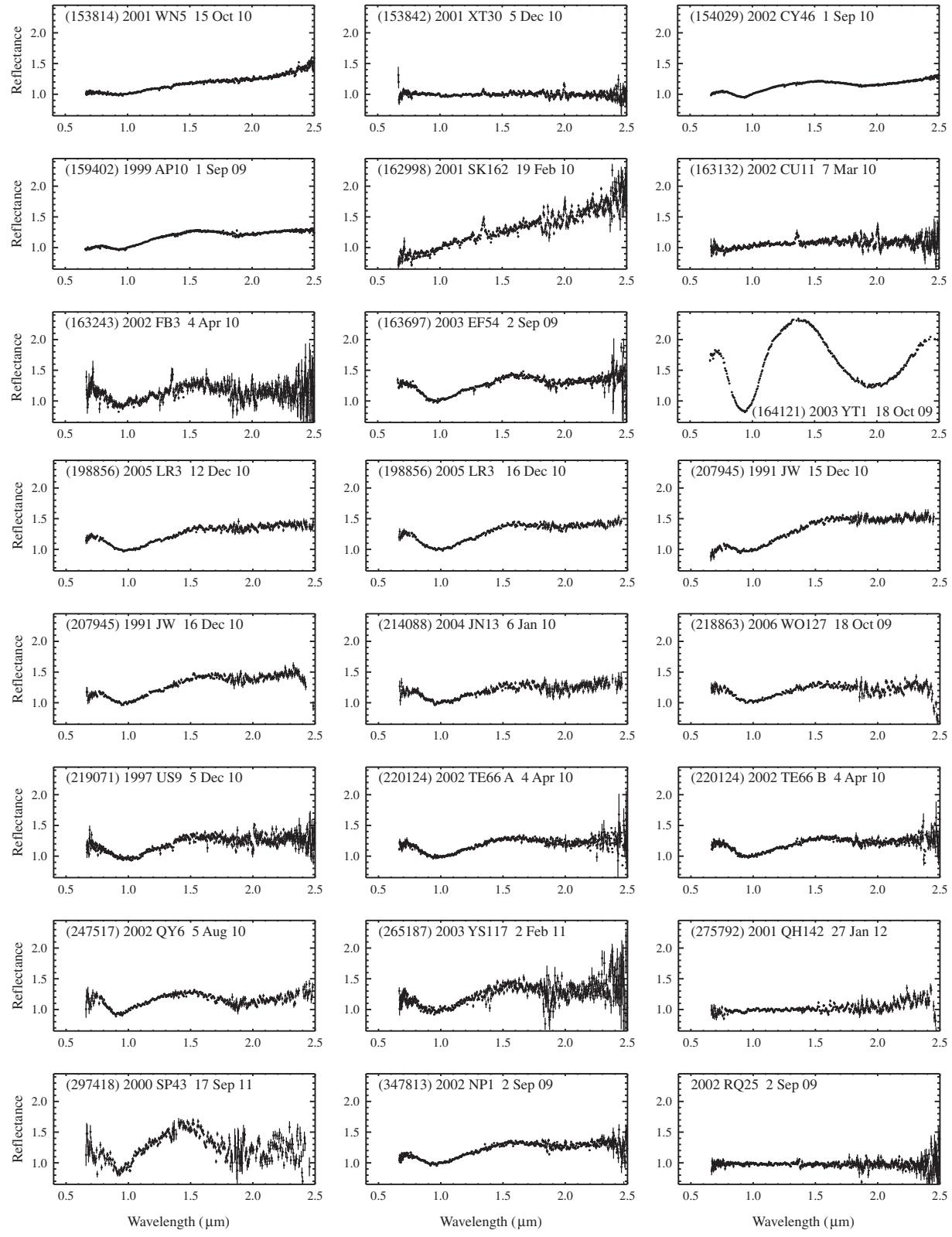
Fig. 9 (*continued*)
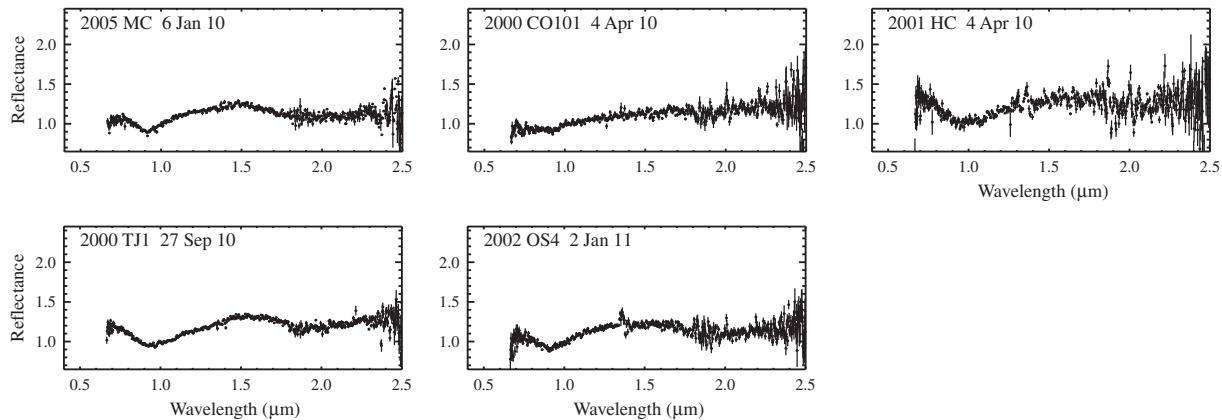
Fig. 9 (*continued*)

Fig. 9 (*continued*)

References

Adams, J.B., 1974. Visible and near-infrared diffuse reflectance spectra of pyroxenes as applied to remote sensing of solid objects in the Solar System. J. Geophys. Res. 79, 4829–4836. http://dx.doi.org/10.1029/JB079i032p04829.

Bell, J.F., Izenberg, N.I., Lucey, P.G., Clark, B.E., Peterson, C., Gaffey, M.J., Joseph, J., Carcich, B., Harch, A., Bell, M.E., Warren, J., Martin, P.D., McFadden, L.A., Wellnitz, D., Murchie, S., Winter, M., Veverka, J., Thomas, P., Robinson, M.S., Malin, M., Cheng, A., 2002. Near-IR reflectance spectroscopy of 433 Eros from the NIS Instrument on the NEAR mission. I. Low phase angle observations. Icarus 155, 119–144. http://dx.doi.org/10.1006/icar.2001.6752.

Binzel, R.P., Rivkin, A.S., Bus, S.J., Sunshine, J.M., Burbine, T.H., 2001. MUSES-C target Asteroid (25143) 1998 SF36: A reddened ordinary chondrite. Meteorit. Planet. Sci. 36, 1167–1172. http://dx.doi.org/10.1111/j.1945-5100.2001.tb01950.x.

Binzel, R.P., Birlan, M., Bus, S.J., Harris, A.W., Rivkin, A.S., Fornasier, S., 2004a. Spectral observations for near-Earth objects including potential target 4660 Nereus: Results from Meudon remote observations at the NASA Infrared Telescope Facility (IRTF). Planet. Space Sci. 52, 291–296. http://dx.doi.org/10.1016/j.pss.2003.10.003.

Binzel, R.P. et al., 2004b. Dynamical and compositional assessment of near-Earth object mission targets. Meteorit. Planet. Sci. 39, 351–366. http://dx.doi.org/10.1111/j.1945-5100.2004.tb00098.x.

Binzel, R.P., Rivkin, A.S., Stuart, J.S., Harris, A.W., Bus, S.J., Burbine, T.H., 2004c. Observed spectral properties of near-Earth objects: Results for population distribution, source regions, and space weathering processes. Icarus 170, 259–294. http://dx.doi.org/10.1016/j.icarus.2004.04.004.

Bottke, W.F., Morbidelli, A., Jedicke, R., Petit, J.-M., Levison, H.F., Michel, P., Metcalfe, T.S., 2002. Debiased orbital and absolute magnitude distribution of the near-Earth objects. Icarus 156, 399–433. http://dx.doi.org/10.1006/icar.2001.6788.

Burbine, T.H., McCoy, T.J., Meibom, A., Gladman, B., Keil, K., 2002. Meteoritic parent bodies: Their number and identification. Asteroids III, 653–667.

Burbine, T.H., Buchanan, P.C., Binzel, R.P., 2007. Deriving formulas from HED spectra for determining the pyroxene mineralogy of Vesta and Vestoids. Lunar Planet. Sci. 38, 2117 (abstracts).

Burbine, T.H., Buchanan, P.C., Dolkar, T., Binzel, R.P., 2009. Pyroxene mineralogies of near-Earth Vestoids. Meteorit. Planet. Sci. 44, 1331–1341. http://dx.doi.org/10.1111/j.1945-5100.2009.tb01225.x.

Burns, R.G., 1993. Mineralogical Applications of Crystal Field Theory, vol. 5. Cambridge University Press.

Burns, R.G., Huggins, F.E., Abu-Eid, R.M., 1972. Polarized absorption spectra of single crystals of lunar pyroxenes and olivines. Moon 4, 93–102. http://dx.doi.org/10.1007/BF00562917.

Bus, S.J., Binzel, R.P., 2002. Phase II of the Small Main-Belt Asteroid Spectroscopic Survey: The observations. Icarus 158, 106–145. http://dx.doi.org/10.1006/icar.2002.6857.

Clark, R.N., Roush, T.L., 1984. Reflectance spectroscopy – Quantitative analysis techniques for remote sensing applications. J. Geophys. Res. 89, 6329–6340. http://dx.doi.org/10.1029/JB089iB07p06329.

Cloutis, E.A., Gaffey, M.J., Jackowski, T.L., Reed, K.L., 1986. Calibrations of phase abundance, composition, and particle size distribution for olivine–orthopyroxene mixtures from reflectance spectra. J. Geophys. Res. 91, 11641. http://dx.doi.org/10.1029/JB091iB11p11641.

Cohen, M., Witteborn, F.C., Roush, T., Bregman, J., Wooden, D., 1998. Spectral irradiance calibration in the infrared. VIII. 5–14 Micron spectroscopy of the Asteroids Ceres, Vesta, and Pallas. Astron. J. 115, 1671–1679. http://dx.doi.org/10.1086/300271.

Cushing, M.C., Vacca, W.D., Rayner, J.T., 2004. Spextool: A spectral extraction package for SpeX, a 0.8–5.5 micron cross-dispersed spectrograph. Publ. Astron. Soc. Pacific 116, 362–376. http://dx.doi.org/10.1086/382907.

de León, J., Licandro, J., Serra-Ricart, M., Pinilla-Alonso, N., Campins, H., 2010. Observations, compositional, and physical characterization of near-Earth and Mars-crosser asteroids from a spectroscopic survey. Astron. Astrophys. 517, A23. http://dx.doi.org/10.1051/0004-6361/200913852.

Delbó, M., Harris, A.W., Binzel, R.P., Pravec, P., Davies, J.K., 2003. Keck observations of near-Earth asteroids in the thermal infrared. Icarus 166, 116–130. http://dx.doi.org/10.1016/j.icarus.2003.07.002.

DeMeo, F.E., Binzel, R.P., Slivan, S.M., Bus, S.J., 2009. An extension of the Bus asteroid taxonomy into the near-infrared. Icarus 202, 160–180. http://dx.doi.org/10.1016/j.icarus.2009.02.005.

Dunn, T.L., McCoy, T.J., Sunshine, J.M., McSween, H.Y., 2010. A coordinated spectral, mineralogical, and compositional study of ordinary chondrites. Icarus 208, 789–797. http://dx.doi.org/10.1016/j.icarus.2010.02.016.

Dunn, T.L., Burbine, T.H., Bottke, W.F., Clark, J.P., 2013. Mineralogies and source regions of near-Earth asteroids. Icarus 222, 273–282. http://dx.doi.org/10.1016/j.icarus.2012.11.007.

Emery, J.P. et al., 2010. Thermophysical characterization of Potential Spacecraft Target (101955) 1999 RQ36. Lunar Planet. Sci. 41, 2282 (abstracts).

Emery, J.P., Burr, D.M., Cruikshank, D.P., 2011. Near-infrared spectroscopy of Trojan asteroids: Evidence for two compositional groups. Astron. J. 141, 25. http://dx.doi.org/10.1088/0004-6256/141/1/25, arXiv:1012.1284.

Fazio, G.G. et al., 2004. The Infrared Array Camera (IRAC) for the Spitzer Space Telescope. Astrophys. J. Suppl. 154, 10–17. http://dx.doi.org/10.1086/422843, arXiv:astro-ph/0405616.

Fieber-Beyer, S.K., Gaffey, M.J., Abell, P.A., 2011. Mineralogical characterization of near-Earth Asteroid (1036) Ganymed. Icarus 212, 149–157. http://dx.doi.org/10.1016/j.icarus.2010.12.013.

Foley, C.N., Nittler, L.R., McCoy, T.J., Lim, L.F., Brown, M.R.M., Starr, R.D., Trombka, J.I., 2006. Minor element evidence that Asteroid 433 Eros is a space-weathered ordinary chondrite parent body. Icarus 184, 338–343. http://dx.doi.org/10.1016/j.icarus.2006.05.011.

Gaffey, M.J., 1984. Rotational spectral variations of Asteroid (8) Flora Implications for the nature of the S-type asteroids and for the parent bodies of the ordinary chondrites. Icarus 60, 83–114. http://dx.doi.org/10.1016/0019-1035(84)90140-4.

Gaffey, M.J., Burbine, T.H., Piatek, J.L., Reed, K.L., Chaky, D.A., Bell, J.F., Brown, R.H., 1993. Mineralogical variations within the S-type asteroid class. Icarus 106, 573. http://dx.doi.org/10.1006/icar.1993.1194.

Gaffey, M., Cloutis, E., Kelley, M., Reed, K., 2002. Mineralogy of asteroids. In: Asteroids III. University of Arizona Press, Tucson, AZ, pp. 183–204.

Harris, A.W., Davies, J.K., 1999. Physical characteristics of near-Earth asteroids from thermal infrared spectrophotometry. Icarus 142, 464–475. http://dx.doi.org/10.1006/icar.1999.6248.

Harris, A.W. et al., 2011. ExploreNEOs. II. The accuracy of the Warm Spitzer near-Earth object survey. Astron. J. 141, 75. http://dx.doi.org/10.1088/0004-6256/141/3/75.

Hicks, M., Truong, T., Somers, J., 2010. Broad-band photometry of the near-Earth Asteroid 154029 (2002 CY46): An unusually steep solar phase curve and evidence for complex rotation. Astronomer's Telegram 1. Abstract 2859

Hinrichs, J.L., Lucey, P.G., 2002. Temperature-dependent near-infrared spectral properties of minerals, meteorites, and lunar soil. Icarus 155, 169–180. http://dx.doi.org/10.1006/icar.2001.6754.

Lebofsky, L.A., Spencer, J.R., 1989. Radiometry and a thermal modeling of asteroids. In: Asteroids II. vol. 1. University of Arizona Press, Tucson, AZ, pp. 128–147.

Lebofsky, L.A., Sykes, M.V., Tedesco, E.F., Veeder, G.J., Matson, D.L., Brown, R.H., Gradie, J.C., Feierberg, M.A., Rudy, R.J., 1986. A refined standard thermal model for asteroids based on observations of 1 Ceres and 2 Pallas. Icarus 68 (2), 239–251.

Li, J., A'Hearn, M.F., McFadden, L.A., 2004. Photometric analysis of Eros from NEAR data. Icarus 172, 415–431. http://dx.doi.org/10.1016/j.icarus.2004.07.024.

Lord, S.D., 1992. A New Software Tool for Computing Earth's Atmospheric Transmission of Near- and Far-infrared Radiation. Tech. Rep.

Mainzer, A. et al., 2011. NEOWISE observations of near-Earth objects: Preliminary results. Astrophys. J. 743, 156. http://dx.doi.org/10.1088/0004-637X/743/2/156, arXiv:1109.6400.

McCoy, T.J. et al., 2001. The composition of 433 Eros: A mineralogical chemical synthesis. Meteorit. Planet. Sci. 36 (12), 1661–1672. http://dx.doi.org/10.1111/j.1945-5100.2001.tb01855.x.

Mommert, M., Hora, J.L., Harris, A.W., Reach, W.T., Emery, J.P., Thomas, C.A., Mueller, M., Cruikshank, D.P., Trilling, D.E., Delbo, M., Smith, H.A. The discovery of cometary activity in near-Earth Asteroid (3552) Don Quixote. Astrophys. J., submitted for publication.

Moroz, L., Schade, U., Wäsch, R., 2000. Reflectance spectra of olivine–orthopyroxene-bearing assemblages at decreased temperatures: Implications for remote sensing of asteroids. Icarus 147, 79–93. http://dx.doi.org/10.1006/icar.2000.6430.

Moskovitz, N.A., Willman, M., Burbine, T.H., Binzel, R.P., Bus, S.J., 2010. A spectroscopic comparison of HED meteorites and V-type asteroids in the inner Main Belt. Icarus 208, 773–788. http://dx.doi.org/10.1016/j.icarus.2010.03.002, arXiv:1003.2580.

Mueller, M. et al., 2011. ExploreNEOs. III. Physical characterization of 65 Potential Spacecraft Target Asteroids. Astron. J. 141, 109. http://dx.doi.org/10.1088/0004-6256/141/4/109.

Müller, T.G. et al., 2012. Physical properties of OSIRIS-REx target Asteroid (101955) 1999 RQ$_{36}$. Derived from Herschel, VLT/VISIR, and Spitzer observations. Astron. Astrophys. 548, A36. http://dx.doi.org/10.1051/0004-6361/201220066, arXiv:1210.5370.

Nakamura, T. et al., 2011. Itokawa dust particles: A direct link between S-type asteroids and ordinary chondrites. Science 333. http://dx.doi.org/10.1126/science.1207758, 1113–.

Rayner, J.T. et al., 2003. SpeX: A medium-resolution 0.8–5.5 micron spectrograph and imager for the NASA Infrared Telescope Facility. Publ. Astron. Soc. Pacific 115, 362–382. http://dx.doi.org/10.1086/367745.

Reddy, V., Gaffey, M.J., Kelley, M.S., Nathues, A., Li, J.-Y., Yarbrough, R., 2010. Compositional heterogeneity of Asteroid 4 Vesta's southern hemisphere: Implications for the Dawn mission. Icarus 210, 693–706. http://dx.doi.org/10.1016/j.icarus.2010.07.015.

Reddy, V., Carvano, J.M., Lazzaro, D., Michtchenko, T.A., Gaffey, M.J., Kelley, M.S., Mothé-Diniz, T., Alvarez-Candal, A., Moskovitz, N.A., Cloutis, E.A., Ryan, E.L., 2011a. Mineralogical characterization of Baptistina Asteroid Family: Implications for K/T impactor source. Icarus 216, 184–197. http://dx.doi.org/10.1016/j.icarus.2011.08.027, arXiv:1110.3414.

Reddy, V., Nathues, A., Gaffey, M.J., 2011b. First fragment of Asteroid 4 Vesta's mantle detected. Icarus 212, 175–179. http://dx.doi.org/10.1016/j.icarus.2010.11.032.

Reddy, V., Nathues, A., Gaffey, M.J., Schaeff, S., 2011c. Mineralogical characterization of potential targets for the ASTEX mission scenario. Planet. Space Sci. 59, 772–778. http://dx.doi.org/10.1016/j.pss.2011.03.005.

Reddy, V. et al., 2012a. Color and albedo heterogeneity of Vesta from Dawn. Science 336. http://dx.doi.org/10.1126/science.1219088, 700–.

Reddy, V., Sanchez, J.A., Gaffey, M.J., Abell, P.A., Corre, L.L., Hardersen, P.S., 2012b. Composition of near-Earth Asteroid (4179) Toutatis. Icarus 221, 1177–1179. http://dx.doi.org/10.1016/j.icarus.2012.10.005, arXiv:1210.2853.

Reddy, V., Sanchez, J.A., Nathues, A., Moskovitz, N.A., Li, J.-Y., Cloutis, E.A., Archer, K., Tucker, R.A., Gaffey, M.J., Paul Mann, J., Sierks, H., Schade, U., 2012c. Photometric, spectral phase and temperature effects on 4 Vesta and HED meteorites: Implications for the Dawn mission. Icarus 217, 153–168. http://dx.doi.org/10.1016/j.icarus.2011.10.010.

Rivkin, A.S., Binzel, R.P., Sunshine, J., Bus, S.J., Burbine, T.H., Saxena, A., 2004. Infrared spectroscopic observations of 69230 Hermes (1937 UB): Possible unweathered endmember among ordinary chondrite analogs. Icarus 172, 408–414. http://dx.doi.org/10.1016/j.icarus.2004.07.006.

Salisbury, J.W., D'Aria, D.M., Jarosewich, E., 1991. Midinfrared (2.5–13.5 μm) reflectance spectra of powdered stony meteorites. Icarus 92 (2), 280–297. http://dx.doi.org/10.1016/0019-1035(91)90052-U, <http://www.sciencedirect.com/science/article/pii/001910359190052U>.

Sanchez, J.A., Reddy, V., Nathues, A., Cloutis, E.A., Mann, P., Hiesinger, H., 2012. Phase reddening on near-Earth asteroids: Implications for mineralogical analysis, space weathering and taxonomic classification. Icarus 220, 36–50, arXiv:1205.0248.

Schade, U., Wäsch, R., 1999. NIR reflectance spectroscopy of mafic minerals in the temperature range between 80 and 473 K. Adv. Space Res. 23, 1253–1256. http://dx.doi.org/10.1016/S0273-1177(99)00193-3.

Skiff, B.A., Bowell, E., Koehn, B.W., Sanborn, J.J., McLelland, K.P., Warner, B.D., 2012. Lowell observatory Near-Earth Asteroid Photometric Survey (NEAPS) – 2008 May through 2008 December. Minor Planet Bull. 39, 111–130.

Somers, J.M. et al., 2010. Optical characterization of planetary radar targets, low-ΔV, and potentially hazardous asteroids: Results from 2009–2010. In: AAS/Division for Planetary Sciences Meeting, vol. 45. Bulletin of the American Astronomical Society, p. 1055 (abstracts).

Sunshine, J.M., Bus, S.J., McCoy, T.J., Burbine, T.H., Corrigan, C.M., Binzel, R.P., 2004. High-calcium pyroxene as an indicator of igneous differentiation in asteroids and meteorites. Meteorit. Planet. Sci. 39 (8), 1343–1357. http://dx.doi.org/10.1111/j.1945-5100.2004.tb00950.x.

Thomas, C.A., Binzel, R.P., 2010. Identifying meteorite source regions through near-Earth object spectroscopy. Icarus 205, 419–429. http://dx.doi.org/10.1016/j.icarus.2009.08.008.

Thomas, C.A. et al., 2011. ExploreNEOs. V. Average albedo by taxonomic complex in the near-Earth asteroid population. Astron. J. 142, 85. http://dx.doi.org/10.1088/0004-6256/142/3/85.

Trilling, D.E., Mommert, M., Mueller, M., Spahr, T.B., Hora, J.L., Harris, A.W., Thomas, C.A., Benner, L., Bhattacharya, B., Bottke, W.F., Delbo, M., Emery, J.P., Fazio, G., Mainzer, A., Penprase, B., Smith, H.A. ExploreNEOs VI: Second data release and preliminary size distribution of near Earth objects. Astron. J., submitted for publication.

Trilling, D.E. et al., 2010. ExploreNEOs. I. Description and first results from the Warm Spitzer near-Earth object survey. Astron. J. 140, 770–784. http://dx.doi.org/10.1088/0004-6256/140/3/770.

Trombka, J.I. et al., 2000. The elemental composition of Asteroid 433 Eros: Results of the NEAR-Shoemaker X-ray spectrometer. Science 289, 2101–2105. http://dx.doi.org/10.1126/science.289.5487.2101.

Usui, F. et al., 2011. Asteroid catalog using Akari: AKARI/IRC mid-infrared asteroid survey. Publ. Astron. Soc. Jpn. 63, 1117–1138.

Vernazza, P. et al., 2008. Compositional differences between meteorites and near-Earth asteroids. Nature 454, 858–860. http://dx.doi.org/10.1038/nature07154.

Werner, M.W. et al., 2004. The Spitzer Space Telescope mission. Astrophys. J. Suppl. 154, 1–9. http://dx.doi.org/10.1086/422992, arXiv:astro-ph/0406223.

Xu, S., Binzel, R.P., Burbine, T.H., Bus, S.J., 1995. Small main-belt asteroid spectroscopic survey: Initial results. Icarus 115, 1–35. http://dx.doi.org/10.1006/icar.1995.1075.

Ye, Q.-z., 2011. BVRI photometry of 53 unusual asteroids. Astron. J. 141, 32. http://dx.doi.org/10.1088/0004-6256/141/2/32, arXiv:1011.0133.